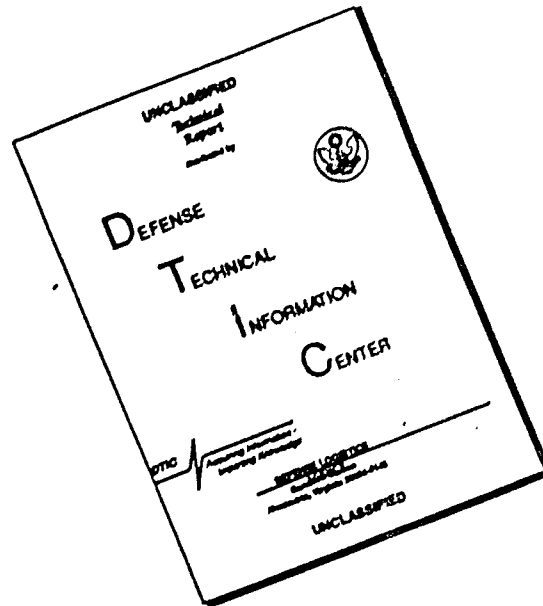# OCEAN-BOTTOM SEISMOMETER
DATA ANALYSIS PROGRAM

AFCRL CONTRACT NO. AF 19(604)-8368

FINAL REPORT

TEXAS INSTRUMENTS
INCORPORATED
SCIENCE SERVICES DIVISION

DISCLAIMER NOTICE

THIS DOCUMENT IS BEST QUALITY AVAILABLE. THE COPY FURNISHED TO DTIC CONTAINED A SIGNIFICANT NUMBER OF PAGES WHICH DO NOT REPRODUCE LEGIBLY.

BLANK PAGES IN THIS DOCUMENT WERE NOT FILMED

OCEAN-BOTTOM SEISMOMETER DATA

COLLECTION AND ANALYSIS

By

William A. Schneider

TEXAS INSTRUMENTS, INCORPORATED
Science Services Division
P. O. Box 5621
Dallas, Texas

Project Manager

Patrick J. Farrell

October 12, 1964

NOTICES

Requests for additional copies by agencies of the Depart-
ment of Defense, their contractors, or other government
agencies should be directed to:

DEFENSE DOCUMENTATION CENTER (DDC)
CAMERON STATION
ALEXANDRIA, VIRGINIA 22314

Department of Defense contractors must be established
for DDC services or have their "need-to-know" certified by
the cognizant military agency of their project or contract.

All other persons and organizations should apply to the:

U.S. DEPARTMENT OF COMMERCE
OFFICE OF TECHNICAL SERVICES
WASHINGTON, D.C. 20230

ACKNOWLEDGEMENT

TABLE OF CONTENTS

TABLE OF CONTENTS (CONTD)

LIST OF ILLUSTRATIONS

LIST OF ILLUSTRATIONS (CONTD)

LIST OF ILLUSTRATIONS (CONTD)

LIST OF TABLES

SECTION I

INTRODUCTION

This final report covers three years of engineering, field measurements and data analysis to investigate seismic energy as recorded in an ocean environment to 22,000 feet.

The work was sponsored by the Air Force Cambridge Research Laboratories (AFCRL) as part of the Advanced Research Projects Agency (ARPA) Project VELA UNIFORM.

The goal of this project is the detection and identification of underground and underwater nuclear explosions, and ARPA, acting through several government agencies, has funded investigations which bear on the problem. In order to be able to detect nuclear explosions, and to distinguish between them and earthquakes, it is desirable to acquire as much knowledge as possible about the transmission and recording of seismic waves through and around the earth. Recordings of many earthquakes and explosions have been studied, but until recently all of these were from land stations.

Ocean-bottom recordings of seismic energy promised to contribute to the objectives of VELA UNIFORM in several ways. First, because the oceans cover 70 per cent of the earth's surface, a favorable location (for reasons other than accessibility) for a seismic recording station is more likely to be in the ocean than on land. Second, it was generally held that the short-period microseisms, (1 to 10 cps band), created by cultural activity or atmospheric disturbance would be absent, or at least highly attenuated, in the deep ocean. If this were true it would allow a reduction in the detection threshold because of the expected improvement in the ratio of signal-to-noise (S/N). Third, ocean-bottom seismograms would be expected to differ from land seismograms because of the thinner and presumably simpler oceanic crust. The difference might appear in phase definition, frequency content, or amplitude ratios.

In addition, knowledge of ocean-bottom noise characteristics such as spectral content, propagation modes, velocities, and direction is necessary for signal enhancement using array techniques.

In this report no effort will be made to repeat what has been published in previous Semi-Annual or Special Reports; however, references will be provided for any reader interested in detail.

A. HISTORY

In March 1961, AFCRL awarded Contract Number AF 19(604)-8368 to Texas Instruments Incorporated (TI) to develop an ocean-bottom seismic monitoring device and use this instrument in a data collection and analysis program.

Two prototype instruments were constructed and used in a data collection program in the vicinity of Santa Catalina Island.

The field operation results, in 42 successful drops and recoveries, provided ocean-bottom seismic data which included five underground nuclear tests from the Nevada Test Site.

These initial results encouraged design and construction of five additional units which were modified to incorporate improvements suggested through experience gained in field testing and data handling. Table I compares the prototype and advanced units.

The advanced units were used in a broad data collection program in three widely separated areas of the Pacific Ocean. Following is a list of these areas and the reasons for their selection.

AREA	REASONS FOR SELECTION	OBJECTIVE
California Coast West of Eureka	Seismically Active	Compare ocean-bottom vs land signal-to-noise ratio (S/N). Investigate propagation of later phases of seismic wave trains.
Aleutian Islands Area	Volcanic Island Arc	Investigate the nature of seismic signals recorded on either side of a volcanic island arc.
Hawaiian Islands	Rapid depth increase in short horizontal distance	Determine the effects of increasing water depth on the ocean-bottom vs land S/N ratio.
All Areas		Determine seasonal micro-seismic activity in an ocean environment. Study pressure vs particle motion relationship in the ocean as it applies to detection and ambient noise studies.

2

TABLE 1

COMPARISON OF PROTOTYPE AND ADVANCED UNITS

INSTRUMENTATION	PROTOTYPE DIGITAL	IMPROVED FM/DIGITAL
Sensors	1 Pressure Transducer 1 Vertical Seismometer 2 Horizontal Seismometers	Same
Tape Recorder	Pemco, 1/2 inch Tape, 10 Track Digital	Parsons, 1 inch Tape, 14 Track FM/Digital
Tape Capacity	800 Ft at 0.355 IPS	1000 Ft at 0.300 IPS
Recording Time	7.5 hr	11.1 hr
Recorder Capacity	4 Data Channels 2 Timing Channels	8 Data Channels 2 Timing Channels
Recording Technique	Digital	FM/Digital
Dynamic Range	36 db per Channel	42 db per Channel 72 db per Sensor
Recording Frequency Range	0.1 to 10 cps Flat 1 - 10 cps	0.1 to 50 cps Flat 1 - 10 cps
Power Requirement	6.3 Watts	8.0 Watts
Timing Method	Crystal 163.8400 kcps	Fork 1600.00 cps
Max Oper Depth	10,000 Ft	20,000 Ft

In carrying out this program the seismographs were dropped and recovered 80 times for a total of 760 hours of ocean-bottom recording of which 500 contained good usable data.

This report will deal mainly with the analysis and interpretation of this data.

B. PREVIOUS REPORTS

Semi-Annual and Special Reports written for this contract are listed below.

REPORT	DATE
Semi-Annual Report No. 1	18 September 1961
Semi-Annual Report No. 2	23 April 1962
Special Report on the Program to Research, Develop, Construct, and Test an Automatic Marine Seismic Monitoring and Recording Instrument	1 March 1962
Special Report on Preliminary Evaluation of Records from Texas Instruments Ocean-Bottom Seismic Monitoring and Recording Instrument	27 April 1962
Semi-Annual Report No. 3	31 October 1962
Semi-Annual Report No. 4	15 March 1963
Special Report on Ocean-Bottom Seismometer Tests at Uinta Basin Observatory and Lake Bend Oreille	1 May 1963
Semi-Annual Report No. 5	15 November 1963
Collection and Analysis of Pacific Ocean-Bottom Seismic Data	2 February 1964

SECTION II

ANALYSIS AND INTERPRETATION

This section includes analysis of ocean-bottom data collected during the summer of 1963 in the three Pacific areas (California Coast, Aleutian Islands and vicinity of the Island of Hawaii) not covered in previous reports.

A total of thirty-one signal events was subjected to spectral analysis to provide signal-to-noise ratio comparisons between the ocean-bottom and land stations. These consist of nine teleseisms, four near-regional quakes, seventeen local shocks, three of which are located, and one nuclear shot from the Nevada Test Site. Table II provides summary information about the signals analyzed in this report as well as those reported previously.

The method of analysis used in the signal-to-noise determination has been described in past reports (Semiannual Technical Reports Number 3 and Number 5). Briefly, it consists of digitally estimating the power spectra of the P-S interval, and S phase of the received signal. The noise spectrum is obtained as an average of four or five individual noise spectra taken approximately one hour apart before and after the signal arrival. These three spectra (P, S and noise) are then displayed on the same graph side by side for the ocean-bottom and land. This type of presentation allows not only comparison of S/N ratio vs frequency, but also direct comparison of signal and noise levels as well as differences in spectral content of signal and noise on the ocean-bottom and land.

In order to further distill and reduce the amount of information contained in these plots, certain statistics on the noise data analyzed to date have been compiled and are presented in Section III. These statistics relate to average noise spectra for the three areas, and average ocean-bottom-to-land-noise ratios.

The spectral analysis results are presented in chronological order starting with the Aleutian recordings, Hawaiian data, and then the California Coast drops. Previous analysis of a California quake and two Aleutian signals covered in special report (Collection and Analysis of Pacific Ocean-Bottom Seismic Data) are not included except in the summary information of Table II and the statistical compilation of Section III.

A. ALEUTIAN DROPS

Figure 1 shows the location of the ocean-bottom instrument for the Aleutian drops as well as the land site which remained fixed throughout the recording period. In addition, approximate hypocentral locations are shown for several near-regional and local events analyzed.

Event No.	Date	Origin Time GMT	Co-ordinates	Area	Land Seis	OB Seis	Hypo-central Depth Km.	Magnitude
				EPICENTER	Approx. Distance			
--	6-29-63	08:09:27.6	40.3°N, 126.9°W	N. Calif.	250 Km	213 Km	33	4.2 (CGS)
3	8-22-63	≈ 22:16	53°N, 177.5°W	Aleutians	220 Km	290 Km	250 est	---
8	8-23-63	13:09:25.3	52.4°N, 159.6°E	Kamchatka	14°	14°	33	4.5 (CGS)
9A	8-26-63	≈ 15:18	52.5°N, 174°W	Aleutians	180 Km	312 Km	--	---
10	8-23-63	16:42:34.2	52.5°N, 159.5°E	Kamchatka	14°	14°	67	4.1 (CGS)
14	8-30-63	≈ 00:06	51.5°N, 175.5°W	Aleutians	60 Km	50 Km	--	---
18	8-30-63	≈ 02:55	51.5°N, 172.5°W	"	366 Km	500 Km	--	---
25	9-7-63	07:13:39.9	45.4°N, 150.8°E	Kurile Is.	22°	22°	33	5.2 (CGS)
26	9-9-63	≈ 01:52	51°N, 175°W	Aleutians	100 Km	70 Km	--	---
27	9-9-63	02:45:45.5	4.4°S, 152.7°E	New Britain	63°	63°	34	5.6 (CGS)
28	9-9-63	≈ 03:44	52°N, 174.5°E	Aleutians	220 Km	200 Km	--	---
30	9-1-63	≈ 22:48	52°.2'N, 178.2'W	"	110 Km	--	--	---
31	8-30-63	00:16:36.3	8.7°S, 108.6°E	Java	87°	87°	33	5.1 (CGS)
32	9-8-63	≈ 10:09	51.5°N, 179°W	Aleutians	164 Km	223 Km	--	3.5 est
39	10-6-63	≈ 22:26	-----	Hawaii Is.	--	--	--	---
41	10-11-63	≈ 23:40	-----	"	--	--	--	---
42	10-11-63	≈ 23:41	-----		--	--	--	---
43	10-13-63	≈ 04:14	-----	"	--	--	--	---
44	10-13-63	05:17:57.1	44.8°N, 149.5°E	Kurile Is.	52°	51°	60	8.5 (PAS)
45	10-13-63	≈ 07:16	-----	Hawaii Is.	--	--	--	---
46	10-12-63	11:26:57.9	44.8°N, 149°E	Kurile Is.	53°	52°	40	7.0 (PAS)
47	10-16-63	≈ 15:12	-----	Hawaii Is.	--	--	--	---
49	10-13-63	≈ 22:06	-----	"	--	--	--	---
51	10-20-63	≈ 12:31	-----	"	--	--	--	---
52	10-20-63	00:53:07.2	44.7°N, 150.7°E	Kurile Is.	52°	54°	25	7.0 (PAS)
53	10-20-63	≈ 02:34	-----	Hawaii Is.	--	--	--	---
54	10-23-63	≈ 05:08	-----		--	--	--	---
55	10-23-63	≈ 07:01	-----		--	--	--	---
57	10-26-63	≈ 16:58	-----		--	--	--	---
59	11-22-63	17:30:00	-----	Nevada Test Site	6°	4.3°	0	---
61	11-29-63	≈ 08:18	-----	N. Calif.	--	--	--	---
62	12-2-63	≈ 13:41	41°N, 125.5°W		120 Km	330 Km	--	---
64	12-2-63	21:05:49	80.1°N, 0.6°W	Svalbard Is.	58°	60°	33	5.1 (CGS)
65	12-4-63	08:24:17.1	46.1°N, 152.9°E	Kurile Is.		66°		5.3 (CGS)

*See Special Report: Collection and Analysis of Pacific Ocean-Bottom Seismic Data.

TABLE 2

SUMMARY OF SIGNAL EVENTS ANALYZED

|	Recording Position -- Land			Recording Position -- Ocean Bottom			
gnitude	Co-ordinates	Area	Elevation from Sea Level Km.	Map Location No.	Co-ordinates	Area	Elevation from Sea Level Km.
(CGS)	40°41'N, 123°59'W	Kneeland, Calif.	-0.46 est	10	40°57'N, 124°32'W	W of Cape Mendocino, Calif.	-0.54*
	51°52.3'N, 176 42.4'W	Adak Is.	+0.05	4	51°5'N, 176°20'W	S of Adak	-3.49
(CGS)	" "	"	"	5S	51°6'N, 176°26'W	S of Adak	-4.06
	" "	"	"	4	54°20.2'N, 174°W	N of Adak	-3.7
(CGS)	" "	"	"	5S	51°6'N, 176°26'W	S of Adak	-4.06
	" "	"	"	13	51°7'N, 176°26'W	"	-4.2
	" "	"	"		" "	"	"
(CGS)	" "	"	"	19	50°15.5'N, 176°11'W	"	-6.27
	" "	" "	"	22	50°45'N, 176°20'W	"	-4.6
(CGS)	" "	" "	"	"	" "	"	"
	" "	" "	"	"	" "	"	"
	" "	" "	"	16	49°11'N, 175°42'W	"	-5.26
(CGS)	" "	"	"	13	51°07'N, 176°26'W	"	-4.2*
est	" "	"	"	21	50°15'N, 176°11'W	"	-6.1*
	19°39'N, 156°0.3'W	Hawaii Is.	+0.02	5	19°35.5'N, 156°09.5'W	W of Hawaii	-2.76
	" "	"	"	9	19°46.8'N, 156°31'W	"	-4.89
	" "	"	"	"	" "	"	"
	" "	"	"	11	19°42.6'N, 156°15.1'W	"	-4.02
(PAS)	" "	"	"	"	" "	"	"
	" "	"	"	"	" "	"	"
(PAS)	" "	"	"	10	19°46.8'N, 156°31'W	"	-4.91
	" "	"	"	13	19°39.6'N, 156°15.9'W	"	-3.98
	" "	"	"	12	19°35.2'N, 156°09.7'W	"	-2.92
	" "	"	"	17	19°40'N, 154°28'W	E of Hawaii	-2.46
(PAS)	" "	"	"	16	19°34.5'N, 154°39'W	"	-2.02
	" "	"	"	"	" "	"	"
	" "	"	"	19	19°31.2'N, 156°02'W	W of Hawaii	-1.46
	" "	"	"	"	" "	"	"
	" "	"	"	21	19°40.4'N, 156°15.6'W	"	-4.22
	40°41'N, 123°59'W	Kneeland, Calif.	+0.46 est	22	36°01'N, 122°10.5'W	SW of Pt. Sur, Calif.	-1.47
	" "	"	"	26	40°38'N, 126°17'W	W of Cape Mendocino, Calif.	-3.1
	" "	"	"	30	38°2.5'N, 125°45'W	W of Pt. Reyes, Calif.	-4.16
(CGS)	" "	"	"	"	" "	"	"
(CGS)	" "	"	"	31	40°41'N, 123°59'W	W of Pt. Conception, Calif.	-4.17
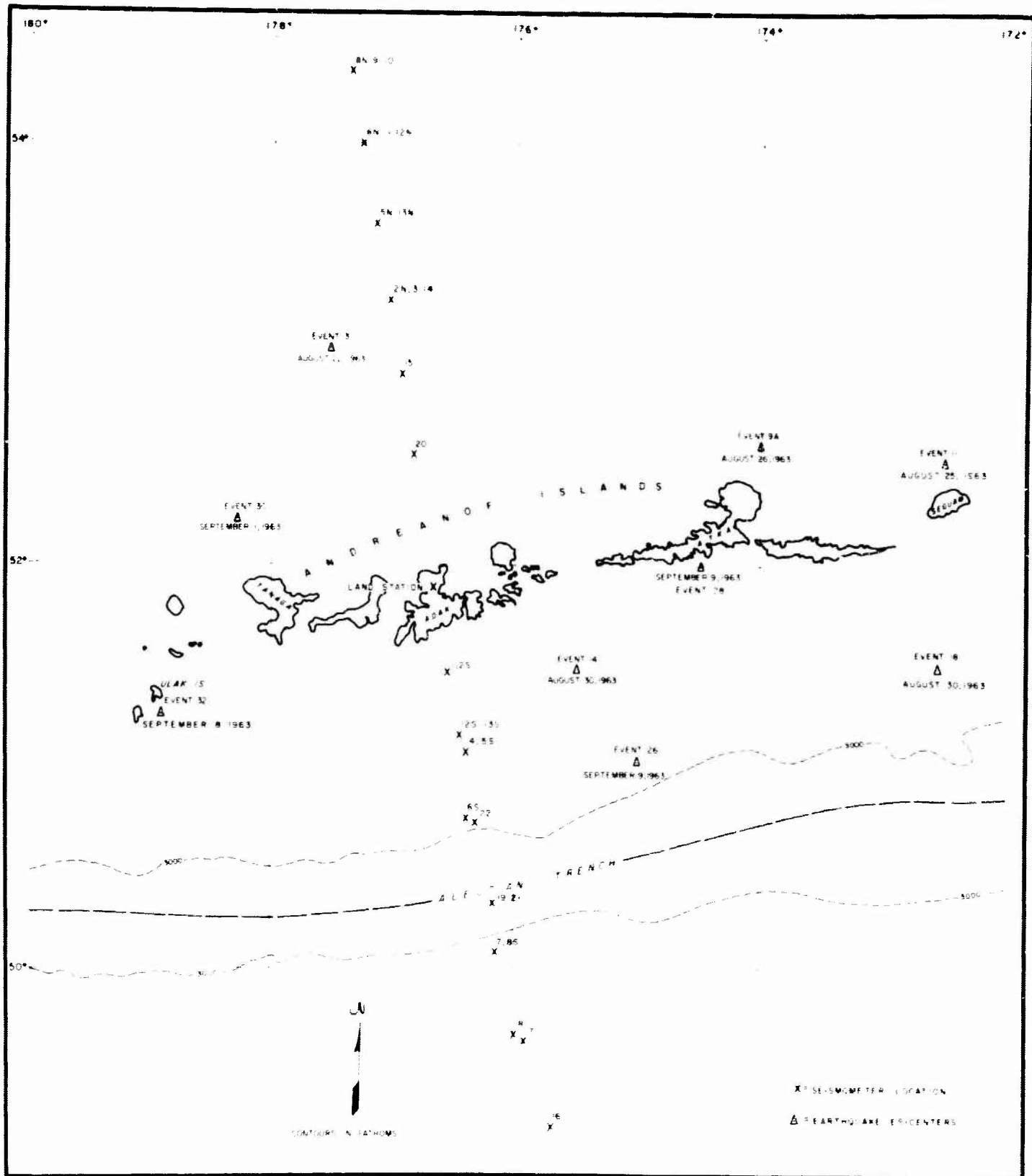
Figure 1. Aleutian Drops Instrument Locations

A great many more events were recorded than have been selected for analysis from the Aleutian data. One requirement for the land and ocean-bottom spectral comparison is that the event be simultaneously recorded at the two sites. Many were eliminated on this basis. Others were discarded if several components were unusable (primarily a problem on the ocean-bottom where occasionally excessive cable noise or improper instrument plant resulted in highly corrupted data). Finally, of the remaining events those were selected which offered the greatest likelihood of providing unambiguous comparisons of S/N, spectral differences, phase development, etc. on the ocean-bottom and land. This implies knowledge of at least the hypocenter, though some unlocated local events are included.

The events will be discussed in the order of decreasing distance, that is, teleseisms, regional, near-regional, local, and a final category of unlocated events most of which are local.

1. Kamchatka Teleseisms of August 23, 1963

Two teleseisms originating from Kamchatka were recorded on the land and ocean-bottom position 5S (Figure 1) approximately 3-1/2 hours apart. These are shown in Figure 2 where the four land traces, indicated as BZ = Benioff vertical, Z = vertical, NS = north-south horizontal, EW = east-west horizontal, and P = ocean-bottom pressure, having been obtained from the high level channels, are displayed. The other ocean-bottom components were inoperative on this drop.

On land, the visual signal-to-noise ratio is better than the ocean-bottom pressure trace, with the former showing a distinct onset. The first shock (event 8) is of slightly larger magnitude than the second (event 10) as is evidenced by the difference in signal-to-noise ratio at the onset. The relative playback gains have been adjusted to equalize the two events for display and are not to be interpreted quantitatively. A local shock can be seen arriving about 20 seconds after the onset of event 8 by the abrupt change in frequency.

The spectra of the two events, 8 and 10, are compared to the average noise spectra for that day in Figure 3.

The signal-to-noise ratio vs frequency is approximately twice as good (in db) on the three land components as for the ocean-bottom pressure sensor. The flattening of the noise curves above 3 cps on all components is indicative of instrument noise level. The broad noise peak on land is characteristic of all the Aleutian noise measurements.

It is interesting to note the similarities in spectra of the two events eminating from approximately the same epicenter. Except for a level difference of about 4 db, many of the spectral details are identical. Without velocity components on the ocean-bottom, little can be said about
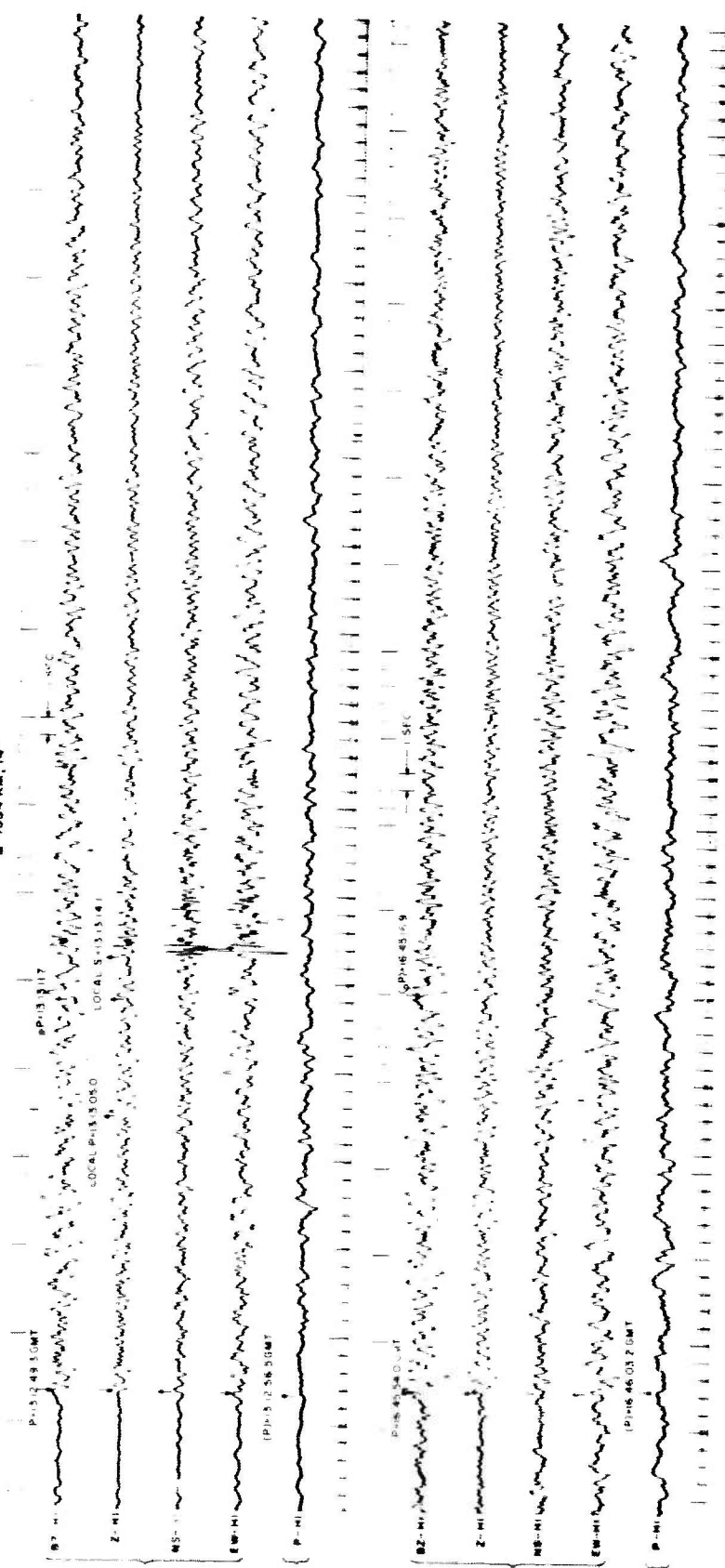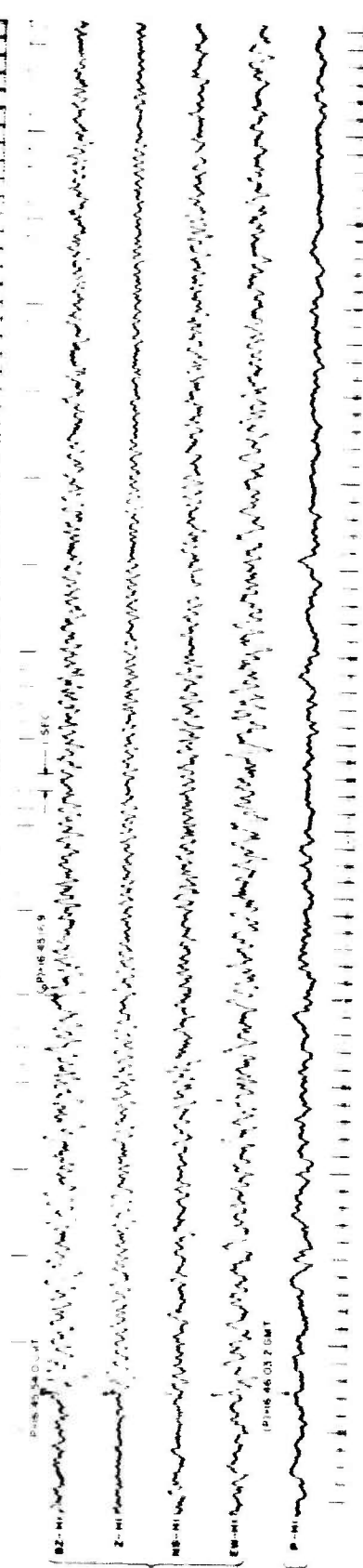
Figure 2. Kamchatka Teleseisms
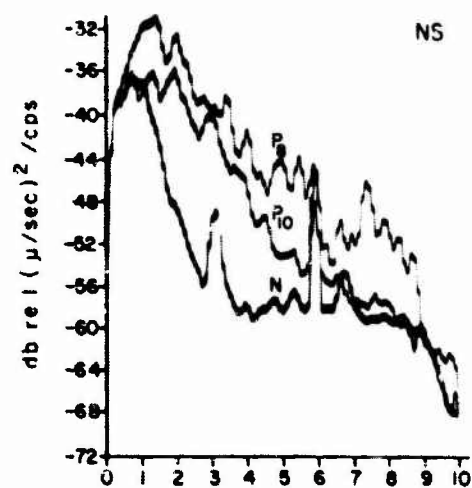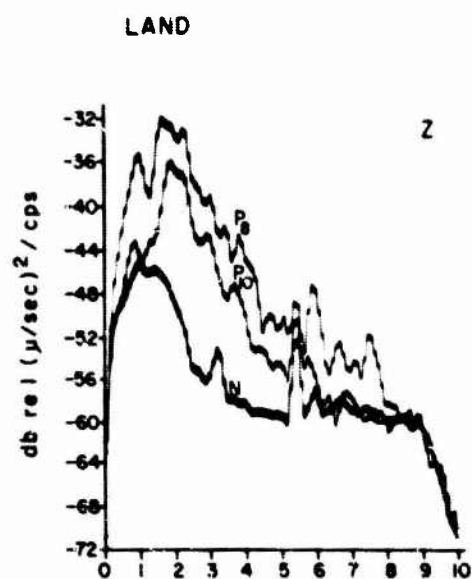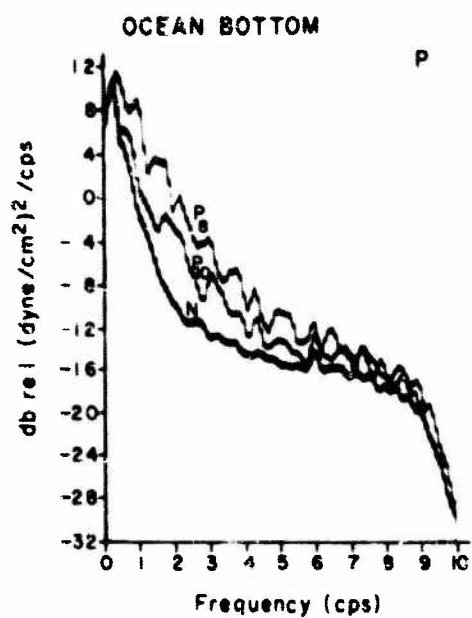
Figure 3.   Kamchatka Teleseism Spectra

comparison of spectral shape or level except that, for a vertically incident planewave, the pressure and vertical velocity spectra should differ by about 24 db. This would place the ocean-bottom Z signal level significantly above the land Z level, (10 db at 2 cps for instance). This phenomenon has been observed for other teleseisms in previous analysis.

2. Kurile Island Teleseism, September 7, 1963

The ocean-bottom and land seismograms for the Kurile Island teleseism (event 25) are presented in Figure 4. Only the ocean-bottom pressure and one horizontal component were operative on this drop (map position 19). The nomenclature used for the ocean-bottom horizontal components is H_u = upper horizontal instrument and H_L = lower horizontal instrument. Orientation was generally not known. All traces displayed except pressure were taken from the low gain (LO) channel in the split-level recording system. Invariably the noise spectra were obtained from the high-gain (HI) channels on which the ambient noise was better modulated. As is evident from the figure, S/N ratio is visibly better on land for this event. When the low frequency pressure ambient is filtered off (bottom half of Figure 4), the pressure S/N ratio fares considerably better; in fact, the first surface bounce can be seen trailing the P onset by about 8.5 sec, the two way travel time in 6.27 km (20,900 ft) of water.

The S/N ratios vs frequency are best studied in Figure 5 showing the spectral plots. The land signal spectra are instrument noise limited above 3 cps (obtained from LO gain traces). Land reception is again favored over the ocean bottom in terms of S/N by about 5 to 10 db in the 1 to 3 cps band. The ocean-bottom noise power level exceeds the land noise on the horizontal components by about 20 db, which is consistent with previous findings.

The pressure noise spectrum is remarkable in that it covers a range of 40 db in one decade (0.4 - 4 cps) after being shaped by the system response, which is down -13 db at 0.4 cps. Thus the true ambient spectrum ranges at least 53 db in this band. The flattening beyond 4 cps is undoubtedly instrument noise level as the dynamic range per channel is about 42 db. The spikes in the land noise spectra at 5.2 cps are believed cultural. They are present on the majority of Adak noise spectra.

3. New Britain Teleseism, September 9, 1963

The New Britain Teleseism (event 27) was well recorded on all land and ocean-bottom components as shown in Figure 6. The unit was located at map position 22 in 4.6 km (15,300 ft) of water. The P onset on the ocean bottom is out of phase between the pressure and vertical component, and the surface bounce delayed by 6 seconds is clearly visible on the vertical. The associated spectra are shown in Figure 7. The S/N ratio vs frequency favors the Z component on land; however, the horizontals are quite comparable. The

EVENT NO 25

SEPTEMBER 7, 1963

MAG = 5.2 (CGS)

Δ = 2400 KM

LAND SEIS
ON ADAK IS

OCEAN BOTTOM SEIS
6.27 KM DEPTH
SOUTH OF ADAK IS
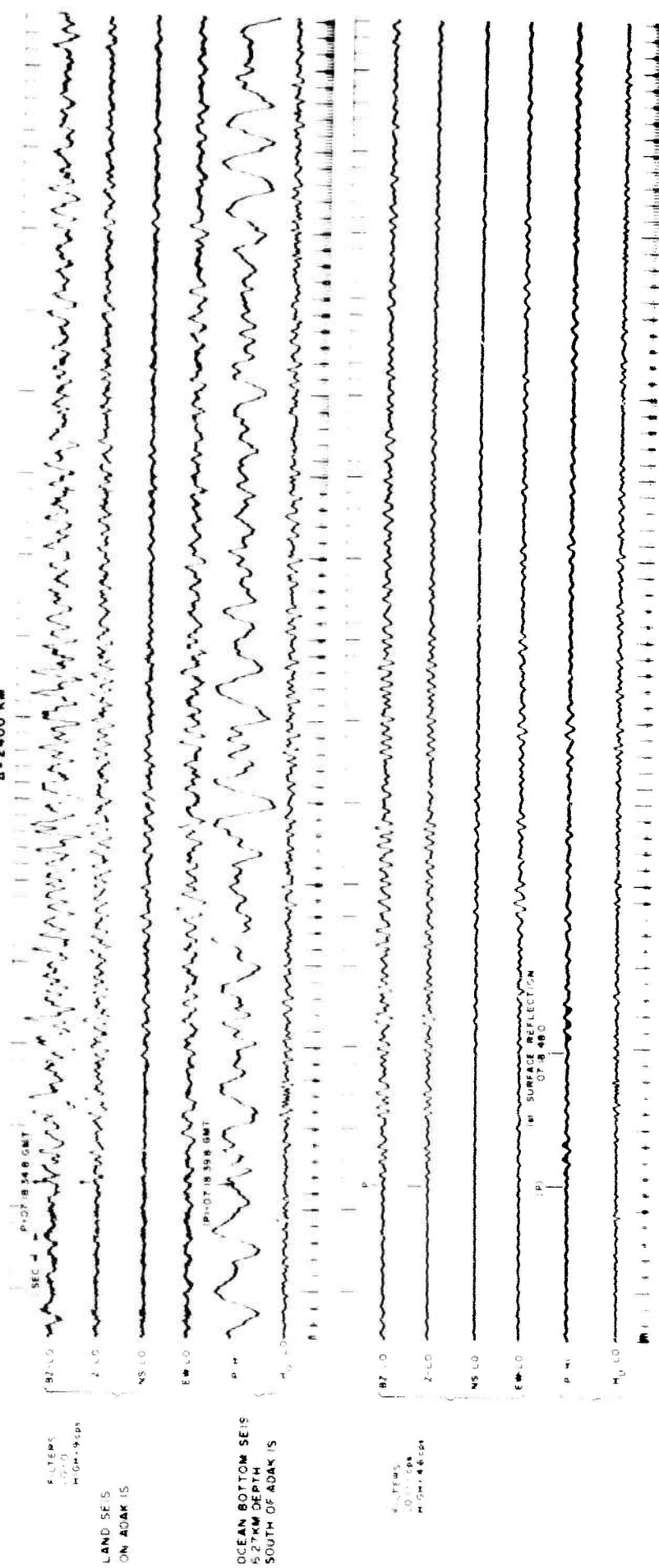
Figure 4. Kurile Teleseism Event No. 25

OCEAN BOTTOM

H_U

LAND

Z

P

NS

INSTRUMENT NOISE

INSTRUMENT NOISE

Frequency (cps)

SEPTEMBER 7, 1963

MAG. = 5.2 (CGS)

Δ   ≈ 2400 KM

LAND SEIS
    ON ADAK ISLAND

OCEAN BOTTOM SEIS.
    6.27 KM DEPTH
    POSITION 19

EW

INSTRUMENT NOISE

Frequency (cps)
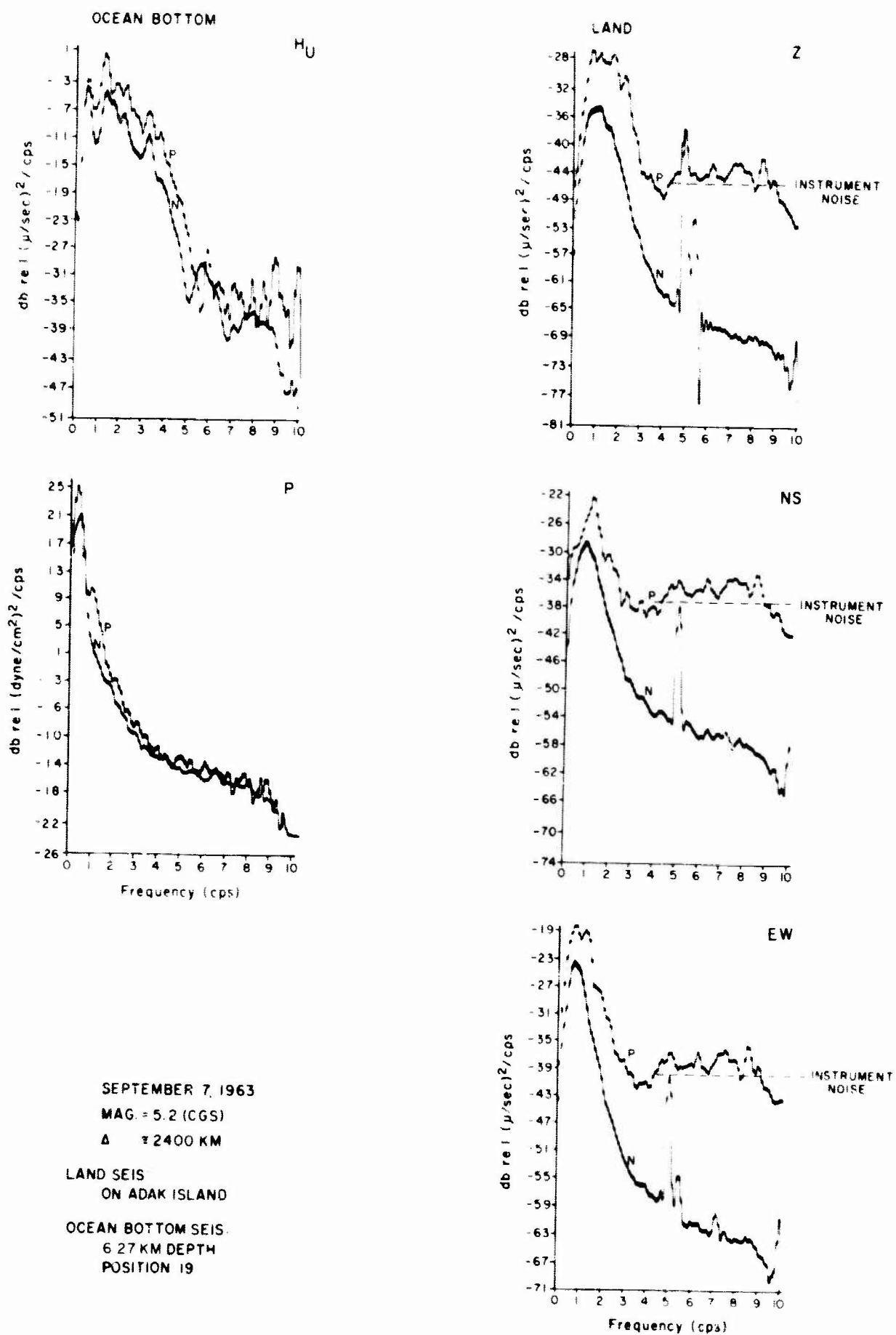
Figure 5.   Kurile Island Event No. 25 Spectra

NEW BRITAIN TELESEISM

EVENT NO. 27

SEPTEMBER 9, 1963
MAG. = 5.6 (CGS)
Δ = 6900 KM, 63°

P = 02 56 03.2 GMT

P = 02 56 01.3 GMT

1 SEC.

FILTERS
LO = 0
HIGH = 9 cps

BZ-LO
Z-LO
NS-LO
EW-LO

LAND SEIS
ON ADAK IS.

P-HI
Z-HI
Mᵤ-LO
Mₗ-LO

OCEAN BOTTOM SEIS.
4.6 KM DEPTH
SOUTH OF ADAK IS.

Figure 6. New Britain Teleseism Event No. 27

16

Figure 7. New Britain Island Area Event No. 27 Spectra

pressure S/N ratio suffers as before for these low frequency signal events. Both signal and noise levels are higher on the ocean bottom. The apparently good S/N ratio on the ocean-bottom Z component between 3 and 10 cps appears to be an instrument or recording difficulty during this time period resulting in the high frequency hash on the Z trace (Figure 6). It is not evident on the other ocean-bottom components. The spectral peak in the ocean-bottom horizontal noise plots at 4 cps is package resonance induced. The signal arrival excites this peak but not to the extent that the horizontal data is unusable.

4. Near Regional Event, August 22, 1963

Event 3 recorded at map position 4 in 3.49 km (11,600 ft) of water is presented in Figure 8. The ocean-bottom H_L component was not operative. The approximate hypocenter location shown also in Figure 1 gives a distance of 290 km and 220 km to the ocean-bottom and land stations respectively. One significant difference between the seismograms is the simple P coda on the ocean bottom relative to that on land. Except for the distinct, well-defined surface reflection on the pre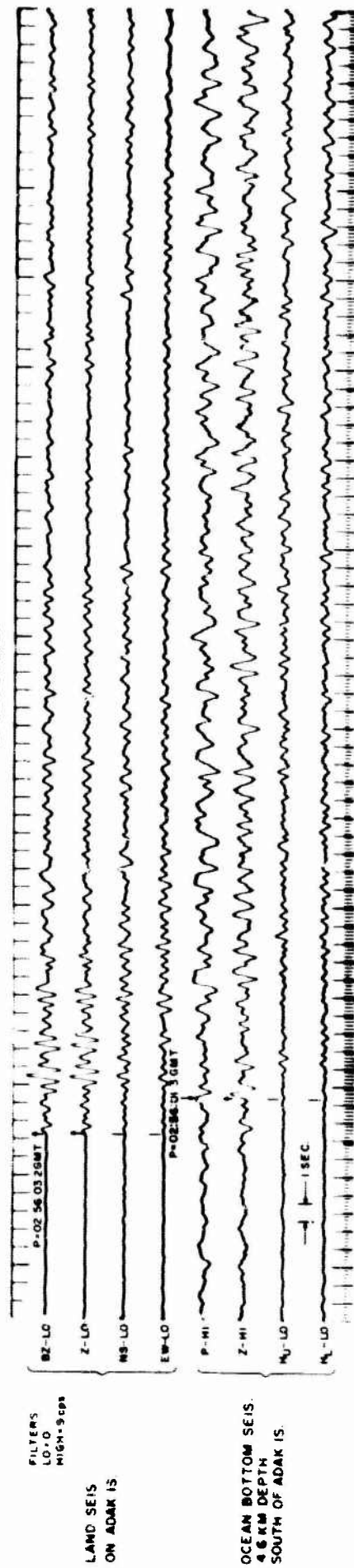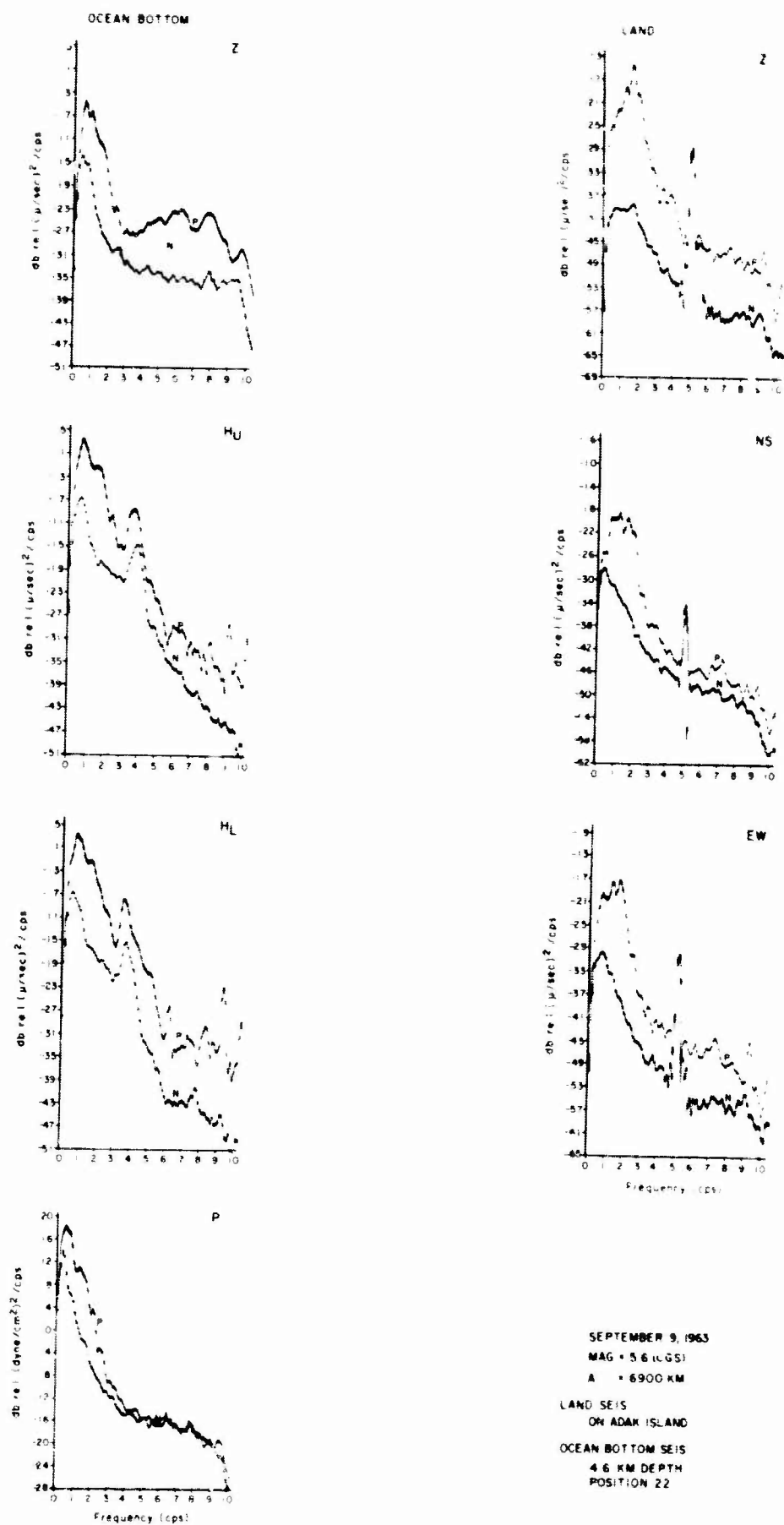ssure and vertical traces, there is little activity between the P onset and the S phase. In addition, the frequency content of the event appears decidedly higher on the ocean bottom than land. Both stations show a well developed S phase.

The spectral plots for event 3 are shown in Figure 9. In this case, S/N ratio favors the ocean-bottom Z over the land Z component though the difference is small. The plots are not corrected for difference in range, which (assuming the refracted phases decay as $(\frac{1}{r^2})$ would increase the ocean-bottom signal-to-noise ratio by $\left(\frac{290}{220}\right)^2$ = 4.8 db. As before, the signal and noise levels are greater on the ocean bottom. Both the ocean-bottom vertical and pressure display richer high frequency content than the land components; for instance, the difference in vertical signal spectrum level between 2 and 7 cps is -3 db and -10 db on the ocean bottom and land respectively. The pressure P spectrum has a maximum at 8.5 cps. The ocean-bottom horizontal H_u component is severly corrupted by package resonance at 4 cps. Another "line" at 6 cps appears on all the ocean-bottom noise components as well as the land noise spectra. This line very likely is instrumental and may have been introduced during transcription of the FM-to-digital tapes. The sudden drop-off of energy above 9 cps in these plots and the previous ones is due to the aliase filters employed in transcription.

5. Near Regional Event, August 26, 1963

Event 9A recorded at map position 9 north of the Aleutian chain in 3.73 km (12,400 ft) of water is shown in Figure 10. The hypocenter in Figure 1 gives an approximate distance of 312 km to the ocean-bottom unit
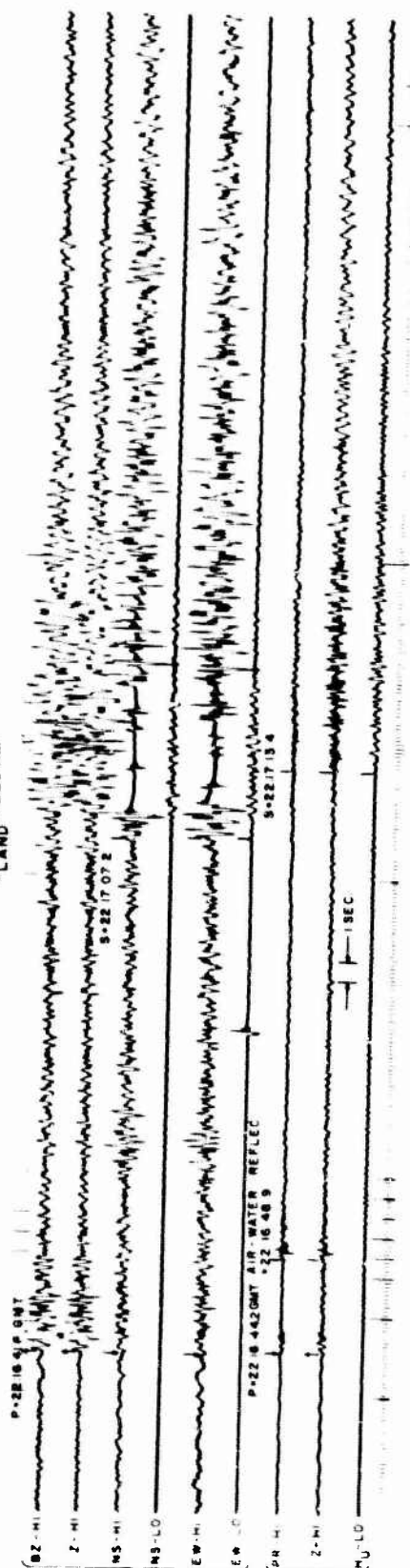
Figure 8. Near Regional Event No. 3
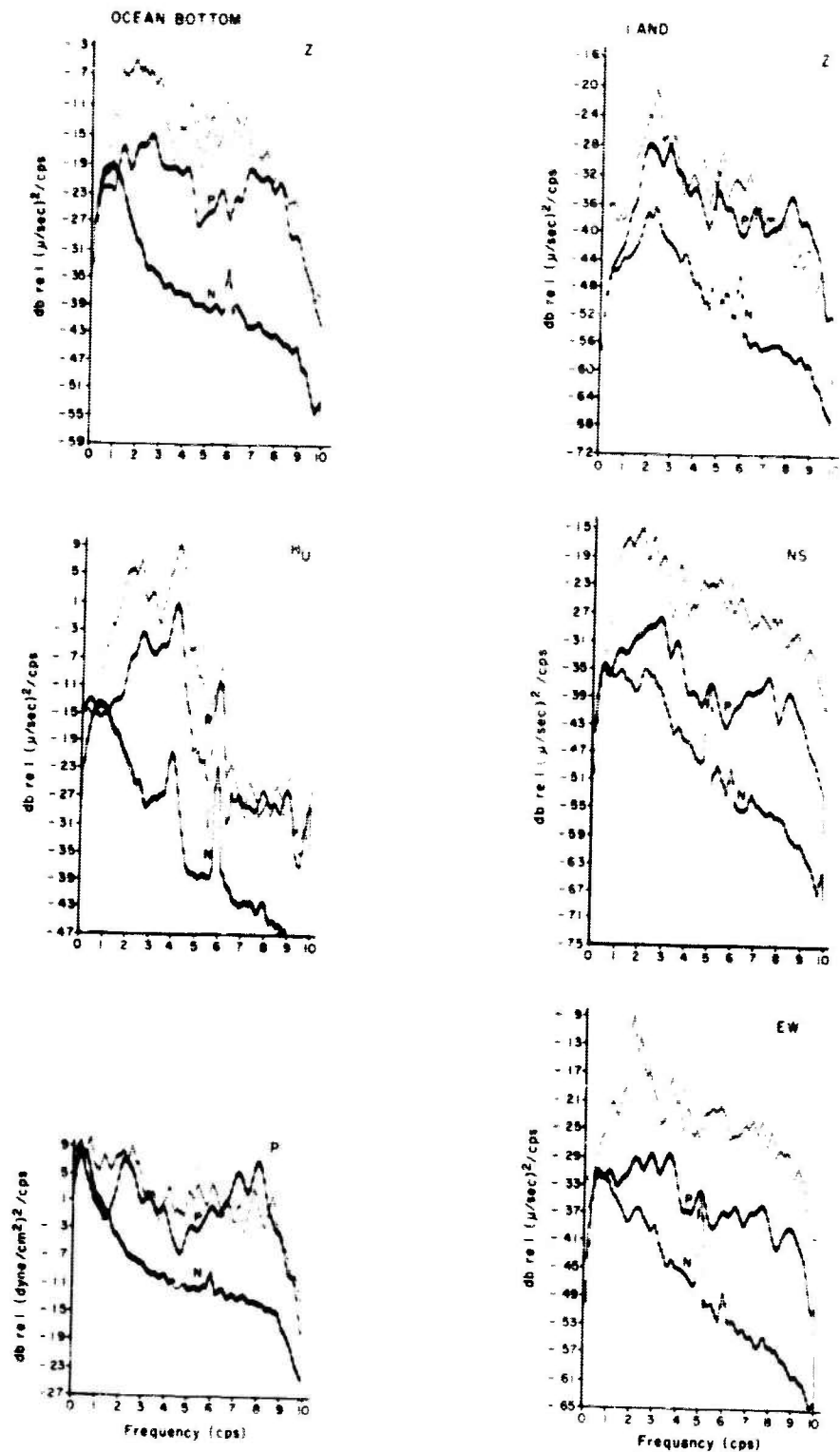
19

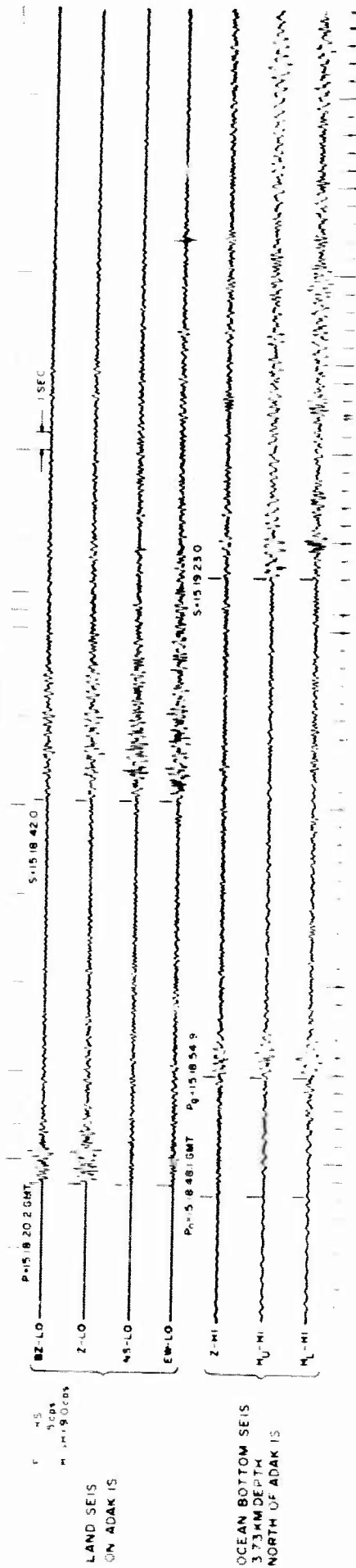Figure 9. Near Regional Event No. 3 Spectra

Figure 10. Near Regional Event No. 9A

and 180 km to the land station. The ocean-bottom path is completely north
of the chain, whereas the path to the land station parallels the island arc.
The pressure component was inoperative for this drop. The P onset on land
is considerably larger than on the ocean bottom. Both stations show a well
developed S phase, and P_g is distinct and well developed on the ocean bottom
but apparently not on land. Considering the difference in distance and possibly
crustal structure over the two paths, it is likely that P_n and P_g arrive close
together on land, thus accounting for the large onset. There does not appear
to be a significant difference in frequency content on land and the ocean bottom
for this event

The spectral plots for event 9A in Figure 11 show S/N ratio vs
frequency favoring the land on all components. The range correction would
add about $\left(\frac{312}{180}\right)^2 \cong 10$ db to the ocean-bottom S/N ratio, improving matters
somewhat but still leaving the ocean-bottom S/N ratio about 6 db below the
land S/N ratio for this event. The noise level is higher on the ocean bottom as
usual, but the signal levels are approximately equal when corrected to the
same range. The ocean bottom ambient spectra do not appear to be limited by
instrument noise on this drop, as evidenced by the continual drop in level
with increasing frequency. The vertical noise spectrum varies by 30 db in the
1 to 9 cps band while the horizontals range 40 db. The land noise spectra show
a peak at about 2.4 cps which does not appear on the ocean bottom.

6. Near Regional Event, August 30, 1963

Figure 12 shows event 18 recorded at map position 13 south of
the chain in 4.1 km (13,640 ft) of water. The hypocenter, located at the right
edge of the figure, is equidistant from the two stations at 366 km. The ocean-
bottom horizontal components were not analyzed because of severe resonance.

The most outstanding difference between the land and ocean-
bottom seismograms is the high level of activity in the P-S interval on the
ocean-bottom, relative to land. This represents the opposite situation from
event 3 with the simple ocean-bottom P coda. The P_g phase appears well
developed on land, but no distinct phases emerge on the ocean bottom until S,
which is well developed at both stations on the velocity components. The
filtered record on the bottom half of Figure 12 shows that the ocean-bottom
signal arrival is richer in high frequencies than the land signal. This is best
seen in the spectral plots of Figure 13.

The S/N ratio vs frequency on the vertical components are
approximately equal for this event in the 2 to 7 cps band. The signal levels
are also comparable at the low frequencies but diverge with increasing
frequency. The mean spectral level at about 7 cps on the ocean bottom is
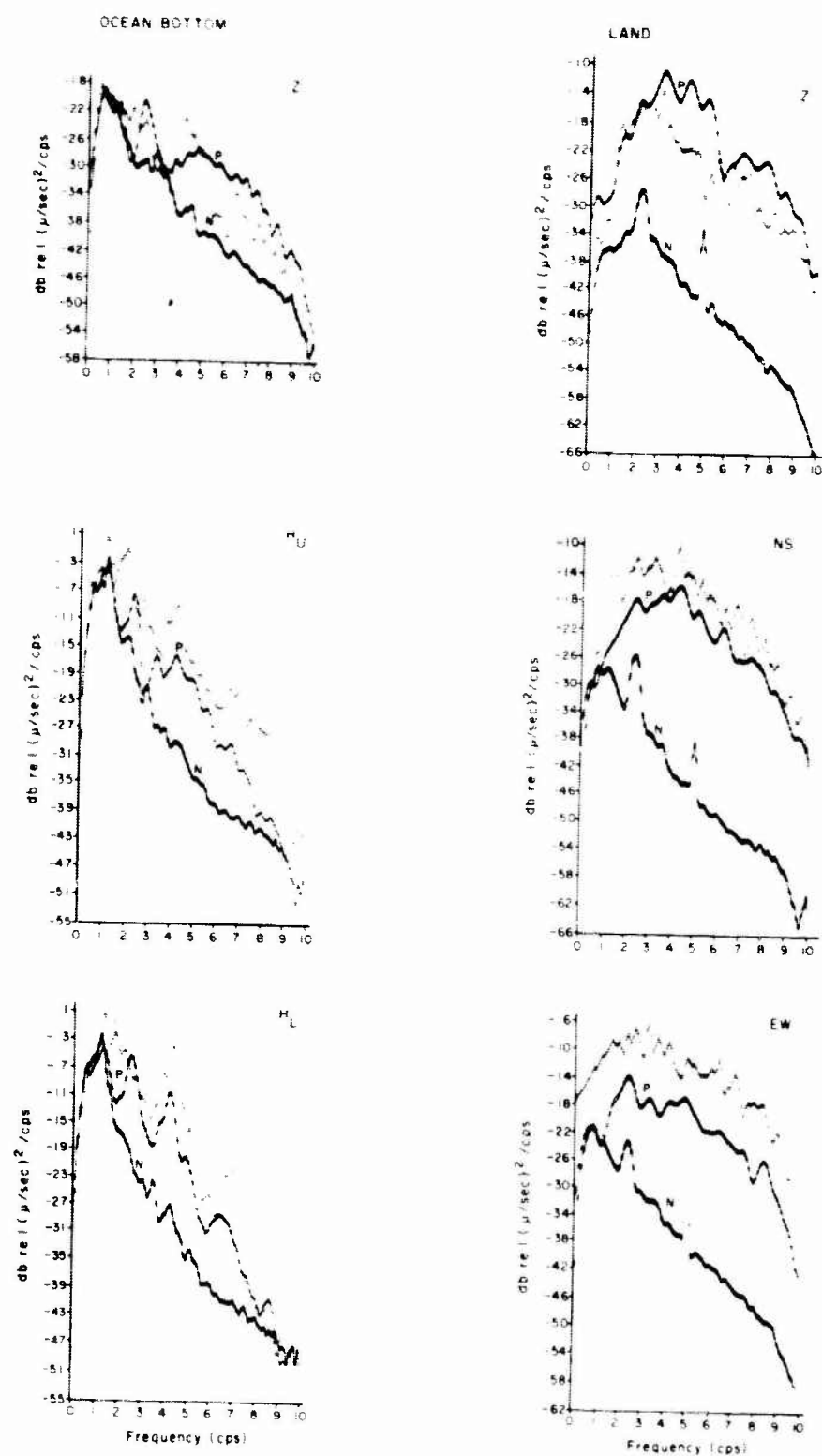
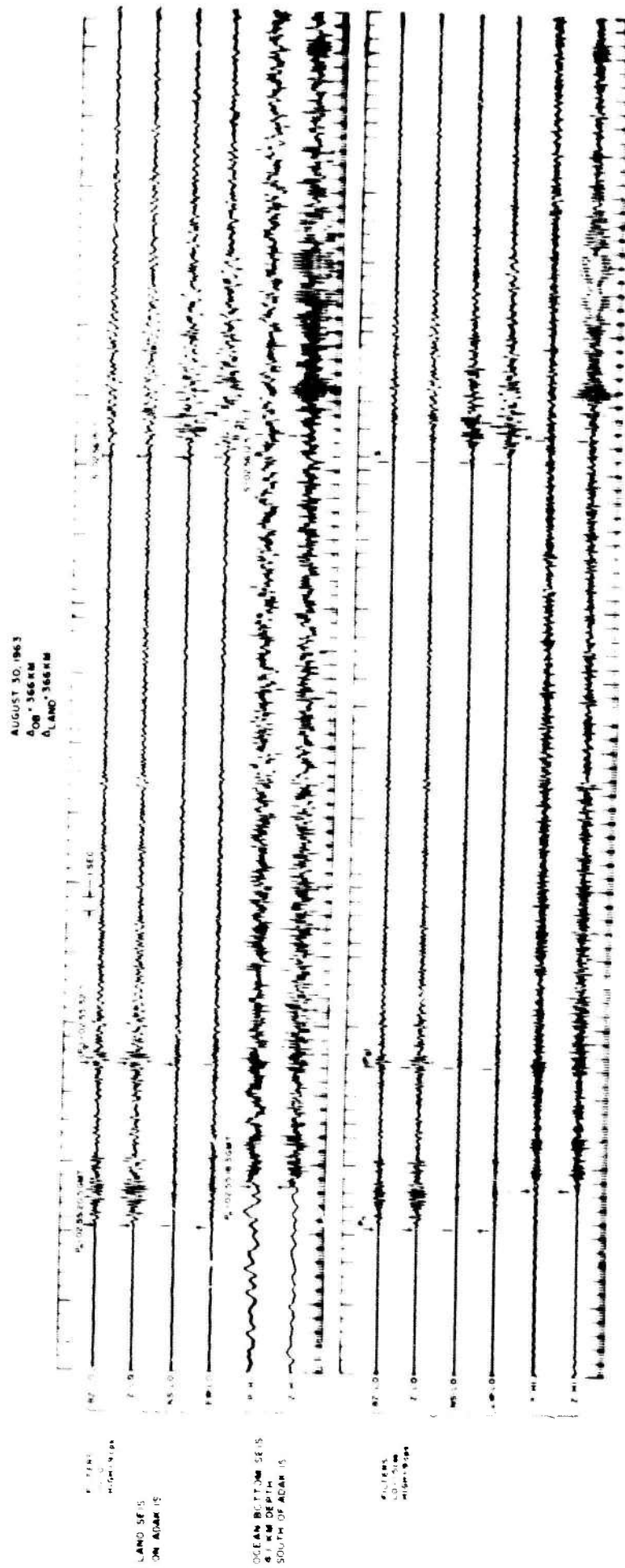Figure 11. Near Regional Event No. 9A Spectra
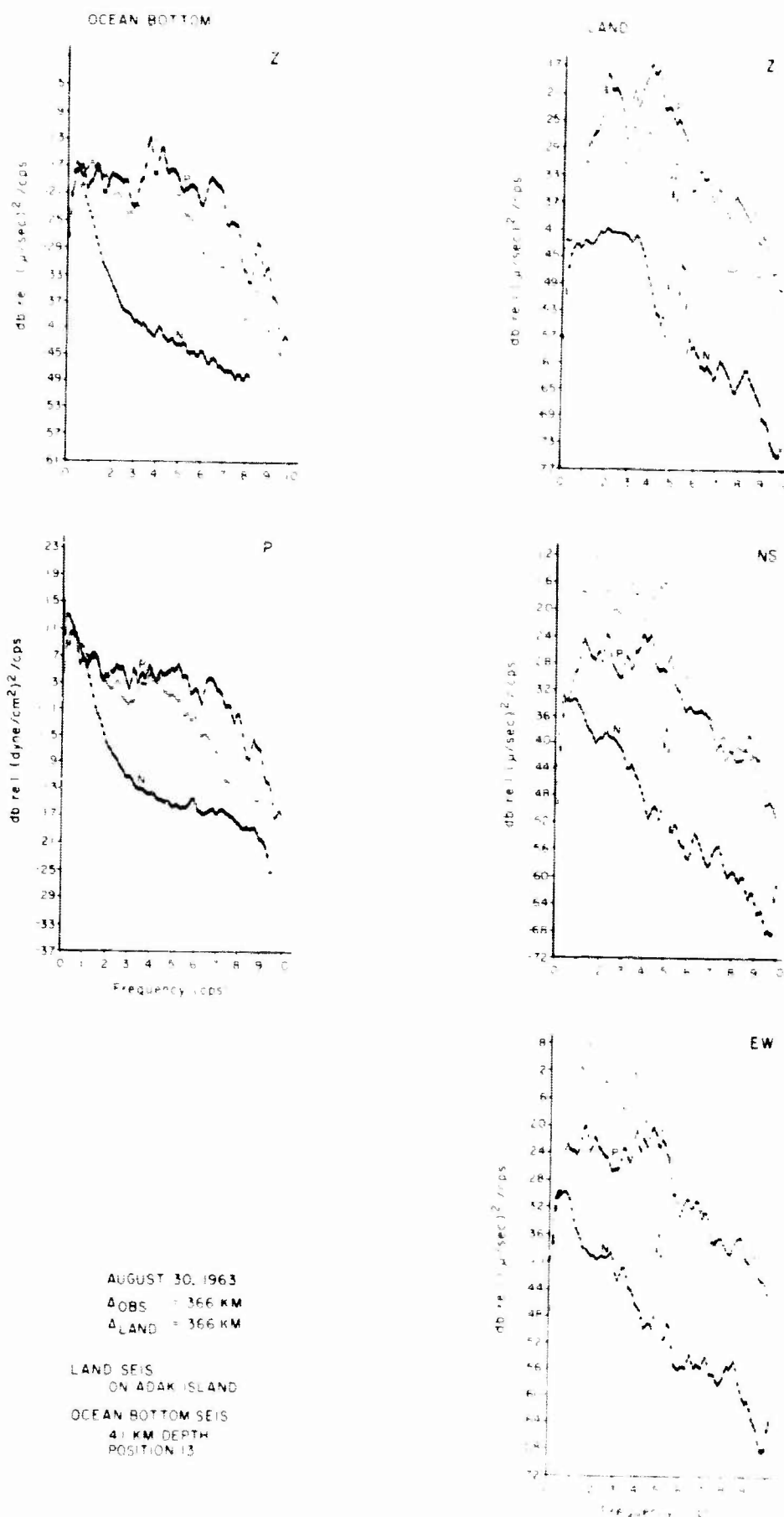
Figure 12. Near Regional Event No. 18

Figure 13.   Near Regional Event No. 18 Spectra

down only a few db from its value at 2 cps, whereas the signal at 7 cps on land is attenuated about -20 db relative to its value at 2 cps. The flatness of the ocean-bottom signal spectrum is even more impressive on the pressure component for the P phase; however, the S/N ratio is not as good. As noted before, the ocean bottom and Adak microseismic background noise spectra do not agree in either shape or level. The broad noise plateau between 0.5 and 4 cps on Adak is decidedly atypical for land stations. In fact, the ocean-bottom vertical noise plot resembles "an average" continental noise spectrum more closely than does the land.

7. Near Regional Event, September 9, 1963

Figure 14 shows the seismograms for event 28 recorded at map position 22 in 4.6 km (15,300 ft) of water south of the Aleutian chain. Again the ocean-bottom horizontals were not analyzed due to resonance problems. The hypocenter is located south of ATKA Island approximately 200 km from the bottom site and 220 km from the land site. The P onset is somewhat better defined on the ocean bottom with the higher frequency wavelet and pressure-vertical out-of-phase relationship. The ocean-bottom traces again exhibit a uniform high level of activity after P onset which persists well after the S phase has decayed on land. No distinct S phase is visible on the ocean-bottom pressure or vertical, save for a signal envelope change at about the correct time. The horizontal components definitely help the land record in this regard. The S phase manifests itself on the land vertical also as a gentle envelope change.

The spectra for event 23 are presented in Figure 15. Clearly the land components have a decided S/N ratio advantage for this event. The small range correction alters the relative S/N by only 2 db. The signal levels on the vertical components are approximately equal in the 2-4 cps band, but as before the land shows more attenuation with increasing frequency than the ocean bottom shows for the P phase. The S phases are approximately the same level at both stations, and attenuate with frequency at the same rate.

8. Local Event, August 30, 1963

The first of several local events selected for analysis is shown in Figure 16. Event 14 was recorded at map position 13 in 4.1 km (13,650 ft) of water. Package resonance corrupted the horizontal components. All channels displayed in the figure are from low gain traces on which the ambient is below instrument noise. The ocean-bottom pressure and vertical traces show a relatively simple P coda. The signal on both records is equally broad band. Clipping occurred on the land S phases; consequently, they are not displayed in the spectral plots of Figure 17. Both the ocean bottom and land recordings of event 14 show rather amazing S/N ratios, with the land being favored by about 10 db. The signal spectra are essentially flat in the 1 to 9 cps band on the ocean bottom and nearly so on land. In addition, the signal levels at the two stations are nearly equal.
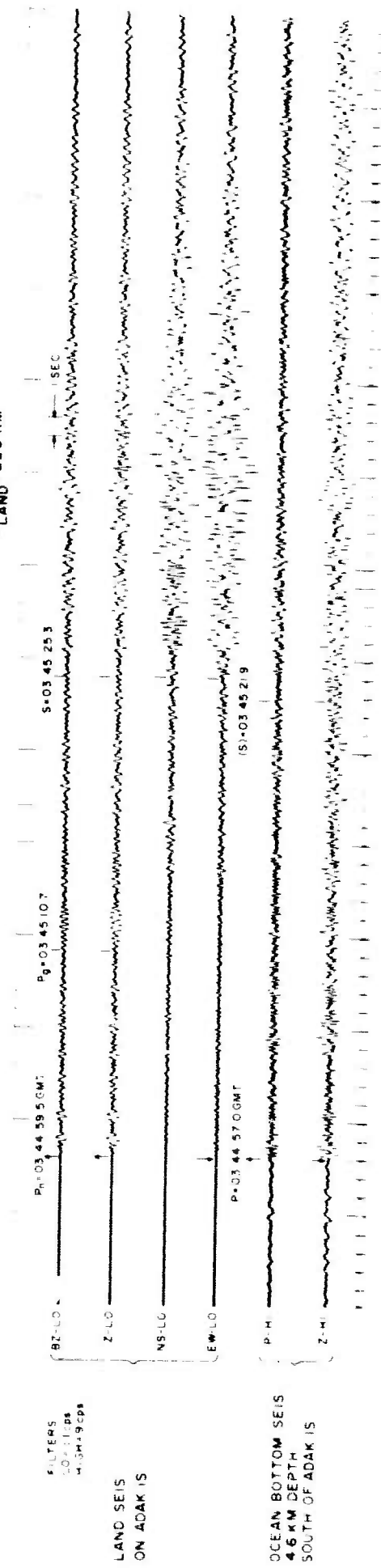
Figure 14. Near Regional Event No. 28

27

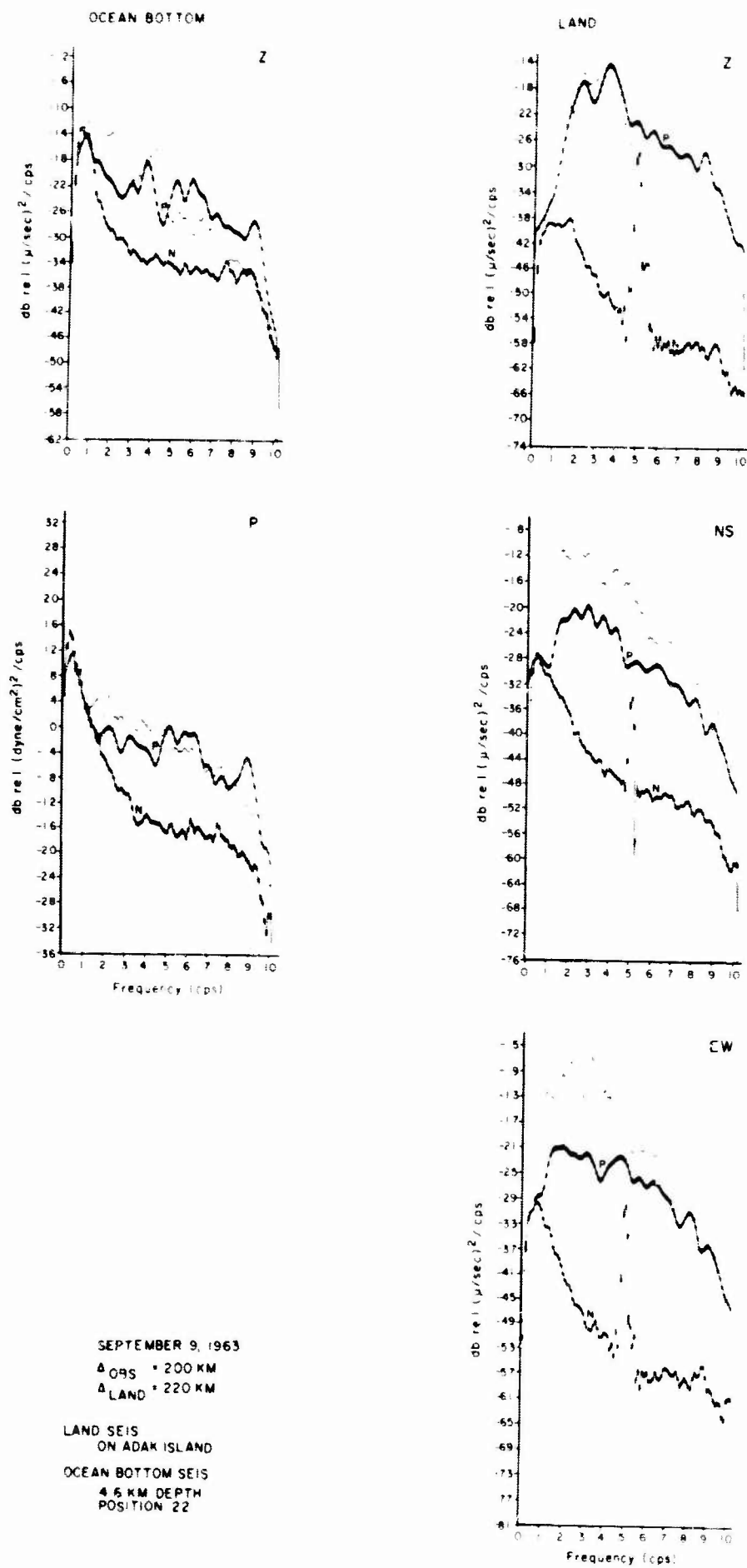Figure 15.　Near Regional Event No. 28 Spectra

AUGUST 30, 1963

$\Delta_{OB} = 50$ KM
$\Delta_{LAND} = 60$ KM
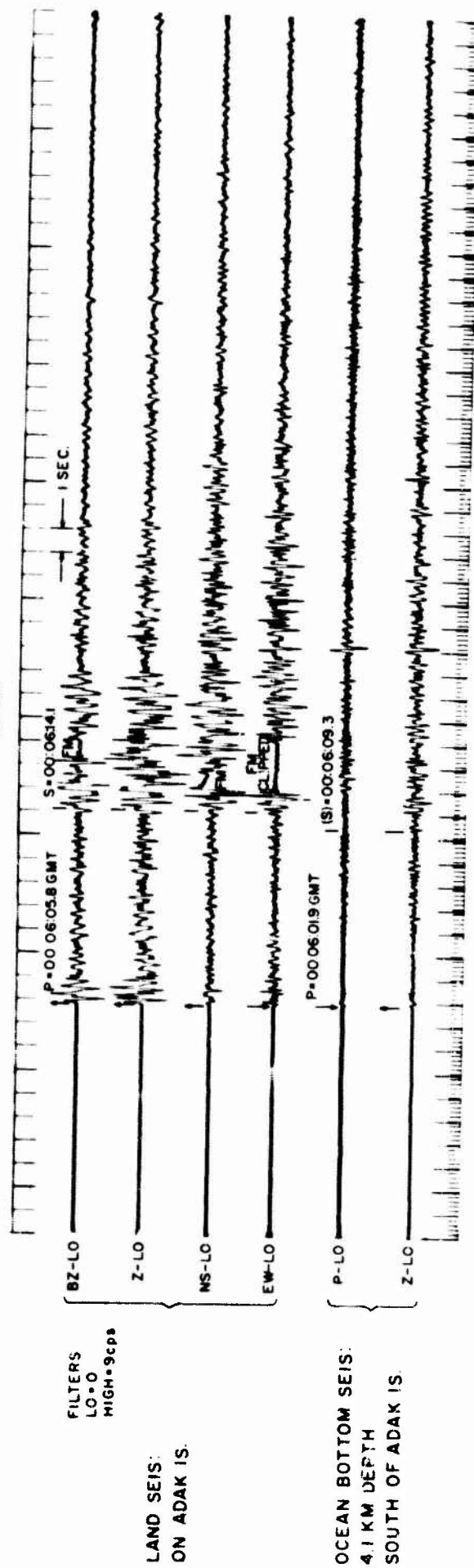
Figure 16.   Local Event No. 14

29

Figure 17.   Local Event No. 14 Spectra

9. Local Event, September 9, 1963

Local event 26 recorded at map position 22 south of the chain in 4.6 km (15,300 ft) of water is shown in Figure 18 for all the land components, and pressure and vertical on the ocean bottom. The hypocenter (Figure 1) is approximately 70 km from ocean-bottom position 22 and 100 km from the Adak land site. The P onset is well developed at both stations, and a later P phase is identified on the ocean-bottom record by the pressure-vertical out-of-phase relationship. The latter is not evident on land. The S phase is strong and distinct at both sites with the major difference that the ocean bottom record continues on well after the land S phase has decayed. The T phase or water arrival from the shock should appear about 30-40 seconds after the P phase. Although there is no clear onset, much of the later activity could be the result of T energy.

The spectra for event 26 are shown in Figure 19. Again S/N favors the land vertical by about 20 db for the P phase when the distance correction is applied. Some ambiguity is involved here in the signal-to-noise comparisons because of instrument noise. The ocean-bottom noise was not as well modulated as the land. Very probably much of the ocean-bottom noise above 2 or 3 cps is in fact instrument noise, at least for the Aleutian data. Attempts were made to obtain better modulated noise in the Hawaii and California drops.

Finally, the P phase signal levels at the two stations are in close agreement.

10. Local Event, September 1, 1963

Event 30 was recorded at position 16 (Figure 1) in 5.26 km (16,000 ft) of water. Only the pressure component was operative on this drop. The hypocenter (Figure 1) is approximately 110 km from the land site and 350 km from ocean-bottom position 16. Both the land and ocean-bottom records (Figure 20) are equally broad band and show distinct P energy onset. The pressure trace has a uniform level of arrivals after P with no distinct later phases other than the surface reflection. This is best seen on the filtered record in the lower half of Figure 20. The land shows a well developed energetic S phase, and otherwise conventional looking seismogram. Spectral plots for event 30, Figure 21, indicate the S/N ratios on land to be about 30 db better than on pressure. The distance correction $\left(\frac{350}{110}\right)^2 = 20$ db reduces the land advantage to about 10 db over the ocean-bottom pressure. One can infer from previous examples that the S/N ratio on the ocean-bottom vertical, had it been recorded, would have been 5 to 10 db poorer than land for this event.
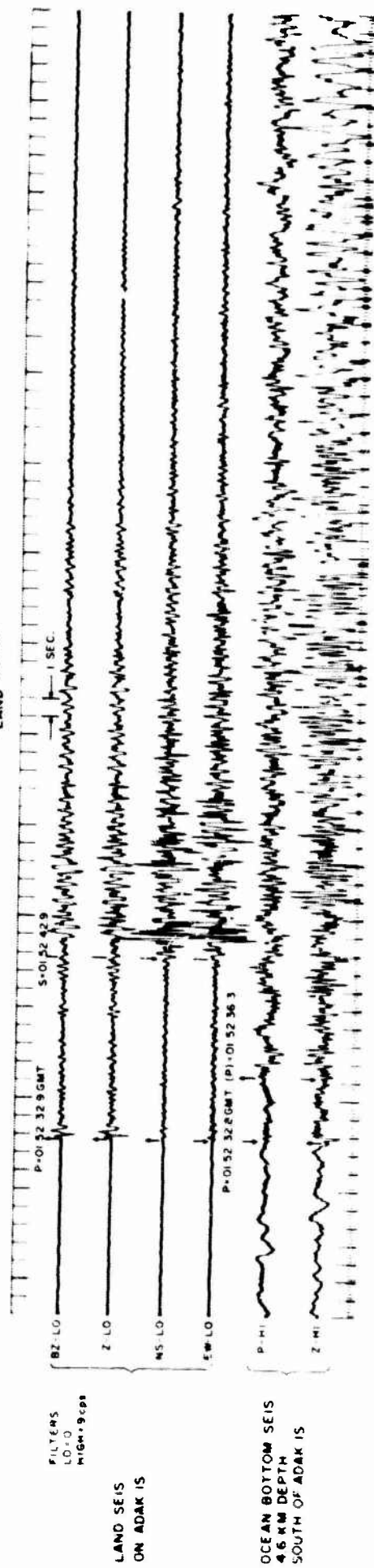
Figure 18. Local Event No. 2b

32
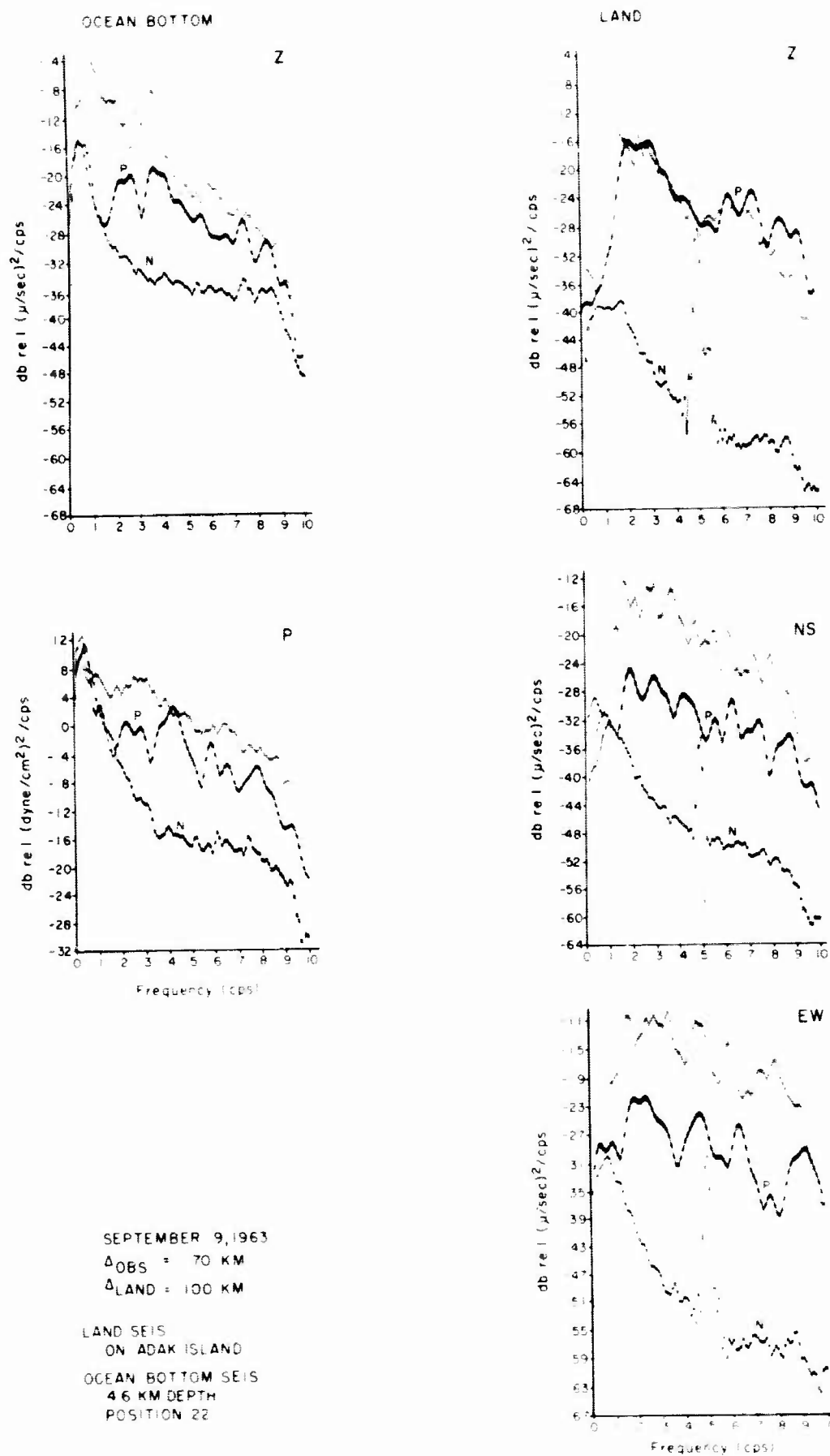
Figure 19. Local Event No. 26 Spectra

Figure 20.   Local Event No. 30

34

OCEAN BOTTOM

LAND

NORTH OF TANAGA
ISLAND, ALEUTIAN ISLANDS

H ≅ 22 48 GMT,
SEPTEMBER 1, 1963

△ LAND ≅ 110 KM
△ OBS ≅ 340 KM

LAND SEIS
ON ADAK ISLAND

OCEAN BOTTOM SEIS
5 26 KM DEPTH
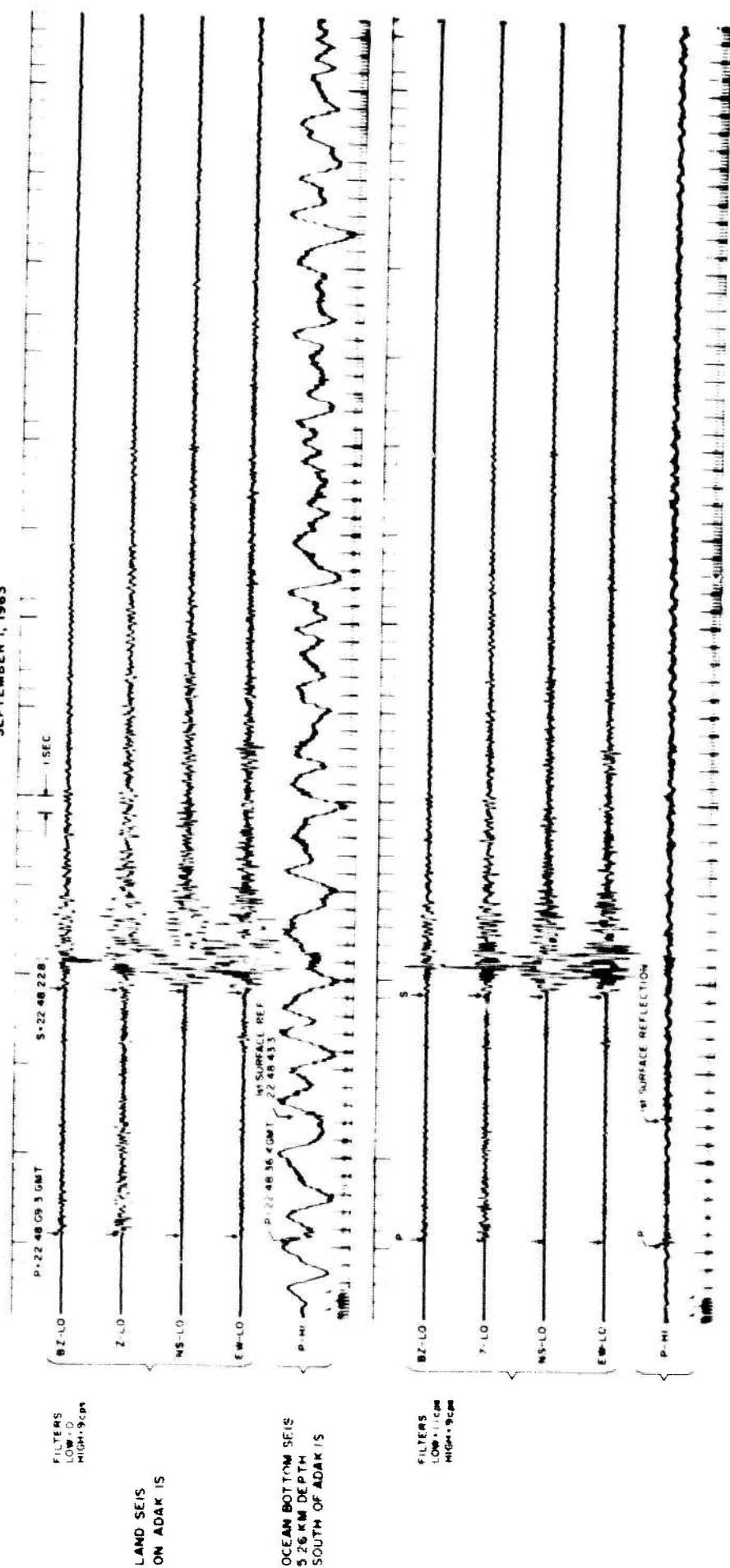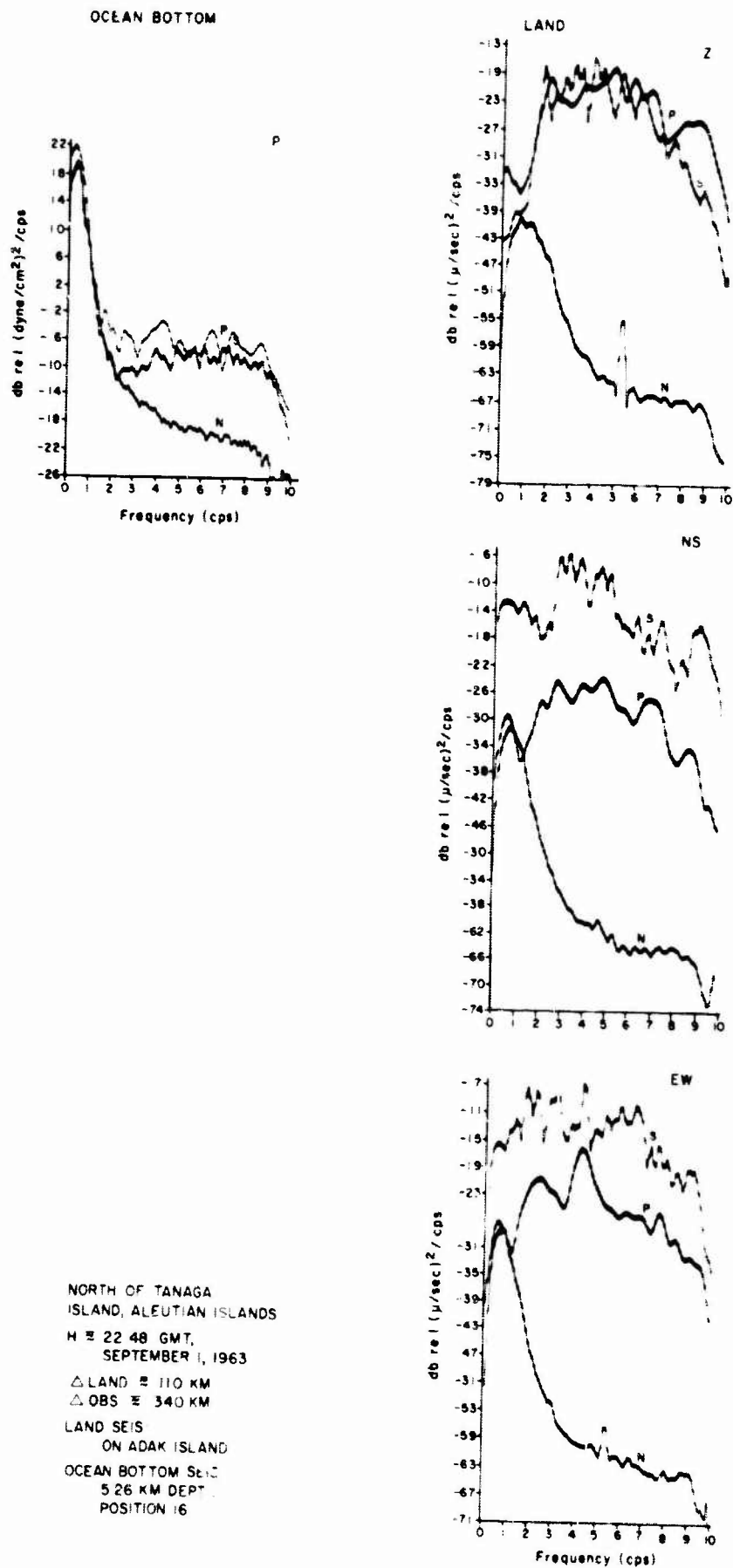POSITION 16

Figure 21.   Local Event No. 30 Spectra

It is significant to note that the pressure signal spectra are "whiter" than the land in spite of the 3 to 1 difference in hypocenter to station range. The implication is that ocean-bottom recording preserves the high frequency signal energy better than land recording, at least in the Aleutians.

11. Summary of Aleutian Signal and Noise Analysis

a. Teleseisms

Of the four teleseisms recorded in the Aleutians, two were recorded only on the ocean-bottom pressure; one, on the pressure and H_u component; and one, on all the ocean-bottom components. The land station recorded all four on all components. The signal events are all low frequency, being confined to the 1 to 4 cps band. The S/N ratios vs frequency favor the land station by about 5 to 10 db except for the horizontal components of event 27 which are comparable.

The ocean-bottom signal levels on the velocity components range 15 to 20 db greater than the corresponding land spectra. This apparent magnification of teleseismic signals on the ocean bottom was observed previously for a magnitude 5.1 shock from Java recorded on August 30, 1963, in the Aleutians at position 13 (Collection and Analysis of Pacific Ocean-Bottom Seismic Data).

b. Near Regional and Local Shocks

The several near-regional and local shocks selected for analysis, range in hypocentral distance from 50 to 360 km. Visual interpretation of the seismograms reveals that the normal P and S phases are present on both ocean-bottom and land records (when ocean-bottom vertical and horizontals are displayed). For two events the ocean-bottom P-S interval appears less complicated than the land (3 and 14), while for other events the converse is true (18, 23 and 26). Arrivals which are present on the ocean bottom and not land are, of course, the water-air reflections and the direct water arrival or T-phase. The latter probably accounts for the duration of event 26 on the ocean bottom relative to land. No consistent differences in phase development or definition, other than the above mentioned, have been observed.

The S/N ratio comparison for these seven events favor the ocean bottom once (event 3), the land five times (events 9A, 28, 14, 26, and 30), and one approximate tie (event 18). Not enough data is available to determine if there are differences in ocean-bottom signal reception north and south of the chain. No significant pattern suggests itself from the signal-to-noise comparison in terms of either hypocenter location or ocean-bottom seismometer location.

The signal spectra on the vertical components are approximately equal in level when corrected to the same hypocentral distance (except event 3 which shows ocean-bottom magnification) though they differ substantially in detail. Recall the teleseisms showed ocean-bottom magnification of 15 to 20 db. It is not clear why the magnification should be dependent on the distance, unless the angle of incidence of the event is a critical factor.

Preservation of high frequency signal information for local, near-regional and possibly regional events does appear to be a consequence of ocean-bottom recording as evidenced by comparisons of the ocean bottom and land vertical P phase spectra for the several events analyzed.

c. Aleutian Ambient Noise

The ambient noise spectra on both the ocean bottom and land show relatively little fluctuation from day to day at the low frequency end (0.2-1 cps) where they differ in level by about 25 db. At the higher frequencies f > 2 cps, the spectra are more variable, particularly on the ocean bottom. We do not place much confidence in the ocean-bottom noise above 2 to 3 cps because of the low modulation level in most of the Aleutian ocean-bottom recordings. More complete statistics on the variations of the noise are presented in Section III of this report.

B. HAWAII DROPS

The location of the 13 drops east and west of the Island of Hawaii are shown in Figure 22. The land station (19°39'N, 156°00'18W) was located approximately 5 miles from the town of Kailua, Kona, and 1 mile from the coast. The proximity of the land site to the coast appears to have resulted in a land noise spectrum unusually rich in frequencies above 2 cps.

During the several Hawaii drops, three teleseisms from the Kurile Islands (one of magnitude 8) and numerous local shocks were recorded. As of this date none of the latter have been located, thereby lessening their usefulness as pertains to signal-to-noise ratio comparison. None-the-less a number of these local shocks have been included in the analysis in the firm belief that any data relating to ocean-bottom seismicity is better than none.

1. Kurile Teleseisms of October 12, 13 and 20, 1963

The three teleseisms originating from the Kurile Islands and recorded on the Hawaii land and ocean-bottom sites 10, 11 and 16 are shown in Figure 23. Event 46 was recorded at 4.91 km (16,400 ft) depth, and event 44 and 52 at 4.02 km (13,400 ft) and 2.02 km (6720 ft), respectively. All components on the ocean bottom and land were operative on these drops.
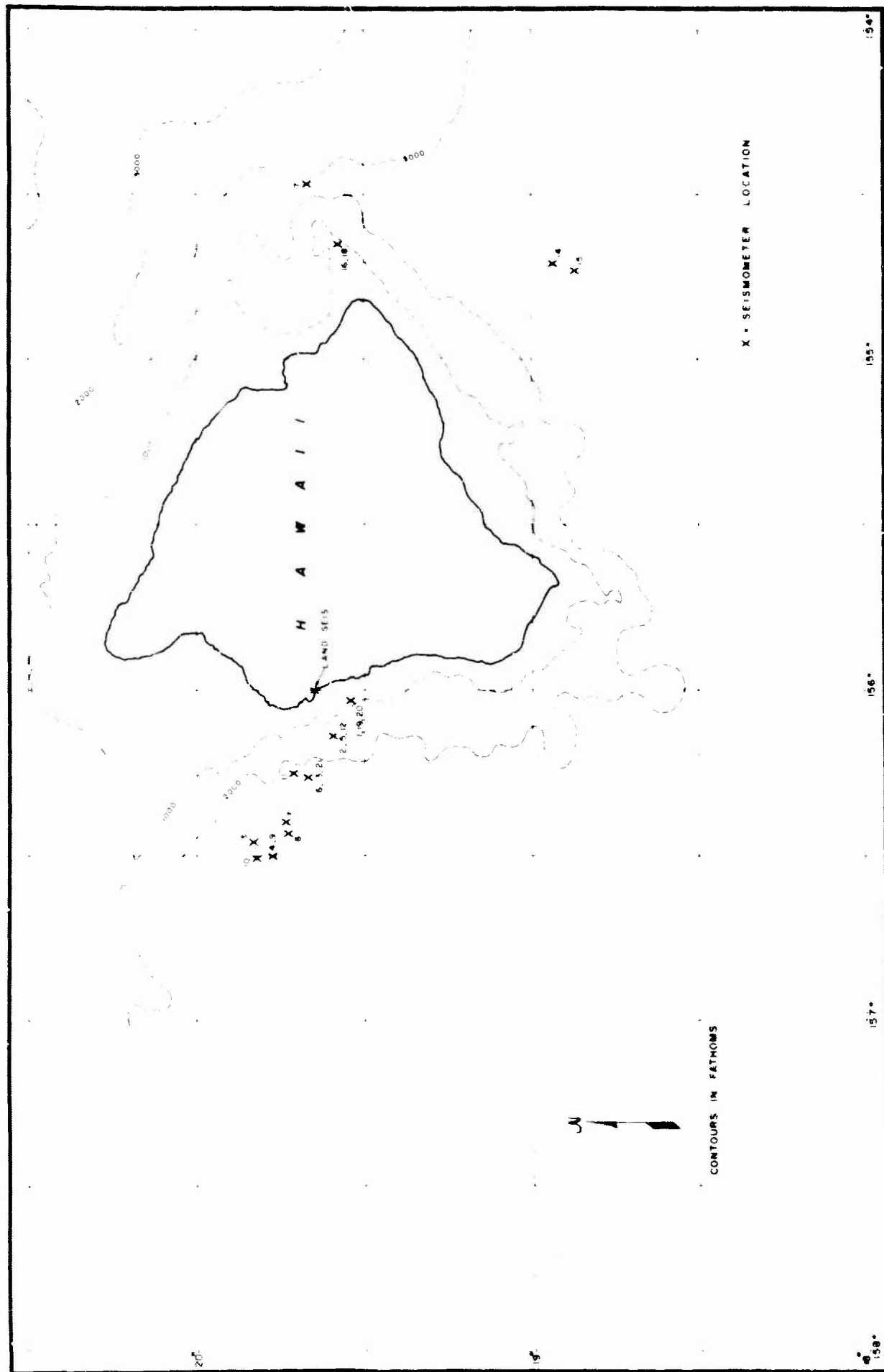
Figure 22. Hawaii Drops Instrument Locations

Figure 23. Kurile Island Teleseismic Events No. 46, 44 and 52

The onset for event 46 is poorly defined on land and somewhat less so on the ocean-bottom. The high frequency energy in the vicinity of the P pick on land is actually part of the ambient, and not the signal. Similar energy bursts can be seen up and down the record both preceding and following the event. A gradual build up in energy is evident, particularly on the ocean bottom with clipping of the high gain channels occuring about 16 seconds after the P onset. The signal and average noise spectra for event 46 are shown in Figure 24.

The S/N ratios vs frequency for the event are nearly equal on the ocean-bottom and land for all components up to 1.5 cps. Above this frequency the ocean-bottom is favored. The flattening of the signal spectra on the ocean bottom for f > 3 cps is the result of instrument or tape noise on the Lo gain traces which were analyzed. There is an approximate 20 db magnification of the signal level on the ocean bottom at 1 cps (a consistent finding for all teleseismic events). The noise levels also differ substantially in both spectral shape and level. The broad noise peak at 2 cps on land is believed due to surf noise. It is present on all the Hawaii noise records at nearly the same level. The possibility of instrument noise is ruled out since the coherence between the land Benioff vertical and vertical component have been computed. The latter is near unity over the entire band of 0.2 to 7.5 cps. In addition, the cross-correlation between horizontals indicate that the noise field is strongly directional (f > 1 cps) coming from the northwest. The difference between ocean bottom and land noise levels at the microseismic peak is about 15 db. This difference diminishes with increasing frequency until a cross-over is reached at about 2 cps beyond which the bottom site is quieter.

The seismograms for event 44 (reference Figure 23) show significantly better signal-to-noise ratios for this very energetic magnitude 8 teleseism than for the previous event 46. The pressure - vertical velocity out-of-phase relationship is visible at the onset, but as for 46, the first arrival on land appears to be lost in the noise; it is not to be associated with the high frequency burst of ambient. Figure 25 shows the spectral plots for event 44. The S/N ratios are slightly better on the ocean-bottom for all components above 0.5 cps. In particular, the land signal level falls below the noise at about 2 cps, while the ocean-bottom shows excess signal up to at least 3 cps. The abrupt flattening of the signal spectrum at about 3 cps on the ocean bottom is similar to event 46 and results from instrument noise. The "bottom clipping" of the pressure signal spectrum results from having exceeded the dynamic range of the plotter. The two peaks in the ocean-bottom horizontal noise spectra at 3.2 and 3.8 cps are package resonance induced. They appear on the vertical to a lesser degree. The noise levels on the ocean bottom are greater than on land by as much as 15 db at low frequencies, but above 2 cps the ocean bottom becomes the quieter of the two stations. The signal level is amplified by about 10 db for this teleseismic event as compared to 20 db for event 46.
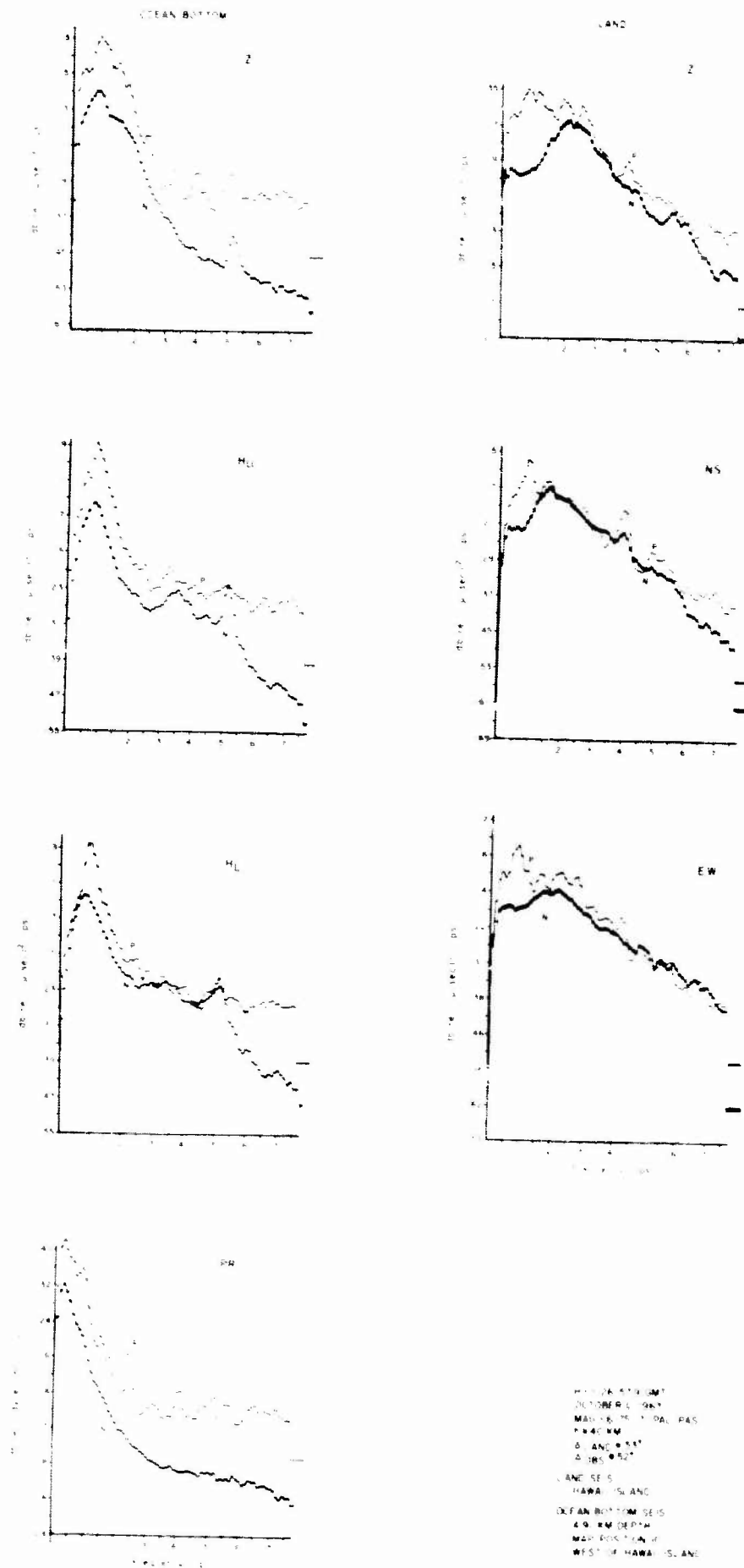
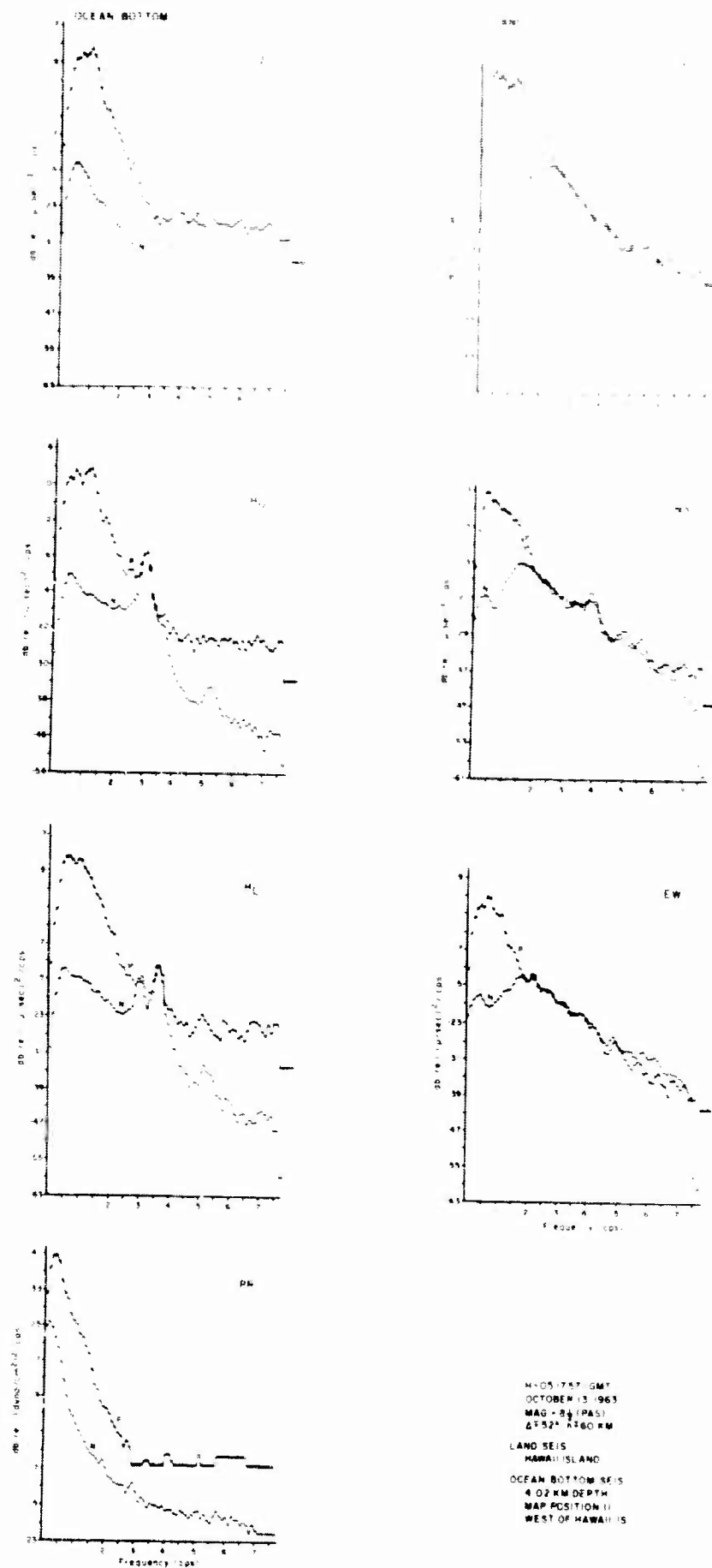Figure 24. Kurile Island Region Event No. 46 Spectra

Figure 25.   Kurile Island Region Event No. 44 Spectra

The seismograms for event 52 (also shown in Figure 23) are very similar in appearance to those for event 46. The onset is poorly defined on both the ocean bottom and land, but the event does build up with time. The horizontals on this drop are more seriously corrupted by resonance as is evident in the spectral plots of Figure 26. The S/N ratios are about equal on the vertical components but favor the ocean-bottom horizontal and pressure over the land by several db. Again, the signal energy is confined to frequencies below 2 cps, and the signal level difference between vertical components favors ocean-bottom reception by 10 db for this teleseism also.

The ambient noise spectra on all components (except for ocean bottom horizontal resonances) are quite stationary, particularly on land, for these three days showing consistent spectral shapes, and minor level changes.

The remaining events analyzed from the Hawaii data pertain to unlocated local shocks characterized by short P to S intervals (5 to 10 sec), and broadband energy content.

2. Local Event 39

Figure 27 shows the seismogram for event 39 recorded at map position 5 in 2.76 km (9190 ft) of water. Only the pressure component on the ocean bottom was operative on this drop. Both the High and Low gain traces are displayed for the latter; however, the later portions of the High gain trace are clipped. Both stations show a distinct but low level onset, and have approximately the same frequency content. A strong S phase is developed on the land horizontal. The pressure trace indicates a later phase about 4 seconds after the onset which coincides with the water bounce time, but probably represents a later P or possibly S phase. The spectra of Figure 28 show the pressure to have a better S/N ratio in the mid frequency band of 2 to 5 cps.

3. Local Events 41, 42 and 49

These three events are grouped in Figure 29. Actually, 41 and 42 occur very close in time, and are presented in the top half of the figure. They were recorded in 4.89 km (16,250 ft) of water at map position 9 (Figure 22). The land recordings show a better developed P and S onset than the ocean bottom traces, which are severely resonance corrupted. The spectral plots for events 41 and 42 are presented in Figure 30.

The signal-to-noise ratio are superior on the ocean bottom for event 42 on all components, both P and S phase; however, the land S/N is favored slightly for event 41. The signal spectra on land are remarkably similar for these two shocks, particularly the S phases which are identical to the smallest detail except for a 4 db difference in level. The same is not true
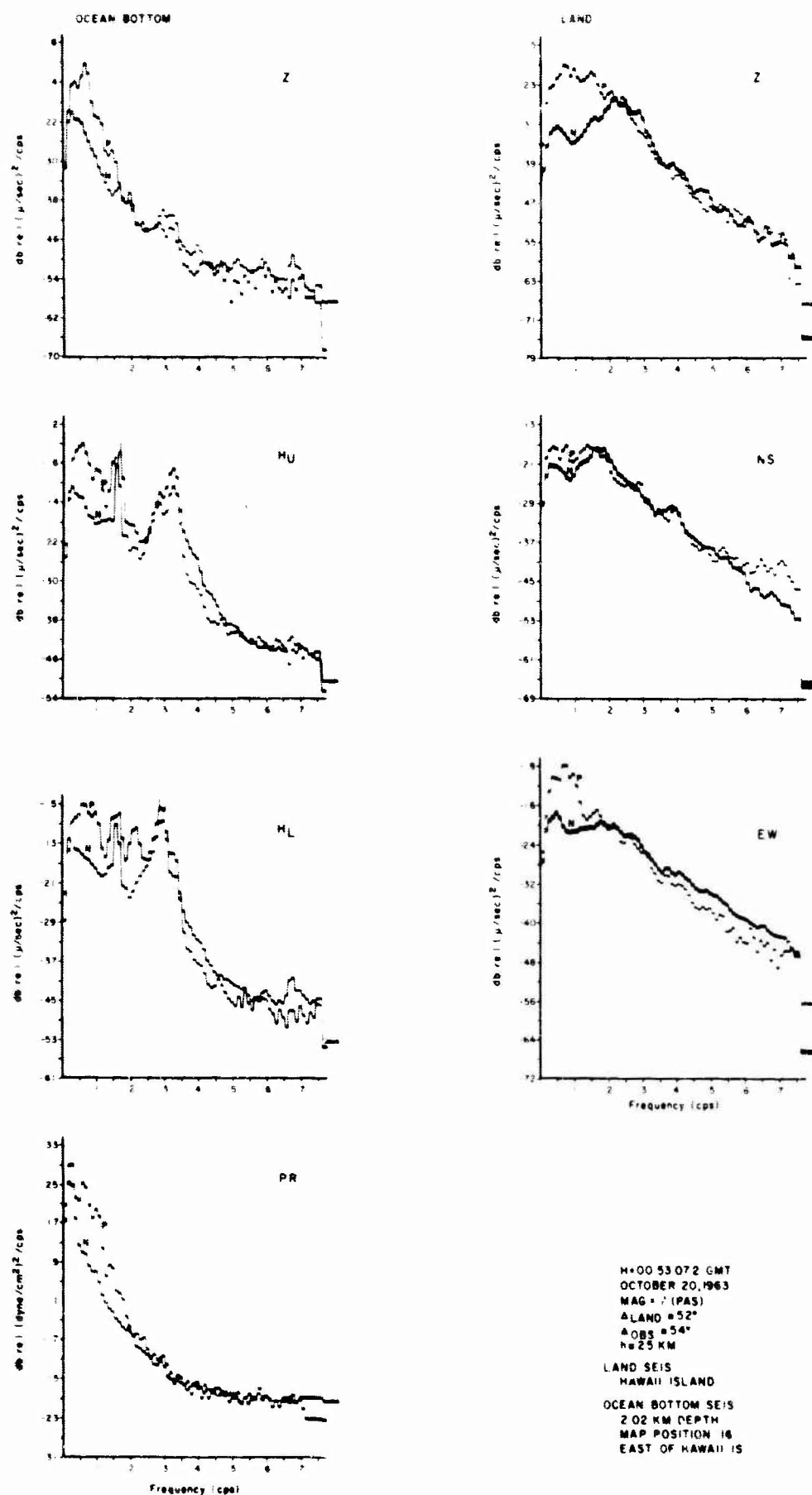
OCEAN BOTTOM

LAND

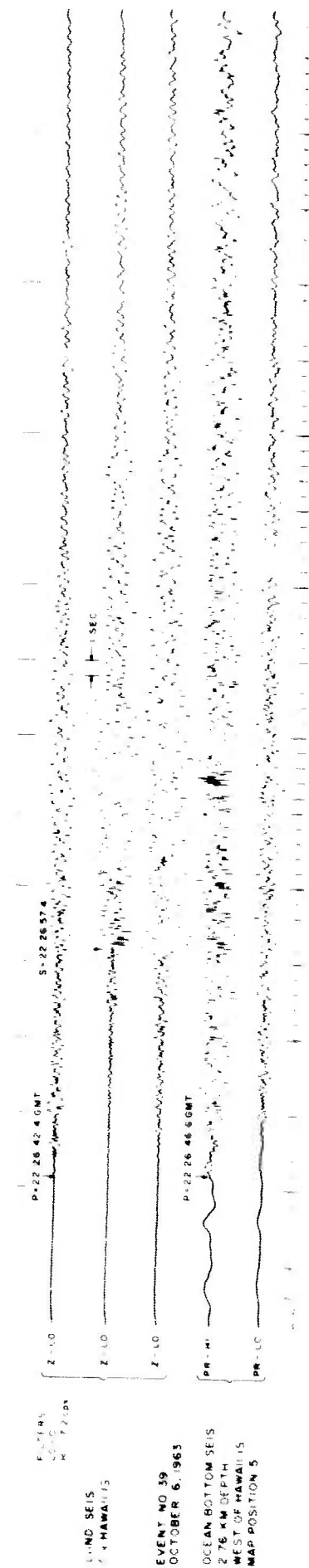Figure 26.   Kurile Island Region Event No. 52 Spectra

44

Figure 27.   Unlocated Event No. 39 (In Vicinity of Hawaii Island)

45

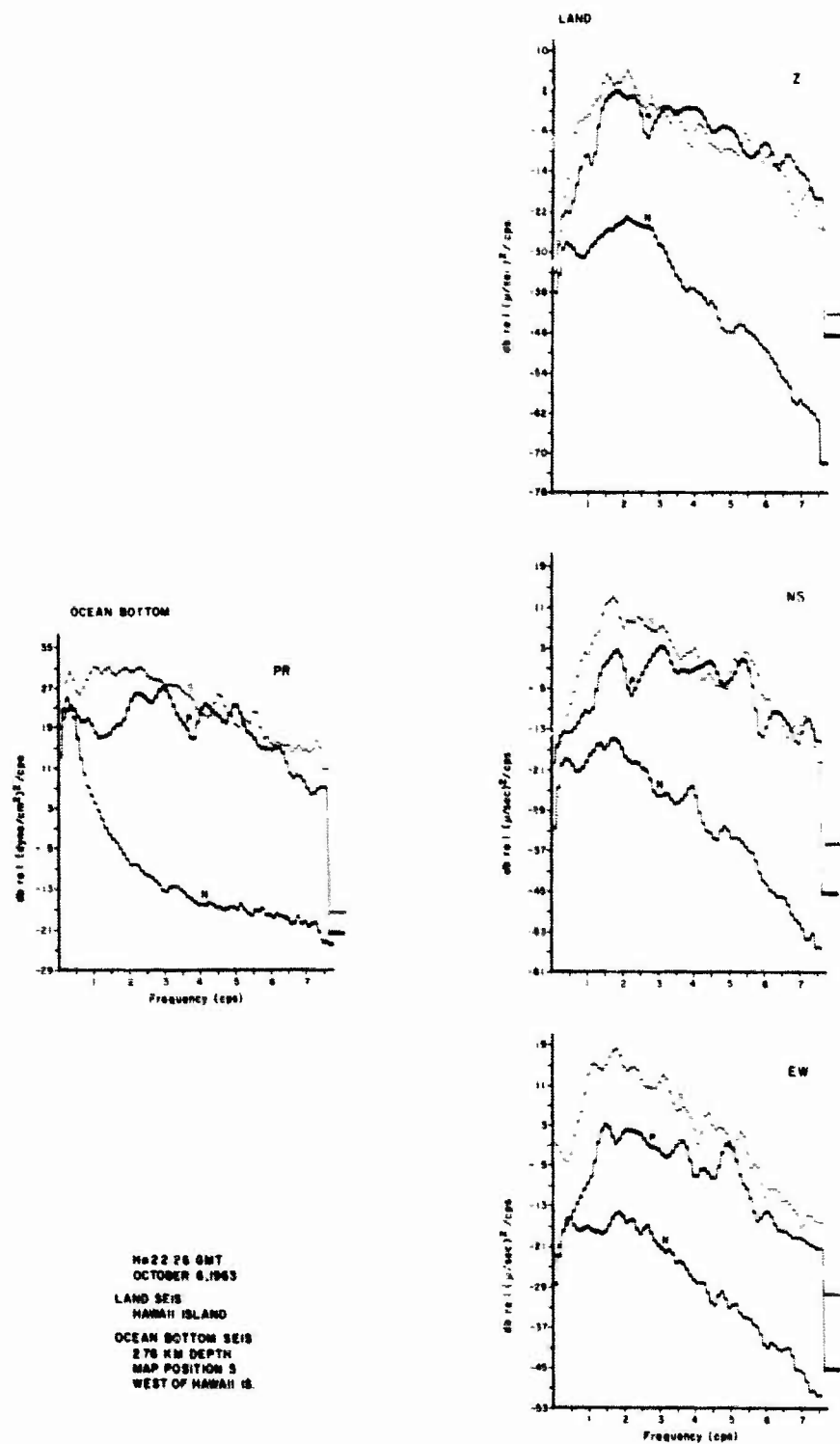Figure 28. Unlocated Event No. 39 Spectra

Figure 29. Unlocated Local Events No. 41, 42 and 49 (In Vicinity of Hawaii Islands)

47

on the ocean bottom. The S phase spectra for the two events show some
similarity on the velocity components at frequencies below the resonance
(f = 5 cps), but the P phases are entirely different. Examination of the
seismograms indicates that the events last considerably longer on the ocean
bottom, consequently the spectral analysis of 42 included arrivals from 41.

Event 49 recorded at map position 12 in 2.92 km (9750 ft) of
water shows well developed P and S phases at both stations. The ocean-bottom
horizontal are again rendered practically useless by the resonance problem.
The spectral plots of this event, as shown in Figure 31, favor the ocean-bottom
components for S/N ratios vs frequency. P to S intervals on land and the ocean
bottom indicate that no significant range correction is required. The signal
spectrum levels are greater on the bottom by approximately 5 to 10 db, and the
ocean-bottom pressure and vertical components indicate slightly less attenuation
of the higher frequencies than observed on land. The excitation of the horizontal
package resonance by the signal is dramatically displayed in the figure.

4. Local Events 43 and 45

Event 43 and 45 are displayed in Figure 32. These were both
recorded on October 13, 1963 at map position 11 in the 4.02 km (13,400 ft)
of water. The P onset is reasonably distinct on land and the ocean bottom for
event 43. A good S phase is developed on the land horizontal; however, their
ocean-bottom counterparts are "ringing" badly. The power spectra of this
event are shown in Figure 33.

The ocean-bottom spectra of this event show better S/N ratios
on all components than on land. Both stations receive equally broadband signals,
and the P phases are of comparable strength. The S phase shows about 10 db
of magnification on the ocean-bottom vertical velocity component.

Event 45 does not differ substantially from 43 except that the
phases are better developed and defined at both stations. As before, the
horizontals on the bottom are resonating. The spectral plots in Figure 34
reveal that the ocean bottom is again favored in S/N ratio (discounting the
horizontal resonances) on all components. The small range corrections
indicated by the difference in P to S phase interval would favor the ocean
bottom. Signal levels differ by very little on the vertical components, and
there does not appear to be any high frequency gain on the ocean bottom for
this event. The average ambient noise spectra for events 43 and 45 were
obtained from different time intervals of the recording on the thirteenth, yet
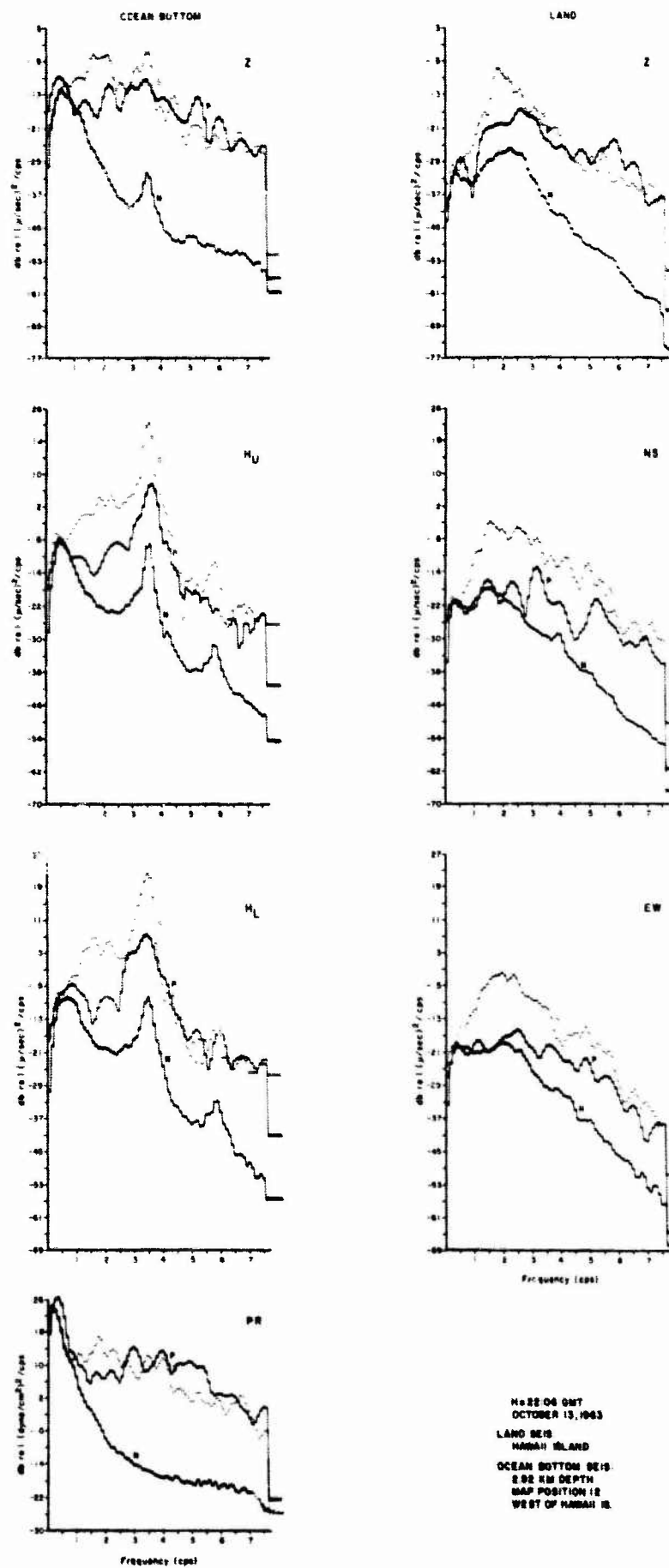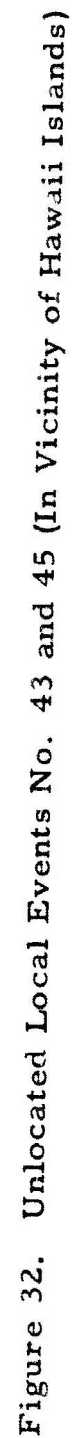are practically overlays in agreement.

Figure 31. Unlocated Event No. 49 Spectra

50

Figure 32. Unlocated Local Events No. 43 and 45 (In Vicinity of Hawaii Islands)
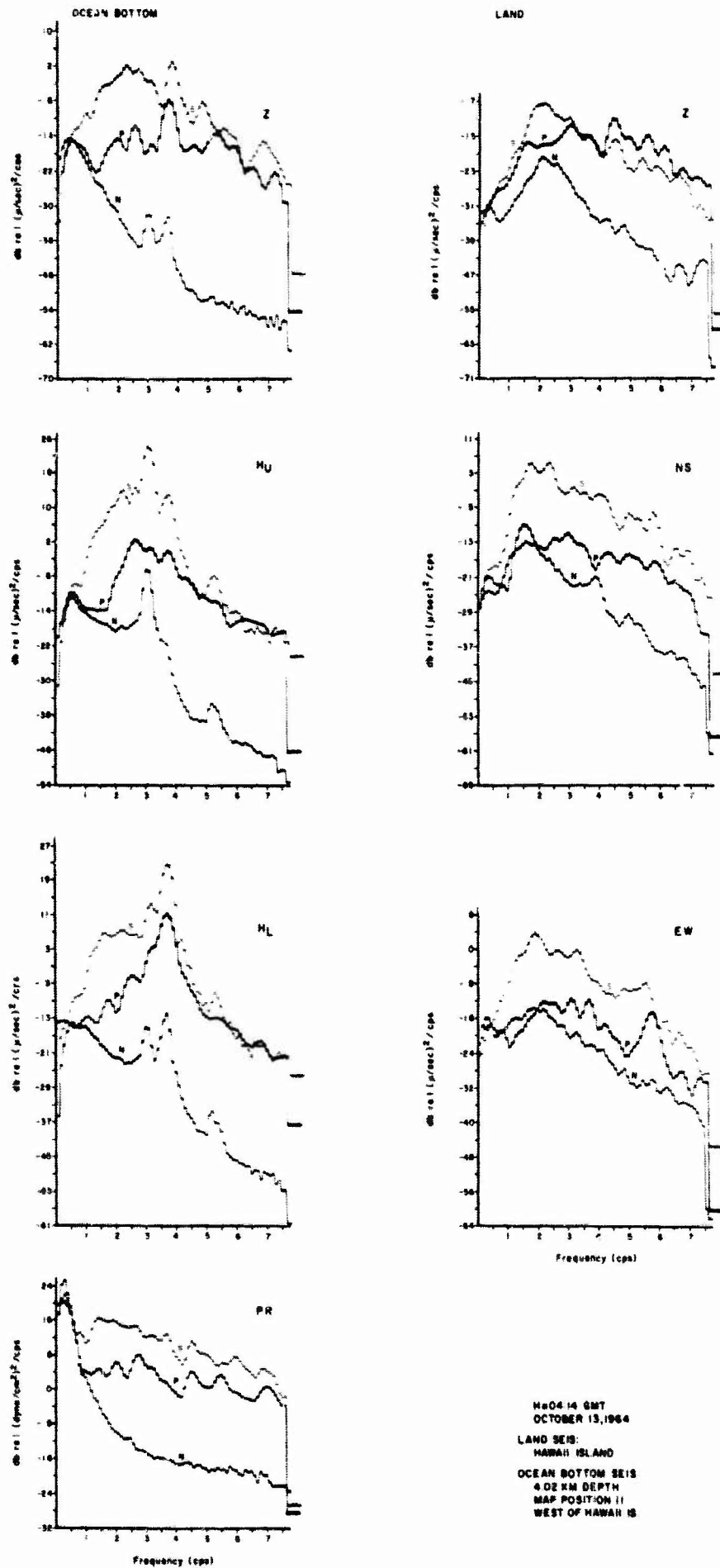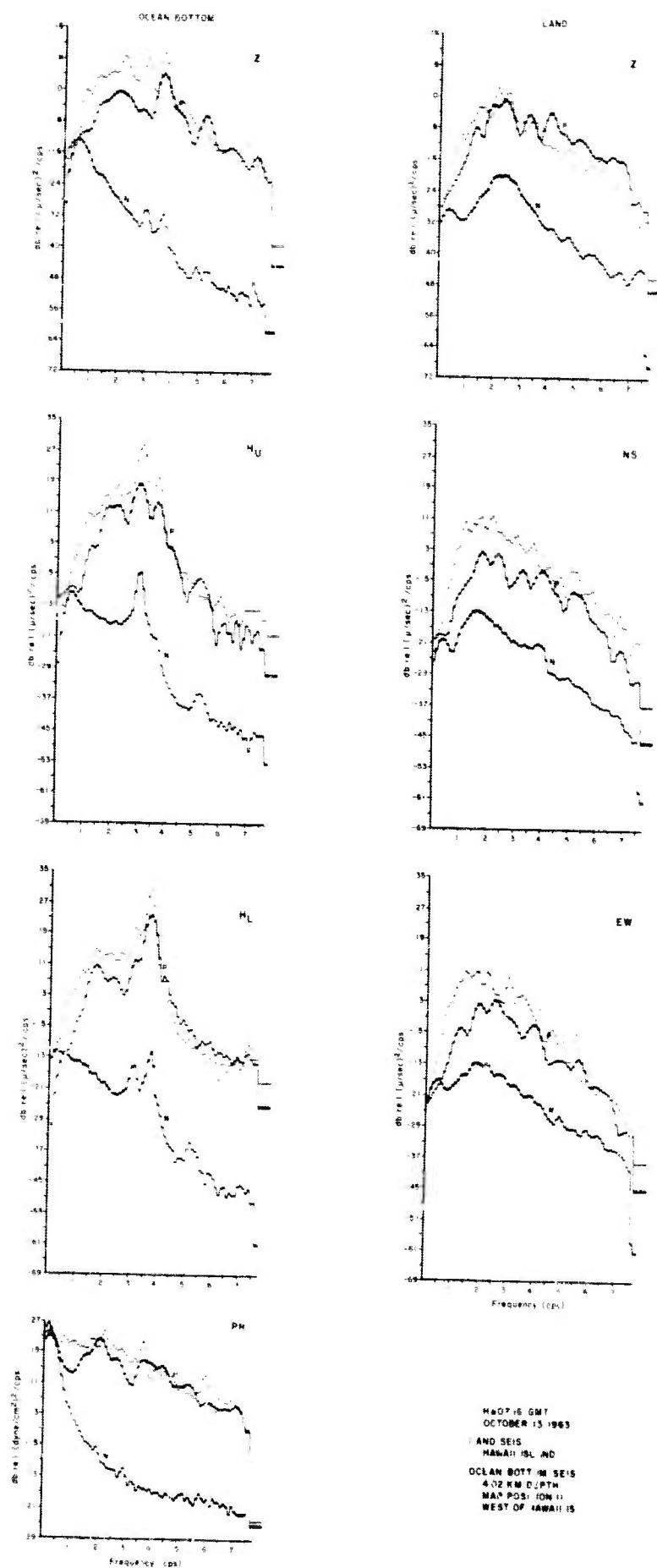
Figure 33. Unlocated Event No. 43 Spectra

Figure 34.   Unlocated Event No. 45 Spectra

5. Local Events 47 and 53

The seismograms of events 47 and 53 are displayed in Figure 35. They were recorded at map positions 13 and 16 in 3.98 km (13,250 ft) and 2.02 km (6720 ft) of water respectively. For event 47, the ocean-bottom vertical was inoperative and the horizontals are exhibiting resonance at about 5 cps. Figure 36 shows the spectral plots for this event.

The horizontal components on the ocean bottom have better S/N ratios than on land for both the P and S phases. The resonance at 5 cps must be discounted. The pressure S/N ratios are several db poorer than any of the land components. As is characteristic of all these local events, the spectrum is quite broad.

The seismograms for local event 53 show slightly better signal-to-noise ratios than for event 47. The land record is somewhat unusual in that the S phase has relatively little expression on the vertical component. The P onset is lower on the ocean bottom than land but somewhat higher in frequency. Power spectra for this event are presented in Figure 37.

S/N ratios favor the land in this instance on all components. The signal level on the vertical seismometer differs by about 20 db in favor of the land, which is the first instance of land magnification observed. It is possible that a significant range correction is involved as the S phase on the ocean bottom is not distinct except for the envelope change of the "ringing" horizontals. The latter may be a poor indicator of the S onset.

6. Local Events 51 and 57

The next pair of unlocated events 51 and 57, are displayed in Figure 38. Positions 17 and 21 were occupied by the ocean-bottom seismometers on these drops in water depths 2.56 km (8200 ft) and 4.22 km (14,000 ft), respectively. Only the pressure channel was operative on the ocean bottom for event 51. All components are shown for 57, but the pressure channel was exhibiting instrumental difficulties at other times, and an average noise spectrum was not obtained. Both event 51 and 57 show about the same features as the previous local events in terms of phase development and spectral content. The spectral plots for events 51 and 57 are shown in Figures 39 and 40.

The pressure spectra has a better S/N ratio above 2 cps than the land components for event 51.

The S/N ratios vs frequency for event 57 also slightly favor the ocean bottom for all components (disregarding the horizontal resonances). In addition, the signal levels are not substantially different though the ocean bottom vertical component shows a "whiter" P spectrum than the corresponding land plot.
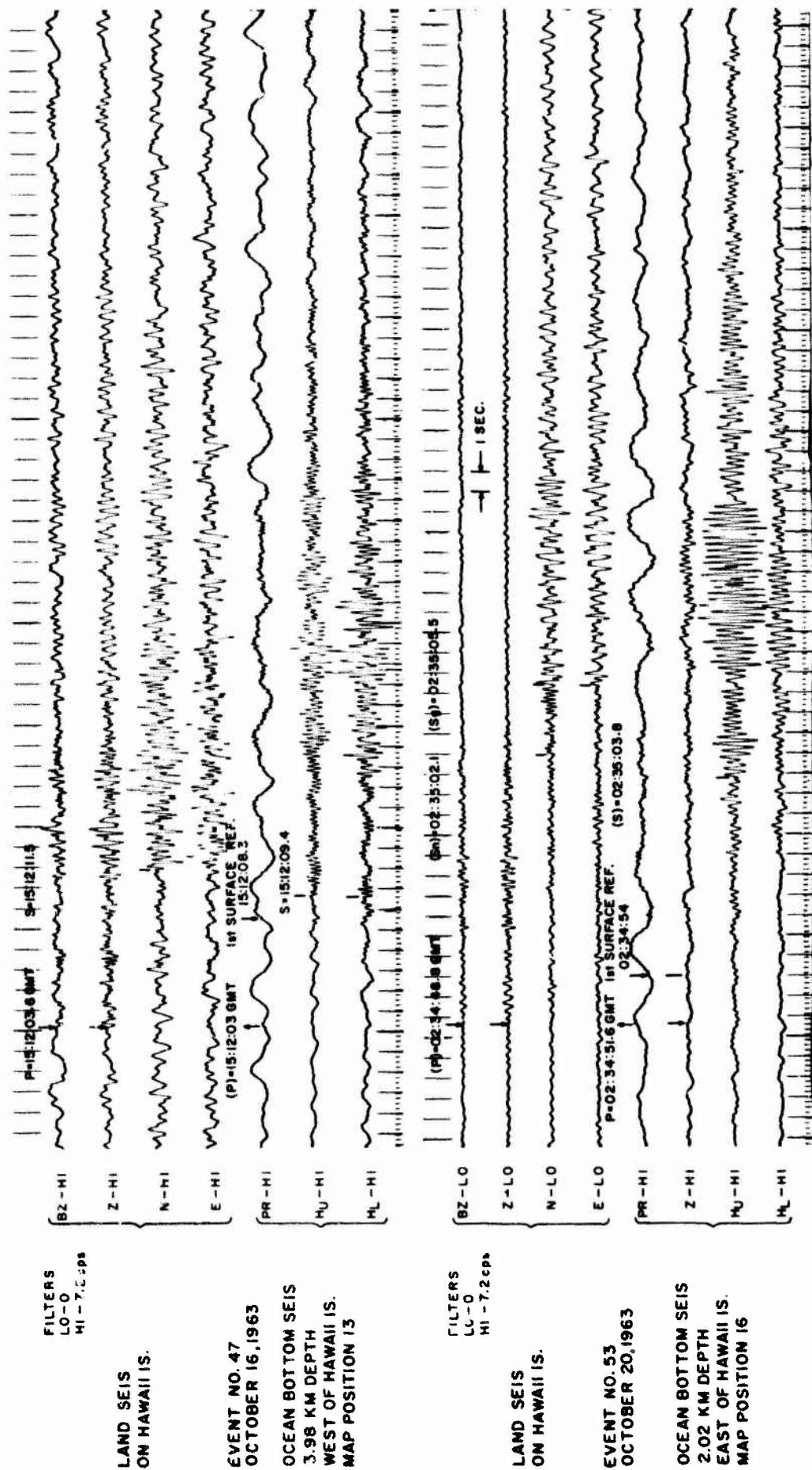
54

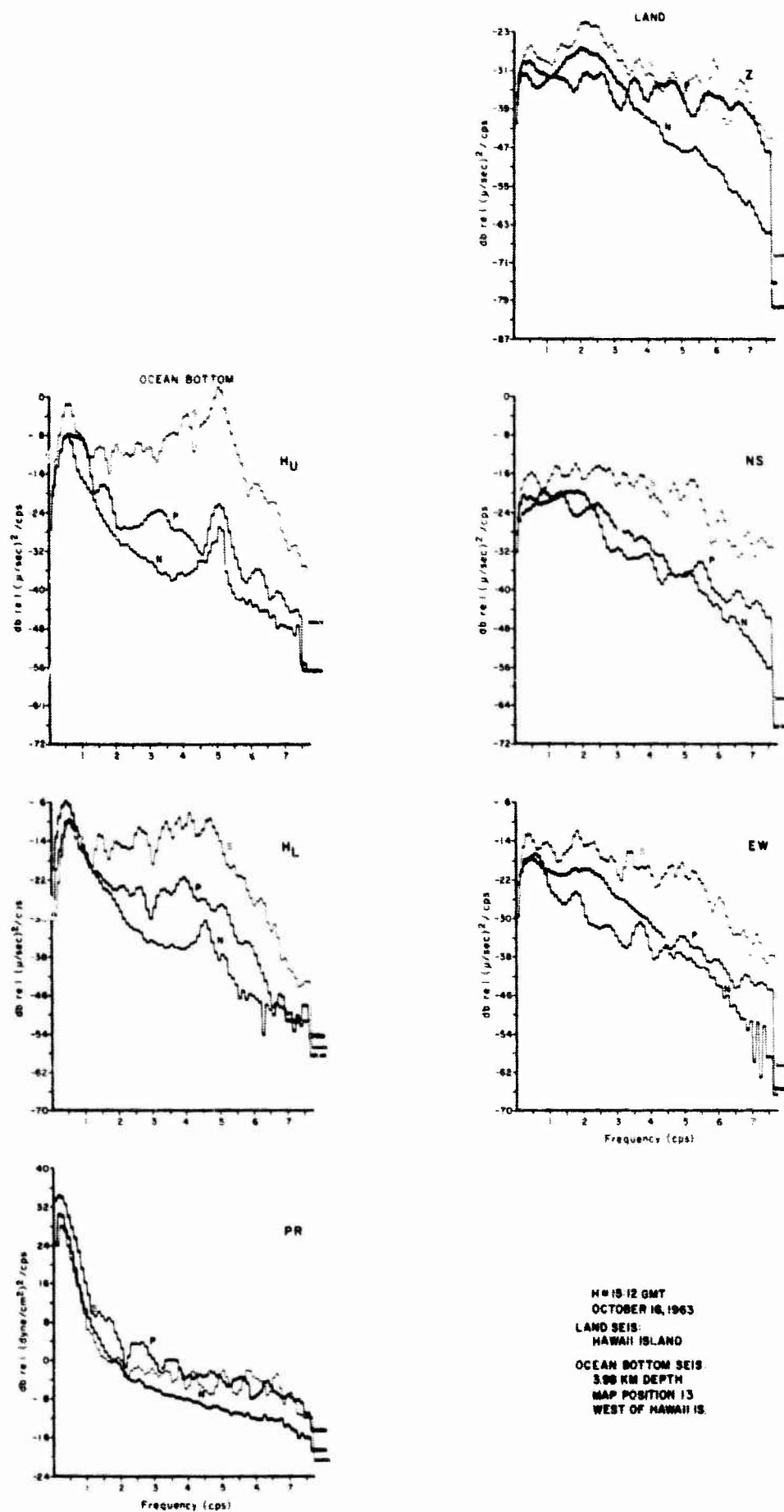Figure 35. Unlocated Local Events No. 47 and No. 53 (In Vicinity of Hawaii)

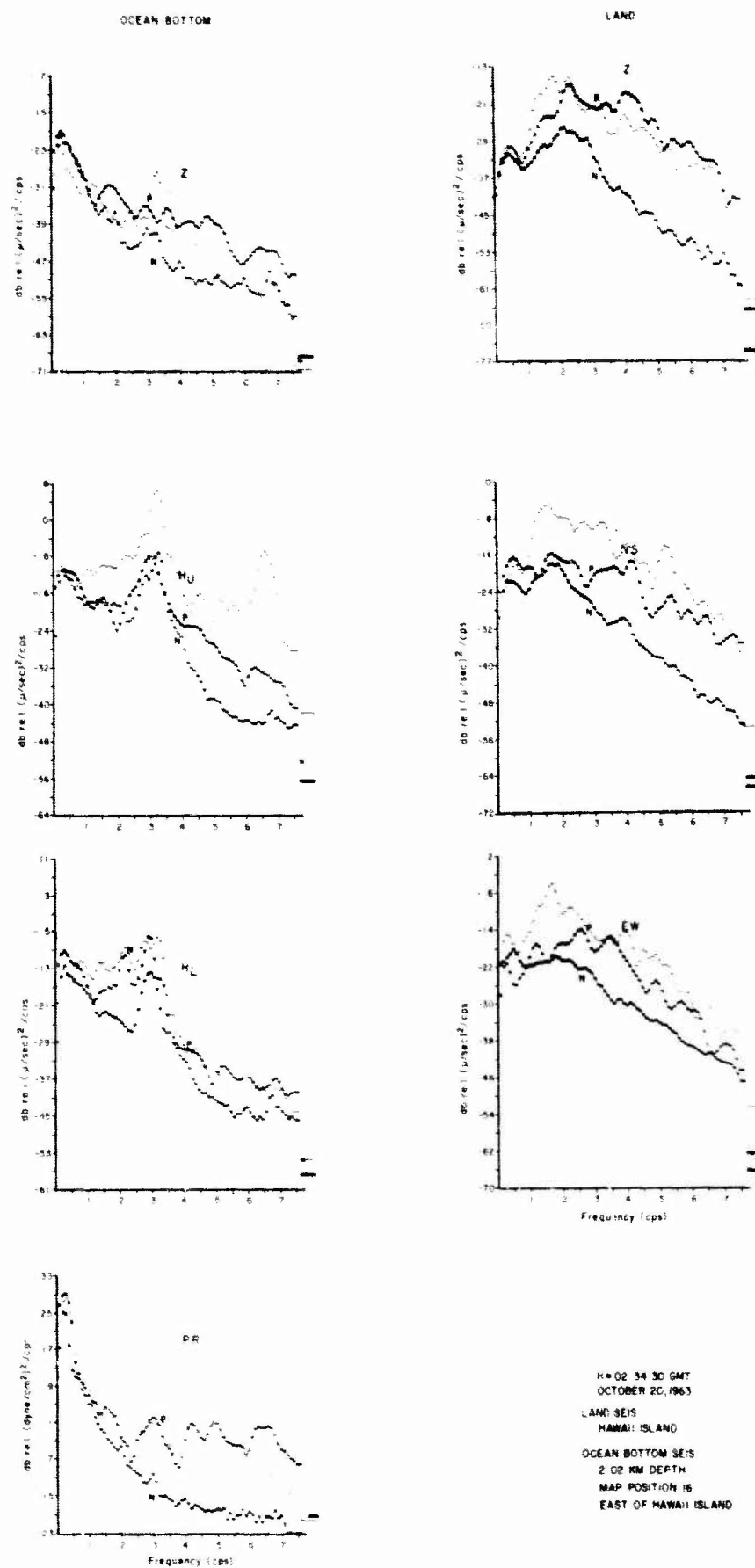Figure 36. Unlocated Event No. 47 Spectra
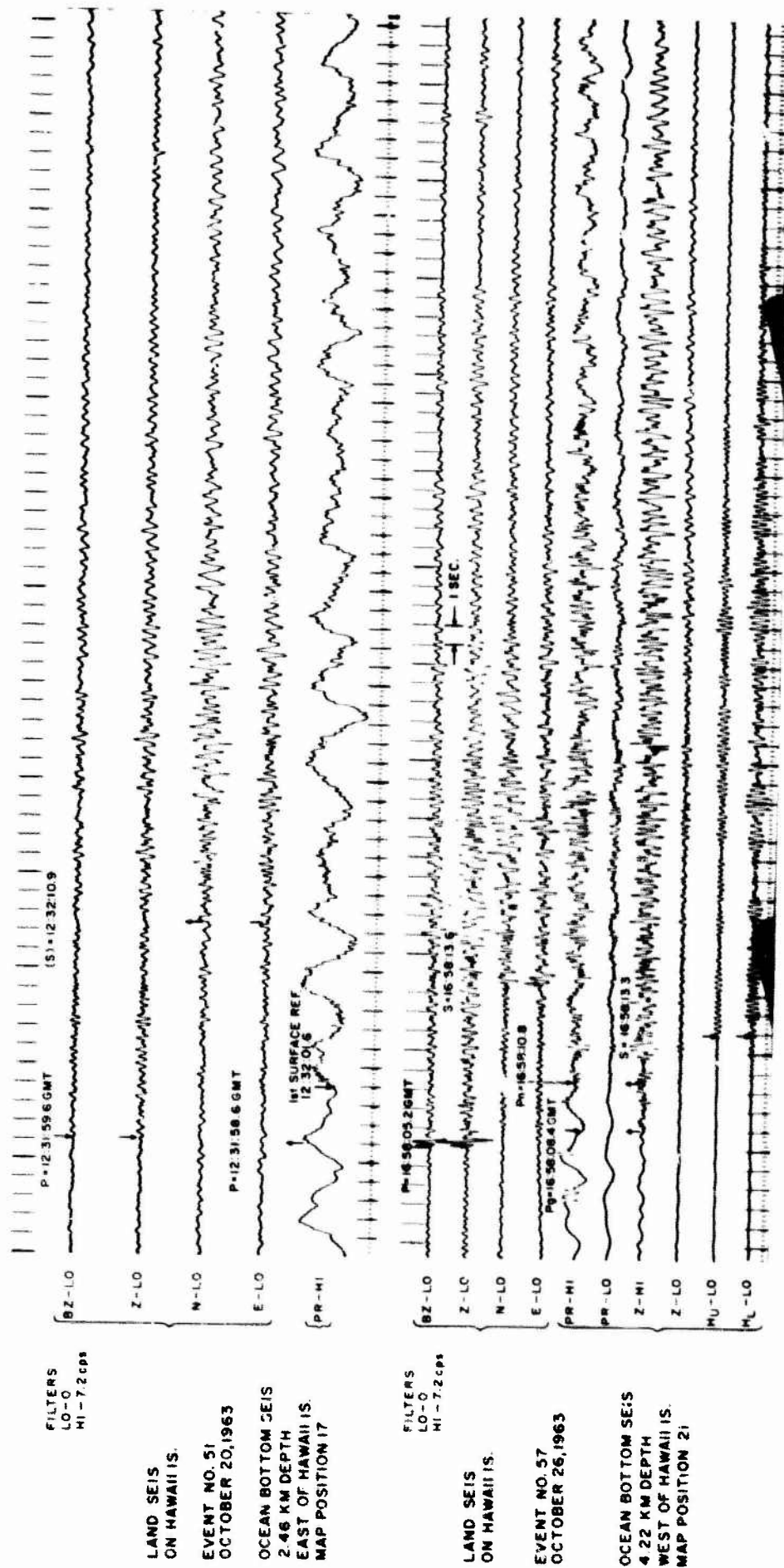
Figure 37.   Unlocated Event No. 53 Spectra

57

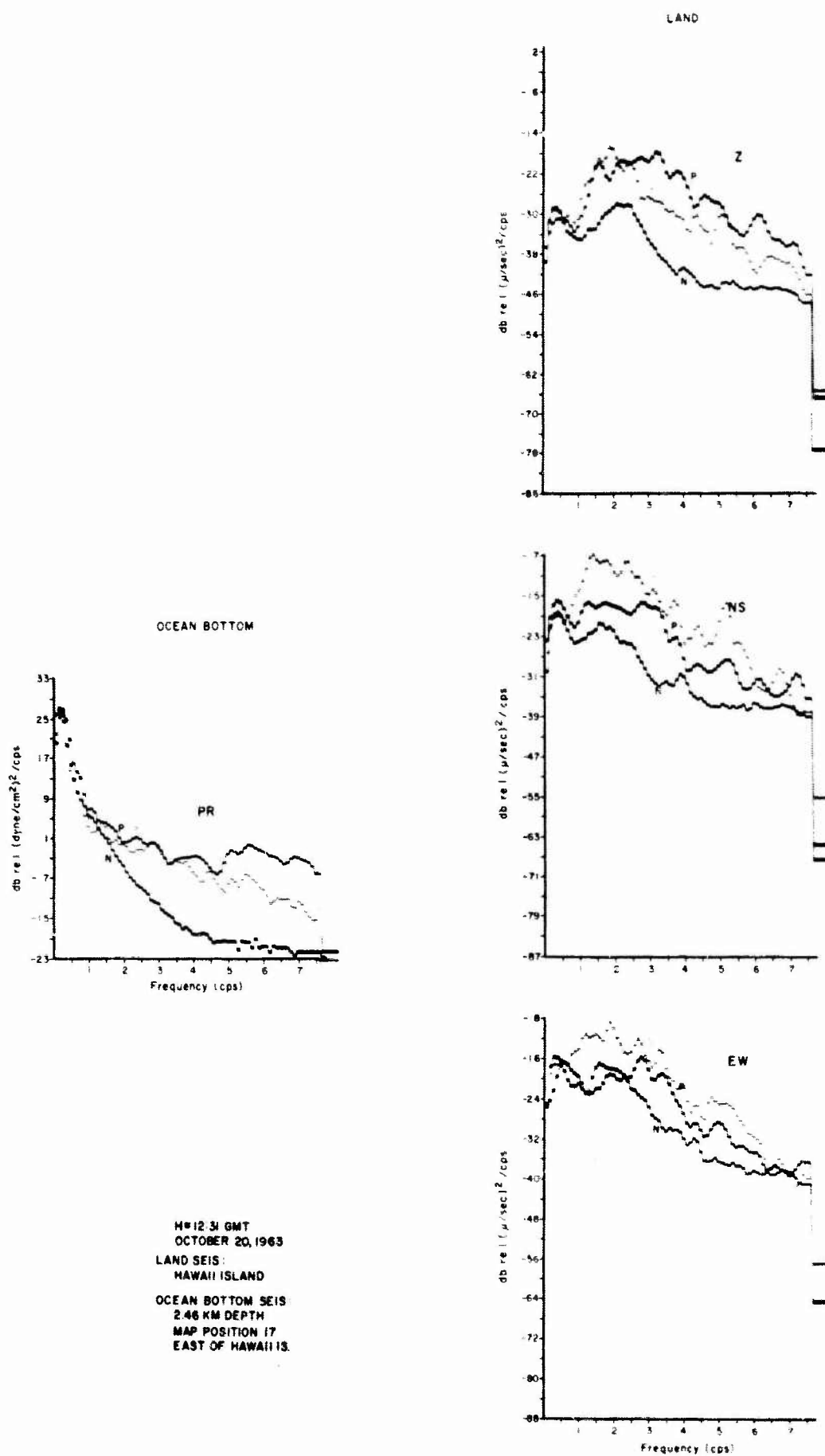Figure 38. Unlocated Local Events No. 51 and No. 57 (In Vicinity of Hawaii)

Figure 39. Unlocated Event No. 51 Spectra
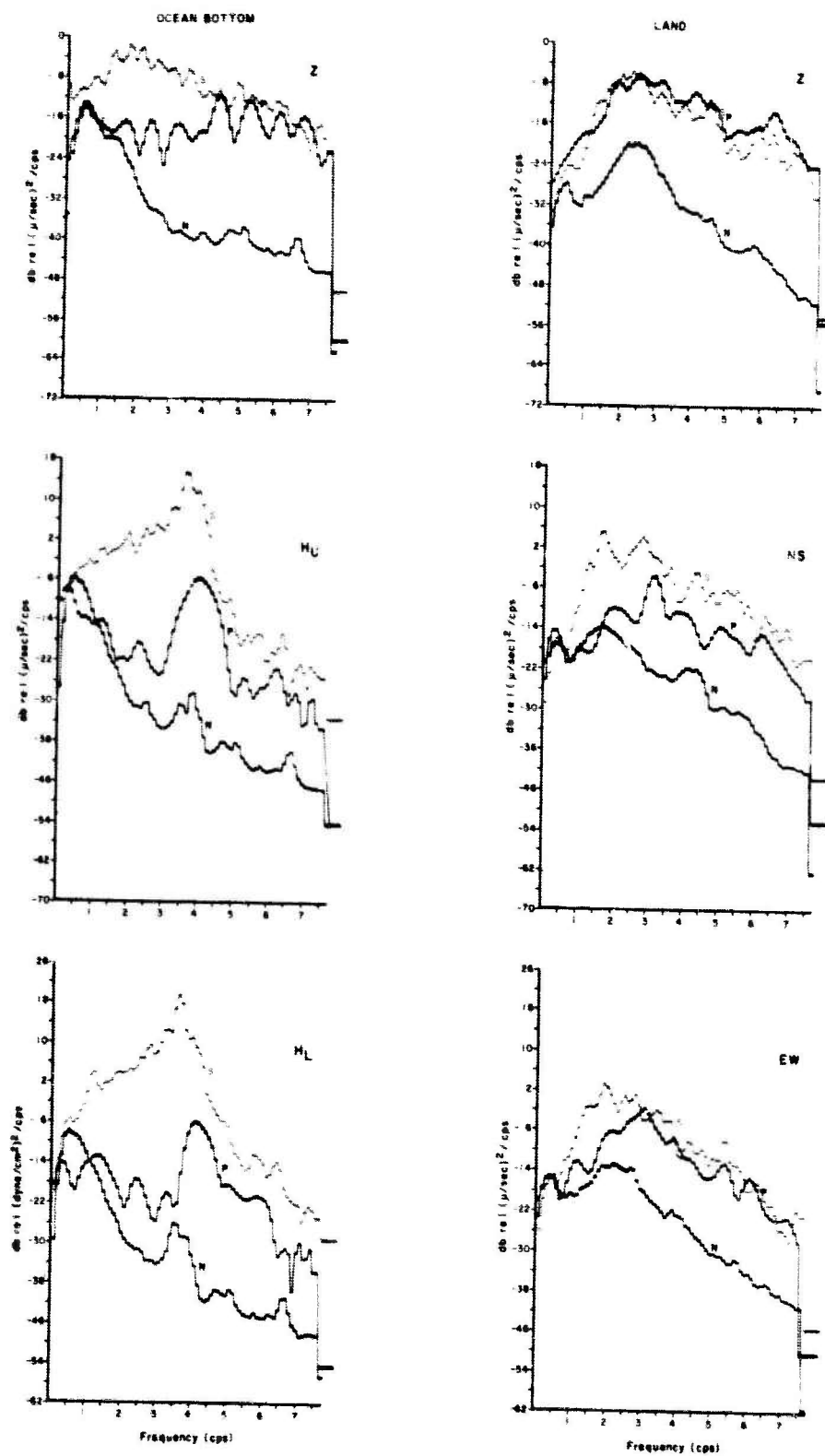
Figure 40. Unlocated Event No. 57 Spectra

7. Local Events 54 and 55

The final two local events analyzed trom the Hawaii data are shown in Figure 41. They were both recorded at position 19 in 1.46 km (4870 ft) of water. All components were operative on the drop. The spectra for these events are presented in Figures 42 and 43.

The S/N ratios are better on the ocean bottom for all components for event 54. The signal levels on the vertical components differ by about 15 db, showing ocean-bottom magnification. In addition, the P phase spectra have better high frequency content on the ocean bottom than on land. The signal strongly excites the horizontal resonance in the 3 to 4 cps band with some corruption of the vertical. The ocean-bottom pressure noise spectrum was obtained from a low gain trace and is instrument-noise limited above 2 cps.

Event 55 also favors the ocean bottom S/N ratios over the land, except on the pressure channel. The spectrum levels on the vertical components are within 6 db of one another and both show rich high frequency content.

8. Summary of Hawaii Signal and Noise Analysis

a. Teleseismic Events

The three major teleseismic events recorded in the Hawaiian Islands were well received on all components on land and the bottom. The signal spectrum is confined to the low frequency band of about 0.5 to 3 cps. In this band the S/N ratio comparisons are approximately equal for events 46 and 52, and slightly favor the ocean bottom for the magnitude 8 event 44. The signal levels on the vertical components show ocean-bottom magnification of 10 and 20 db for events 44, 52 and 46, respectively.

b. Unlocated Local Events

The great majority of the Hawaii signal events fall in this category. All are characterized by broad spectral content and simple phase development. P and S are always present on land. while S is less well defined on the ocean bottom.

The S/N ratio comparisons for these twelve events favor the ocean bottom ten times (events 39, 43, 45, 47, 49, 51, 54, 55, and 57) and the land twice (events 41 and 53). The average differences in S/N ratio are, however, not large. The effect of water depth does not appear to be a factor in the S/N ratio in the Hawaii area. Better ocean-bottom ratios are observed at both shallow and deep sites; for example, event 55 in 1.47 km (4900 ft) and event 57 in 4.22 km (14,100 ft) of water both show superior S/N ratios on the bottom. The lack of depth dependence of of S/N ratio is undoubtedly related to the lack of depth dependence of the noise itself as will subsequently be discussed.
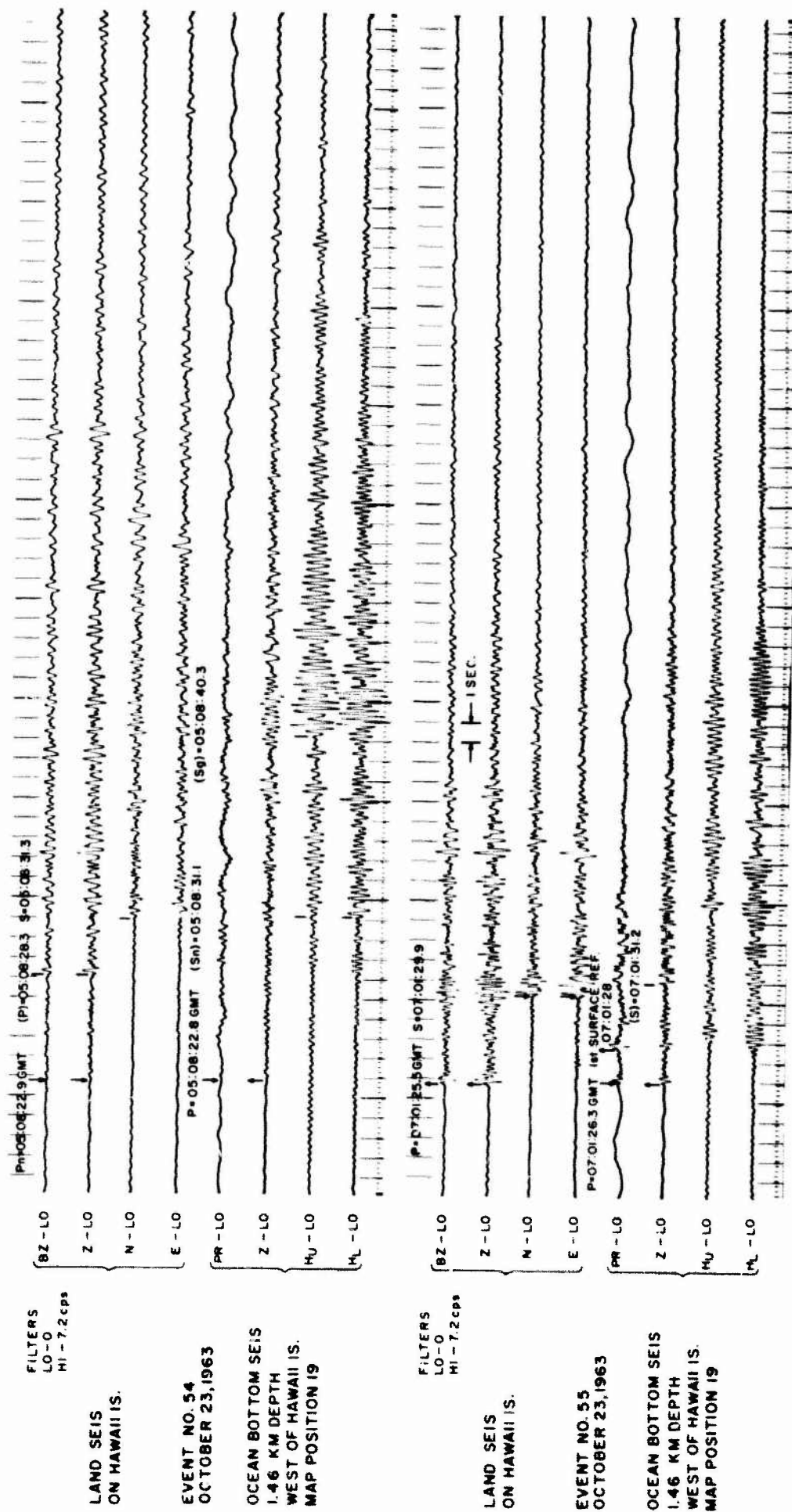
Figure 41. Unlocated Local Events No. 54 and No. 55 (In Vicinity of Hawaii)
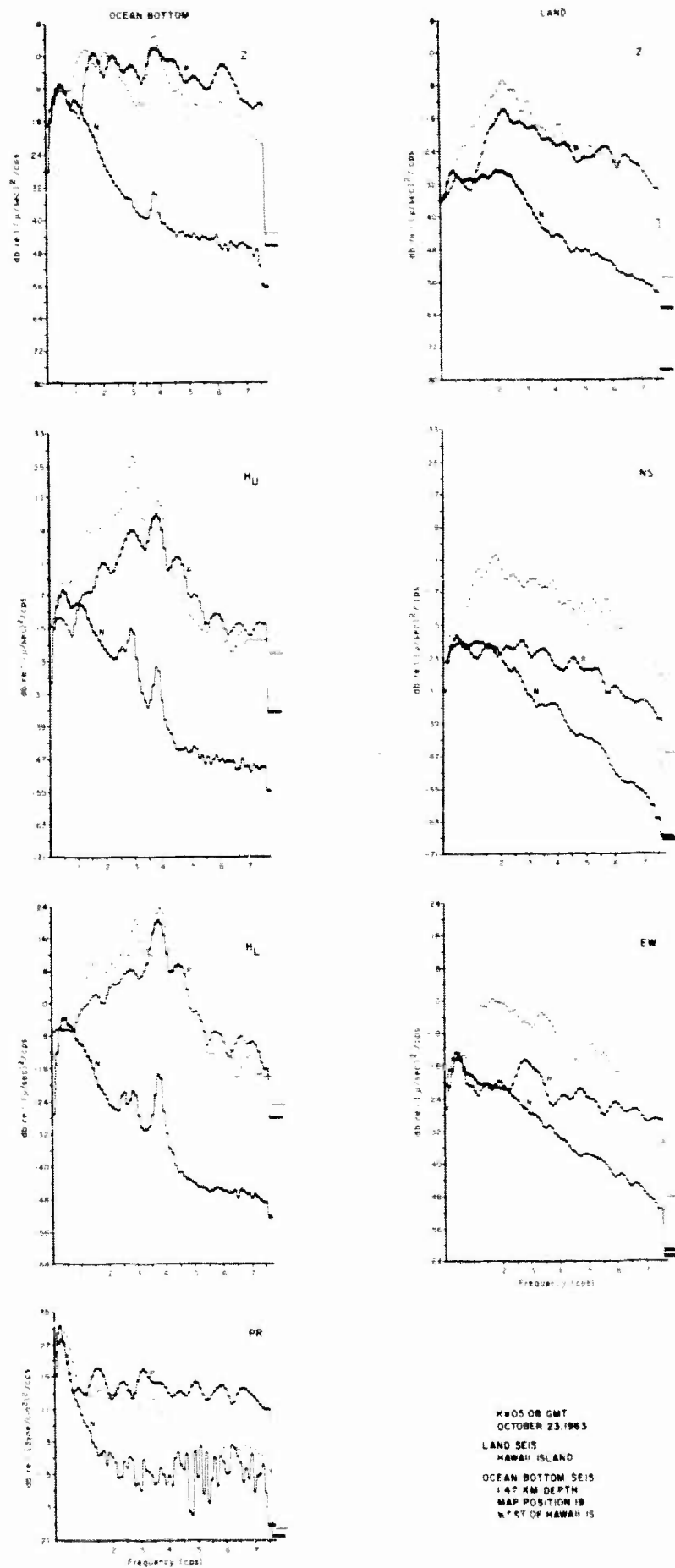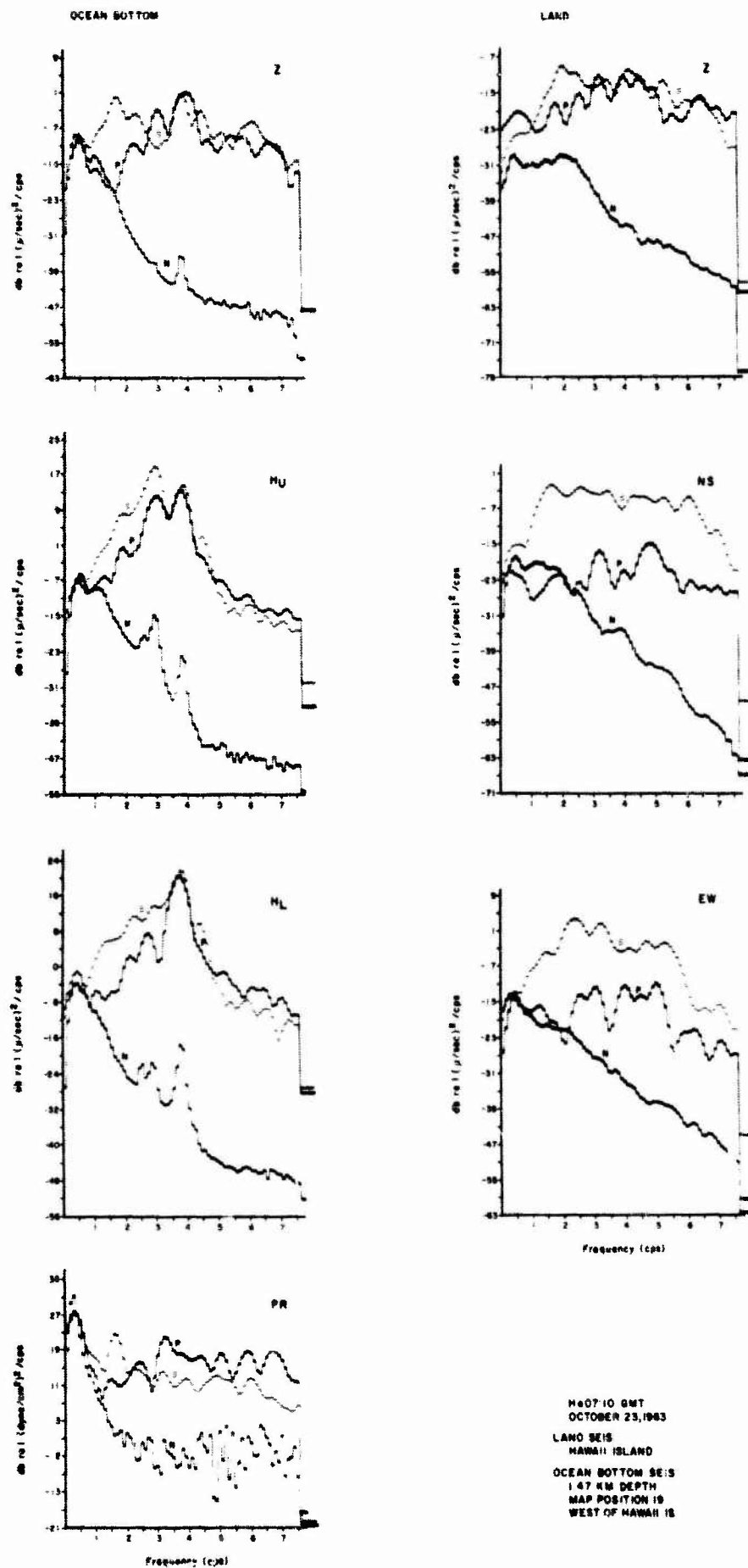
Figure 42. Unlocated Event No. 54 Spectra

Figure 43.   Unlocated Event No. 55 Spectra

The signal levels indicate ocean-bottom magnification for several local events though it is not nearly so consistent as for the teleseismic signals. In addition, the uncertainty about range or distance correction makes generalization in this regard highly tenuous.

The evidence for high frequency signal preservation on the ocean bottom vs land in the Hawaii area is considerably less striking than in the Aleutians. Both land and ocean-bottom signal spectra are substantially "white" for these local shocks.

c. Hawaii Ambient Noise

The ocean-bottom ambient, measured at the several positions shown in Figure 22 in water depths from 4900 ft to 17,932 ft, average about 15 db higher than the land spectra in the 0.5 to 1.5 cps band. At higher frequencies the land noise has more power than the ocean bottom. We believe, however, that the land spectra are probably not representative of an interior station far removed from the coastal surf. If the latter were correct, it very likely would alter many of the S/N results obtained in the Hawaii area.

The ocean-bottom noise spectrum does not appear to have any simple dependence on water depth. Plotted in Figure 44 are the pressure ambient spectra vs water depth. The arrow heading each column of data gives the date and map position of the drop. The horizontal ties connect the same frequency (0.2, 0.4, 0.6, etc.) at each drop position. Depth dependence of the pressure noise spectrum vs frequency may be inferred from the behavior of the horizontal ties. No significant variations with depth are evident for the frequencies shown. In fact, the pressure spectrum at 4900 ft is within several db of the spectrum at 17,900 ft. The fluctuations with depth that are present may be due to level changes in the regional ambient pressure field from day to day. Simultaneous measurements with multiple ocean-bottom units over this depth range would resolve the question. Similar results apply to the vertical component as regards depth dependence.

C. CALIFORNIA DROPS

The California Coast drop positions and land site locations are shown in Figure 45. Ocean bottom sites 1 through 21 were occupied during June and July of 1963 and have been reported on in Semiannual Technical Report Number 5, and Special Report, "Collection and Analysis of Pacific Ocean Bottom Seismic Data." Drops 22 through 31 were made during November and December of 1963 and are covered in this report.

In spite of the seismicity of the Mendocino area only four usable natural events of analysis quality were recorded during the November and December drops, and two of these were teleseisms. The remaining two
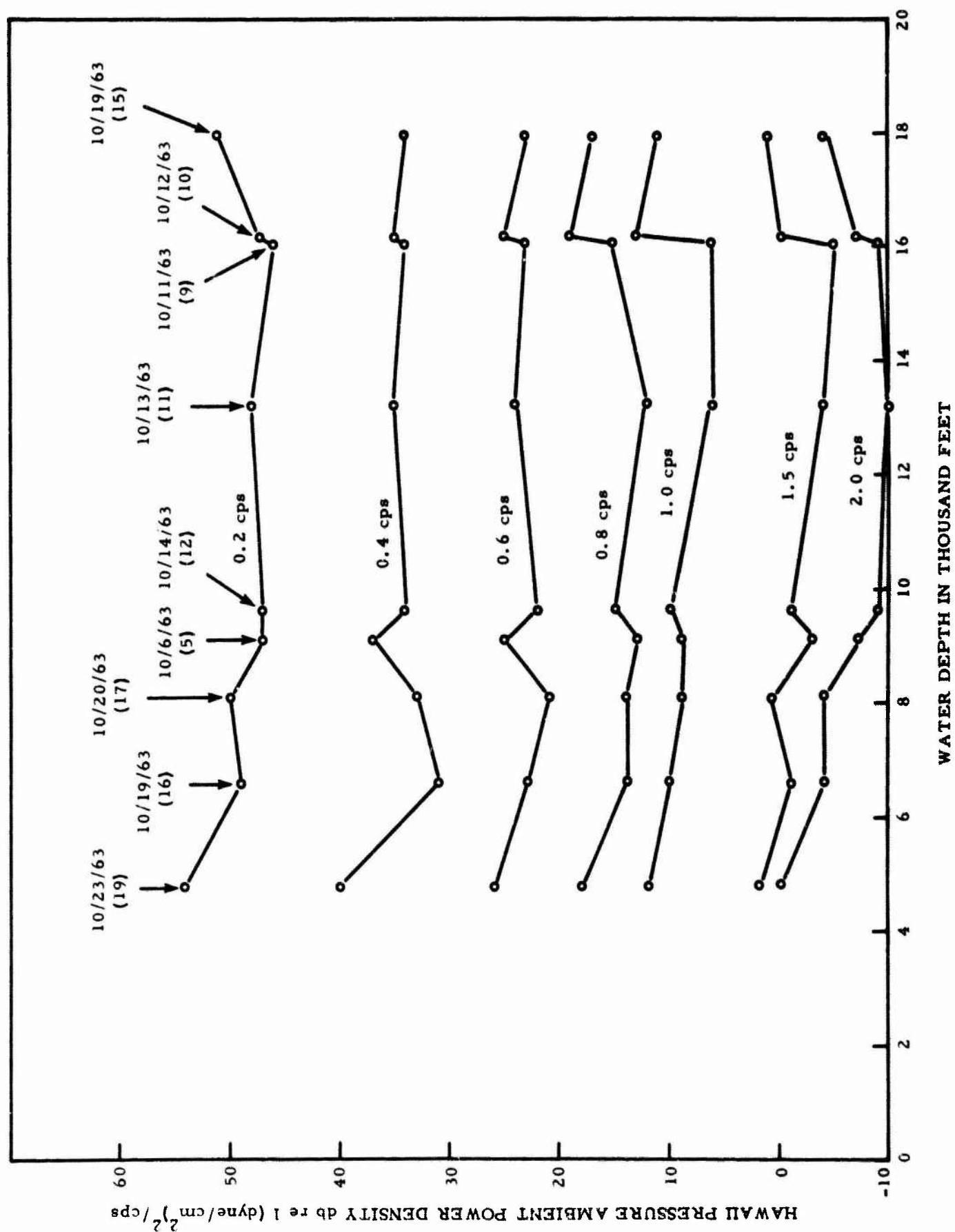
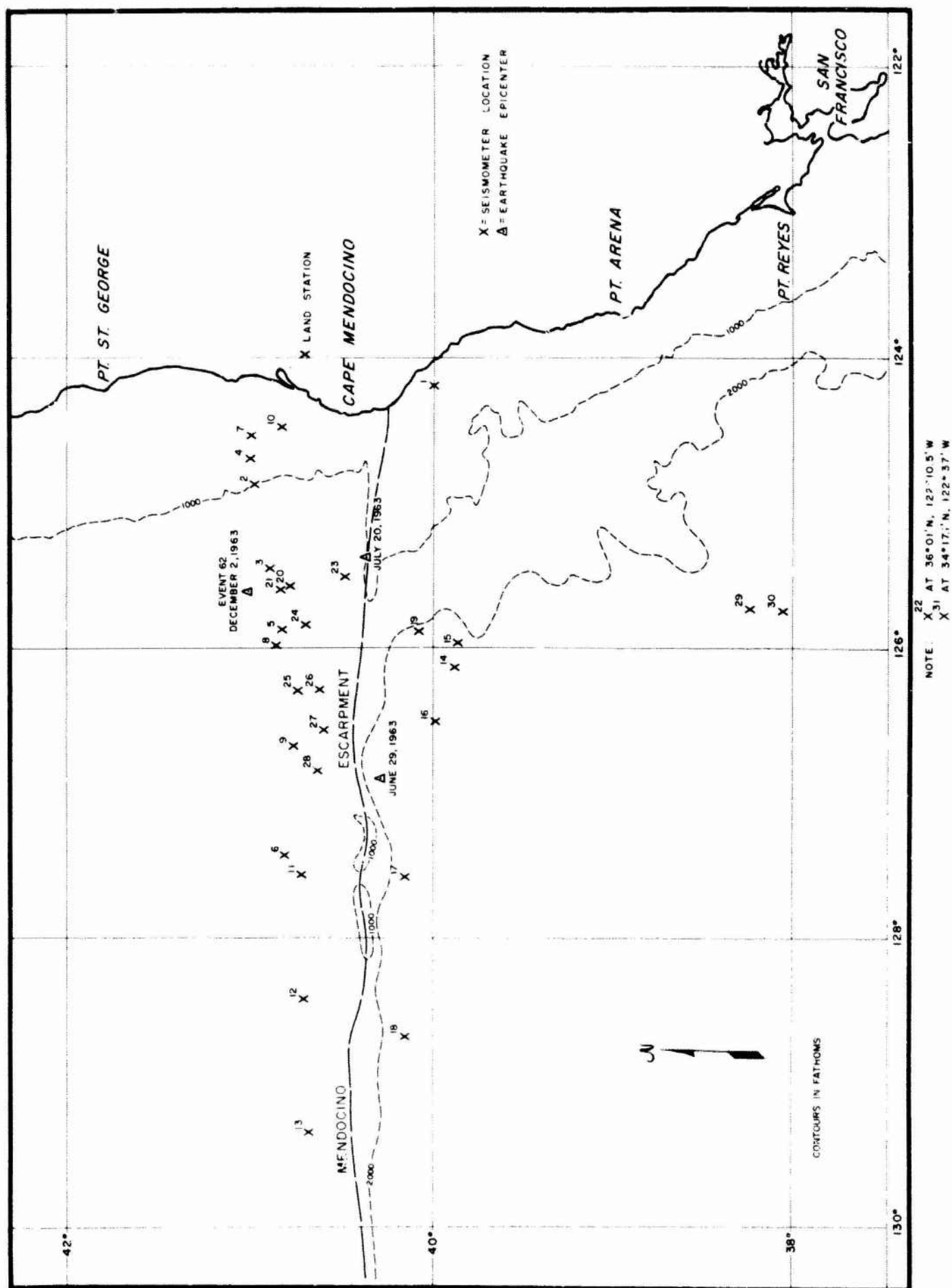Figure 44. Pressure Ambient Noise vs Depth Dependence

Figure 45. California Coast Drops Instrument Locations

consisted of a near-regional and unlocated local event. The spectra of these
are presented in the following.

1. Local and Near-Regional Events 61 and 62

The seismograms for these two events are shown in Figure 46.
All components were recorded for both events. Event 61 was recorded in
3.10 km (10,300 ft) of water at map position 26. The land recording is decidely
cleaner with better phase development and definition than on the ocean bottom.
A strong resonance component on the horizontal following the S_g phase shows
cross-coupling on the vertical trace, but not the pressure. The spectra for
event 61, Figure 47, verify what the seismograms made obvious, that the S/N
ratio is decidedly superior on the land. The difference in P to S interval times
indicates a significant range correction, but not enough to equalize the S/N
ratios. The P signal levels differ by about the range correction (10-15 db);
however, the ocean bottom signal spectrum is considerably "whiter" than on
the land vertical. The ambient levels are approximately 25 db higher on the
ocean bottom velocity components at the microseismic peak (0.5 cps). This is
in good agreement with the data collected six months earlier which showed 20
db difference in ambient level.

Event 62 was recorded in 4.16 km (13,850 ft) of water at
position 30 off Point Reyes, California. The hypocenter is located approximately
120 km from land and 330 km from the bottom site. The land components show
better phase development and definition as well as superior signal-to-noise ratio.
The ocean bottom event is, however, decidedly higher frequency. This is best
seen in the spectral plots of Figure 48. The ocean-bottom signal spectra for
P and S phases on the vertical and pressure are substantially flat out to 7.5
cps, whereas the land vertical components show about 20 db attenuation of the
high frequency energy relative to that at 1 cps. The low frequency signal levels
on the vertical components are approximately equalized when corrected for

difference in range $\left(\dfrac{330}{120}\right)^2 = 17.5$ db. The ocean bottom S/N ratio, however,

is still inferior to that on land.

The ocean bottom and land noise levels are considerably lower
than average on this day. More significant, however, is the peculiar noise
observed on the bottom at this position. The vertical component is about 20 db
lower than the ocean-bottom horizontals, which in itself, is unusual. The
vertical noise spectrum barely stands above the instrument noise level in the
plot (Figure 48). The interesting feature of the horizontal data is the harmonic
structure which can be seen superimposed on the broad noise peak at about 0.5
to 2 cps. This effect was observed to persist over nine hours of recording on
that date. In addition, the cross-correlation between horizontals indicate that

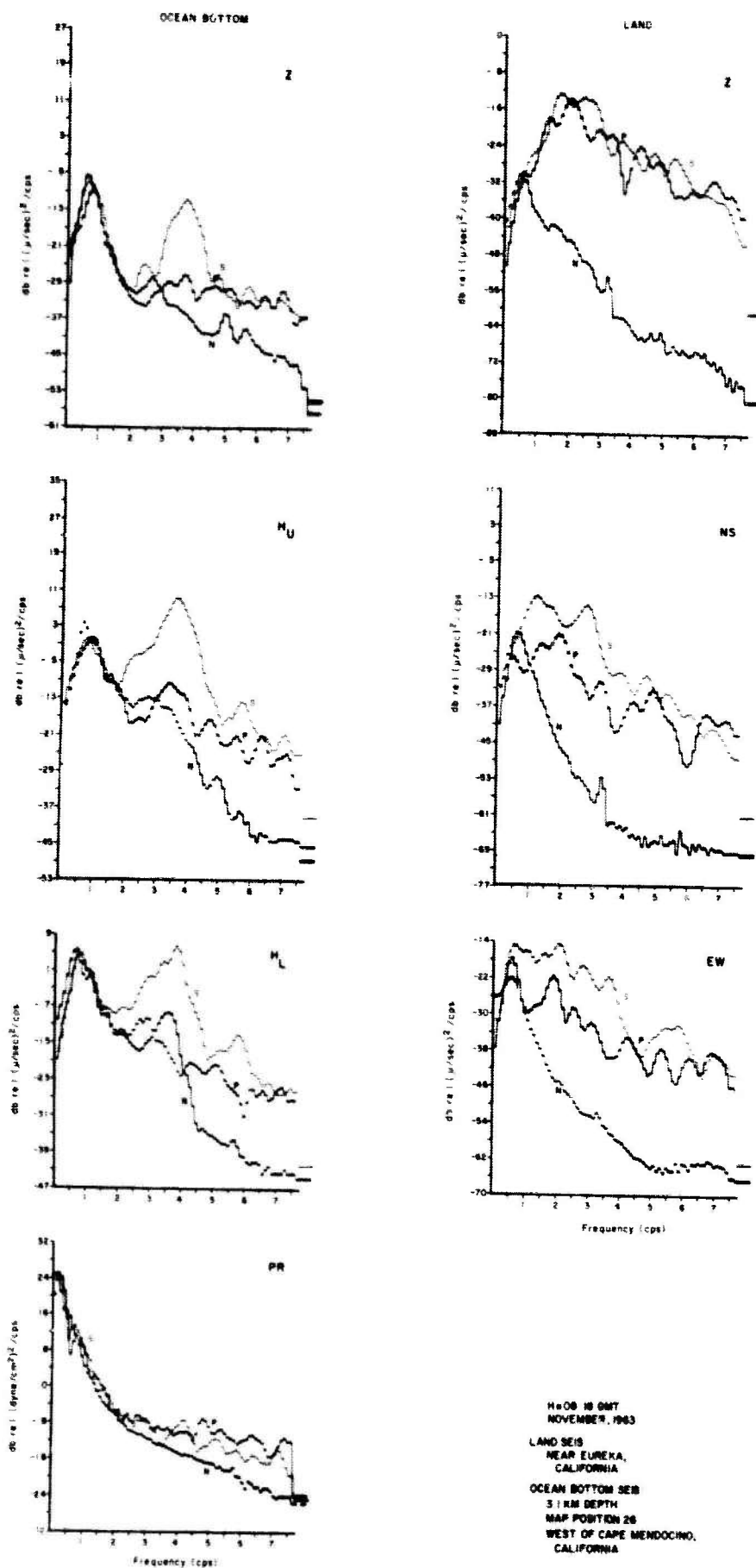Figure 46.   Local Events No. 61 and No. 62 (Near Cape Mendocino, Calif.)

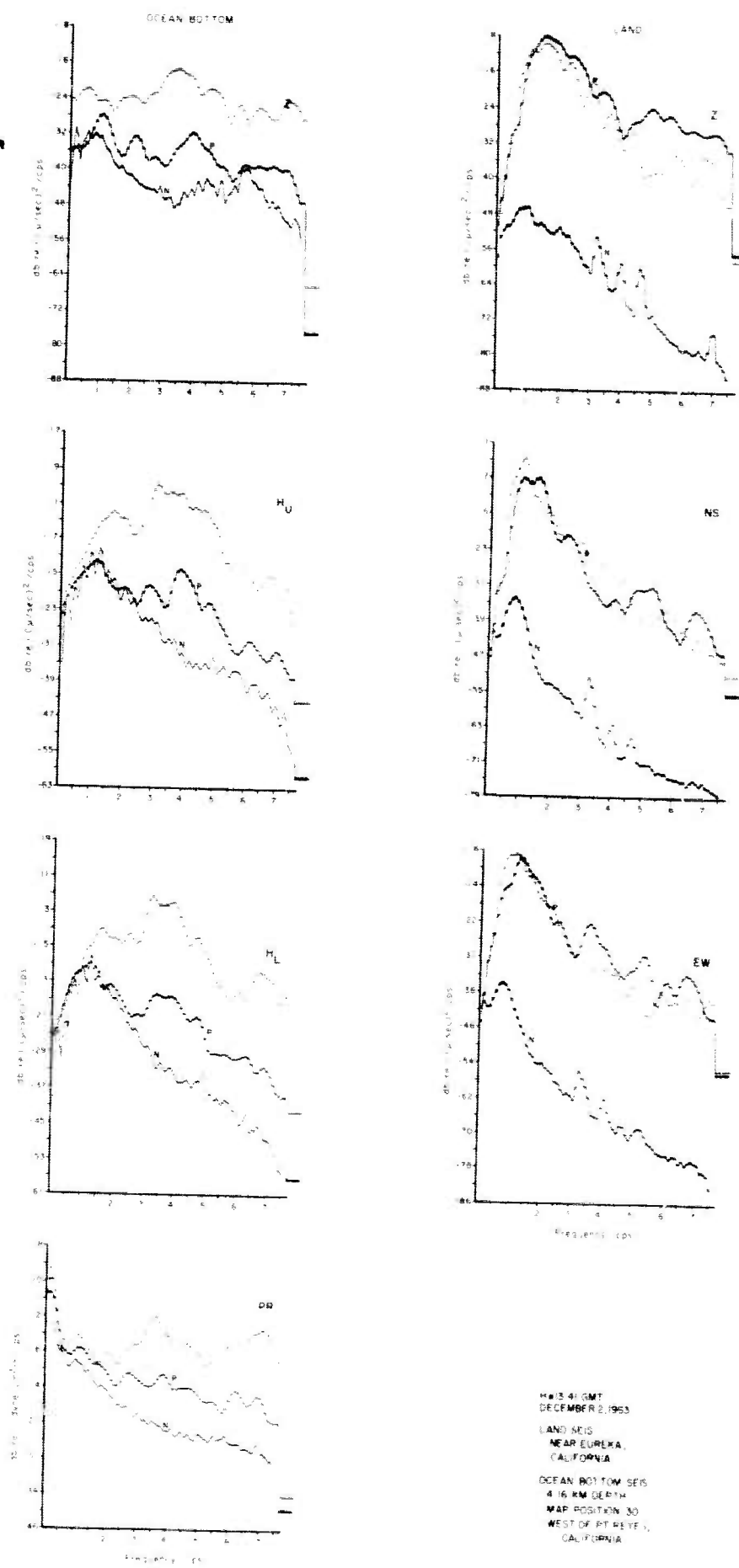Figure 47.   Unlocated Event No. 61 Spectra

Figure 48.   Local Event No. 62 Spectra

the noise field was highly directional (direction unknown) for the duration of the recording. The implication is that the bottom motion consisted predominantly of shear motion, perhaps propagating as Love waves. The resonances are as yet unexplained, but may be related to normal or leaky Love wave propagation involving sub-bottom crustal layering.

2. Teleseismic Events 64 and 65

Teleseisms 64 and 65 from the Svalbard Island and Kurile Island regions are shown in Figure 49. Neither of these events particularly distinguishes itself above the noise. Event 64 was recorded at position 30 in 4.16 km (13,850 ft) of water. The power spectra plots in Figure 50 reveal a signal of about 4 db on the ocean-bottom vertical and pressure in the 0.5 to 1.5 cps band. The same band on the land vertical shows a comparable signal-to-noise ratio. At higher frequencies, the "signal" plots drop below the noise spectra, which means, in actuality, the noise level for this sample was below the average at those frequencies. Neither the ocean-bottom nor land horizontals show any signal energy. An ocean-bottom magnification of about 10-12 db is indicated on the vertical components.

Event 65 from the Kuriles was recorded at position 31 in 4.17 km (13,900 ft) of water. Although the ocean-bottom velocity components are displayed, due to severe cable induced resonance problems which prevented obtaining an average noise spectrum, they were not analyzed. The pressure and land spectra are shown in Figure 51 for this event. The land vertical and North-South horizontal show about 4 to 6 db of S/N ratio at 1 cps. The pressure indicates about 3 db in the 0.5 to 1.5 cps band. The pressure noise level increase between 4 and 7 cps is the result of cable jerks present on other sections of the tape.

3. Nuclear Test Shot, November 22, 1963

The only nuclear blast recorded during the collection phase is presented in Figure 52. The top half of the figure is unfiltered on the low end and the bottom half has been played back through a 1.2 cps low-cut filter. The event was recorded in 1.47 km (4900 ft) of water, 25 miles SW of Pt. Sur, California (not shown in Figure 45). The epicenter distance is approximately 700 km from the land site and 450 km from the ocean-bottom station. The records show a weak onset and gradual buildup of energy with no clear phase definition for the ocean-bottom recording.

The land on the other hand appears to have ample character; however, what can be seen on the record is mainly noise with perhaps a strong cultural component on this day. The verification of this comes from the spectra of Figure 53. The land "signal" spectra are similar to the average noise.

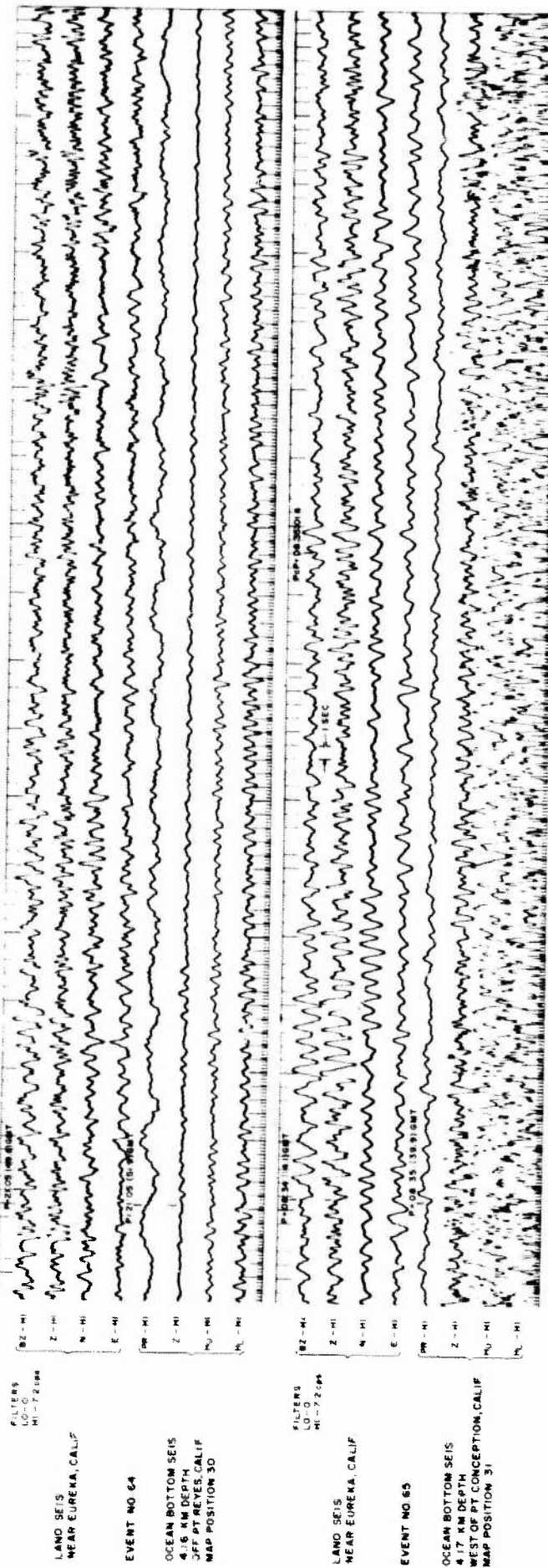Figure 49. Teleseismic Events No. 64 and 65
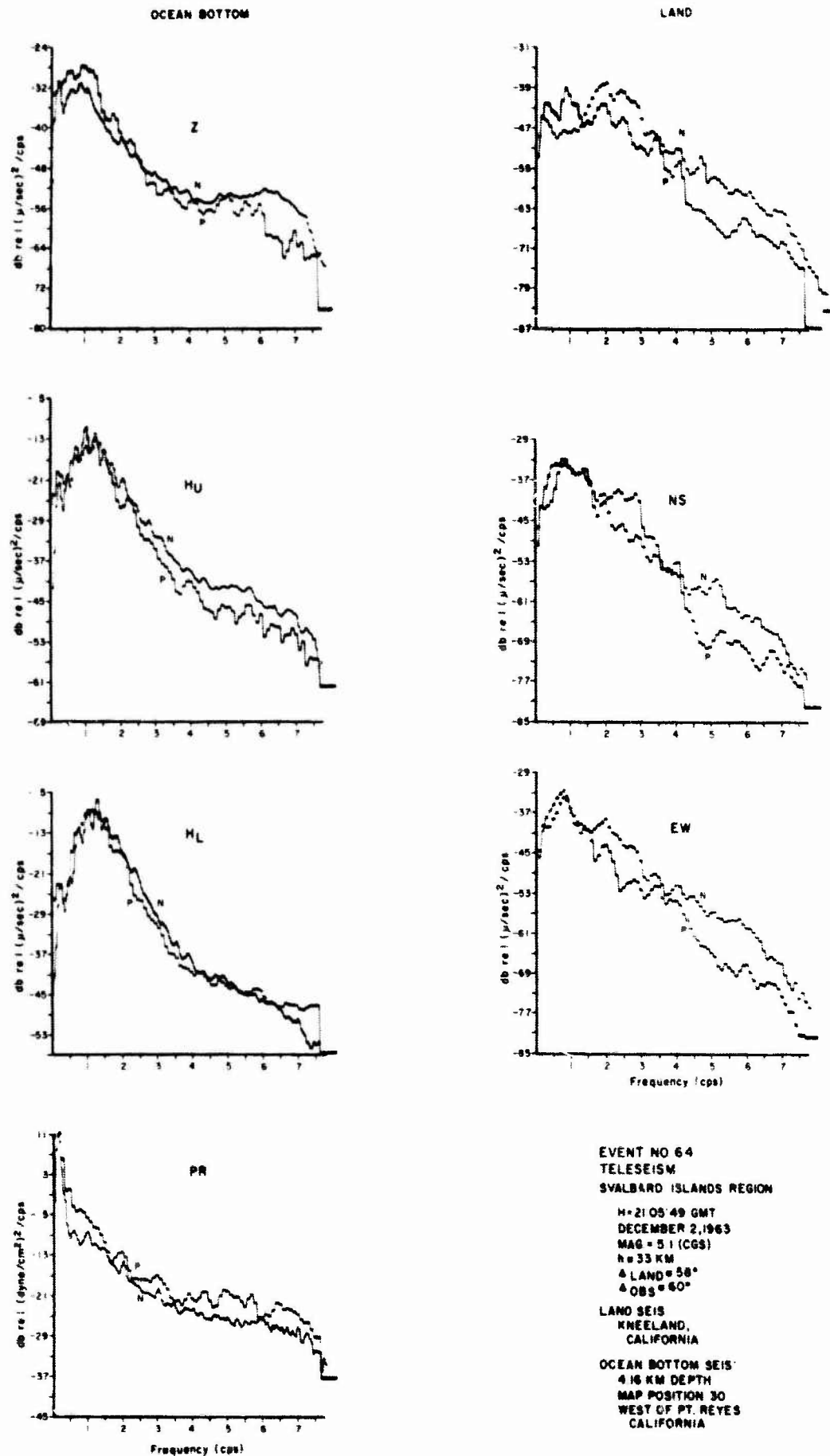
Figure 50.   Event No. 64 Spectra
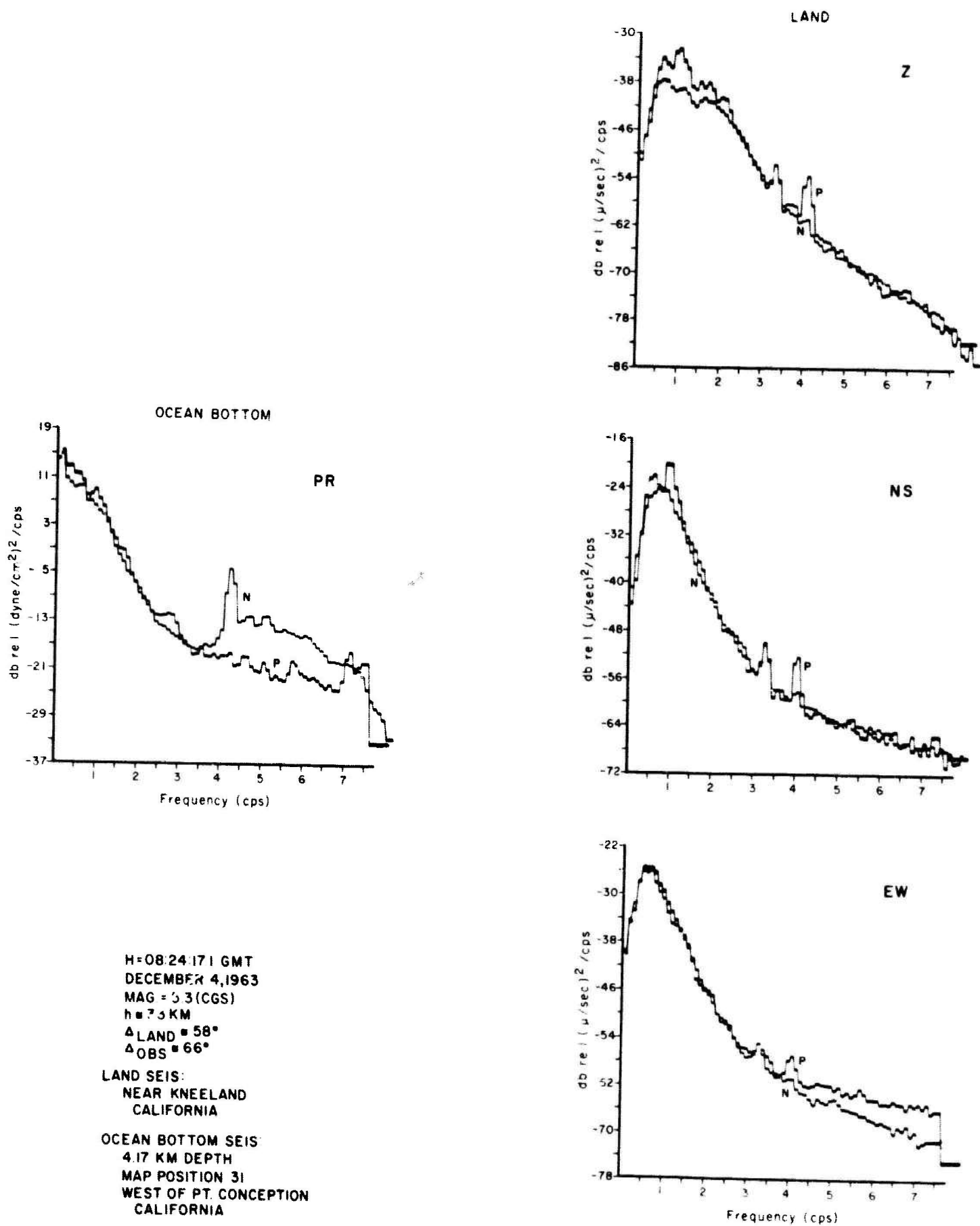
Figure 51.   Event No. 65 Spectra

Figure 52. Nuclear Test Shot, Event No. 59

OCEAN BOTTOM

LAND

NUCLEAR TEST SHOT
NEVADA

H #17 30 00 GMT
NOVEMBER 22,1963
Δ LAND # 6°
Δ OBS # 4 3°

LAND SEIS
NEAR EUREKA,
CALIFORNIA

OCEAN BOTTOM SEIS
1 47 KM DEPTH
25 MILES SW OF
PT SUR,
CALIFORNIA

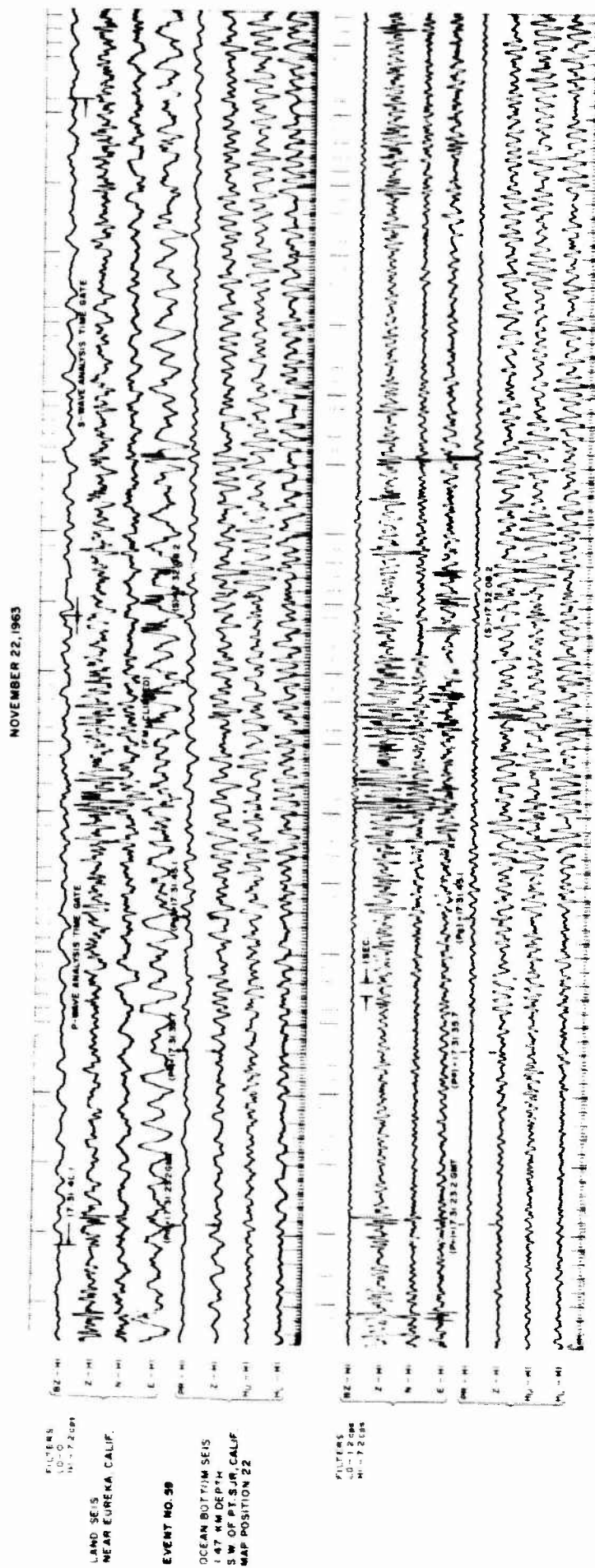Figure 53.   Event No. 59 Spectra

77

Whether or not any actual signal is present above the noise is problematical. The presence of signal on the ocean bottom on the other hand is undeniable. Signal-to-noise ratios are good on all components out to about 5 cps. The interference of direct and reflected arrivals off the water surface can be seen in the ocean-bottom signal spectra on all components. This results in notches in the pressure spectrum and peaks in the velocity spectra at f = 0.5, 1.0, 1.5 etc. At least four of these can be seen on the pressure component. If signal is present on land, the difference in level between the vertical components is about 25 db. The range correction reduces this to about 17 db, which is rather surprising and significant if true. For this event the ocean-bottom horizontals appear to be well behaved and essentially resonance free.

It is unfortunate that the land site did not record the nuclear blast, for it may have provided useful information relating to possible classification criteria differences between land and ocean-bottom recorded nuclear events at first zone distances.

In summary, the California drops during November and December yielded: 1) two teleseisms showing similar S/N ratios, and the now familiar ocean-bottom magnification; 2) two local events favoring the land in S/N ratio and the ocean-bottom in high frequency content; and 3) one nuclear shot well recorded on the ocean bottom and probably not recorded on land. In addition, one location (position 30 off Point Reyes) resulted in very interesting and unusual ocean-bottom noise consisting of highly directional bottom shear motion with a well developed odd-harmonic structure.

D. ALEUTIAN REFRACTION PROFILE

As part of the Aleutian data collection program, a refraction profile was planned across the Island arc using two-ship recording and shooting large charges at almost all of the positions shown in Figure 1. Due to unfavorable weather conditions, very few of the simultaneous shot and drop measurements were conducted. All of the shots were, however, recorded at the Adak land station giving two single coverage refraction profiles north and south of the chain. An initial analysis of the data was reported on in Semiannual Technical Report Number Five. The same data has subsequently been reanalyzed with somewhat more care and greater detail. Keeping in mind the uncertainty of single coverage refraction profiles, the following results are presented.

Figure 54 shows the seismograms recorded on the Adak vertical component for the suit of shots north and south of the chain. The charge size, as well as well as distance and shot number (or map position), is indicated. The traces have been equalized on a mean amplitude basis for visual presentation. The equalization factors are the numbers by which the traces should be multiplied to convert them to their correct relative levels. All the traces
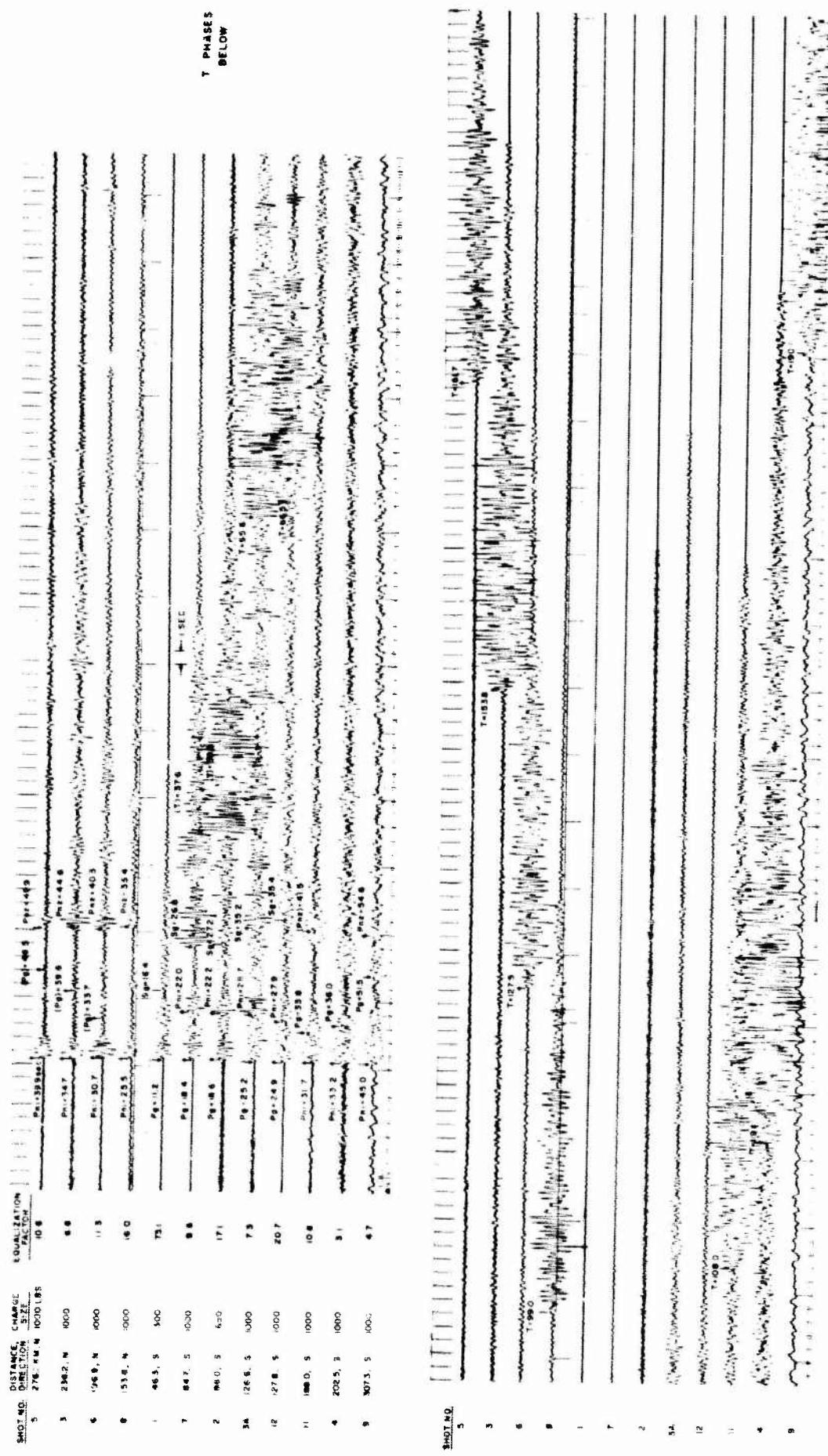
78

Figure 54. Refraction Shots Vertical Component, Recorded on Adak Island

79

are aligned on the first arrival. A number of phases are evident on the seismogram, the more common of which are P_n, P_g, S_g and the water arrival or T phase. In addition, the north shots show arrivals delayed by 10 seconds which are equally strong as the first arrival and similar in waveform. A likely explanation for this arrival is shown in Figure 55 where the various phases have been plotted in the usual time-distance manner. On the north, P_{n1}, or the first arrival with mantle P velocity, is followed by a second phase with the same phase velocity of 8.5 km/sec, but delayed by 10 sec as previously stated. Using a crustal thickness of 14 km north of the chain, Shor, 1962, an event which traverses the path shown for P_{n2} would have the correct delay and phase velocity. There is no evidence of a water bottom reflection on the north side, suggesting the bottom reflection coefficient at these frequencies is quite small. P_g north of the arc is highly tentative, which leaves essentially only the two P_n phases shown. The higher-than-normal mantle velocity could be due to increasing crustal thickness towards the chain. Without a reverse profile, this is only a supposition. The situation south of the arc is considerably more complicated with not only P_n but also P_g and S_g. South of the trench, there is also some evidence of a P_{n2} phase which requires an 11 km crust. A distinct disturbance in the phases occurs at about the position of the trench. P_n appears to be displaced by about 4.5 seconds with an apparent change in velocity and S_g is difficult to pick at greater offsets. Only P_g carries across reasonably undisturbed, though none of the later picks on the south side can be called unambiguous. The indicated structure below the Island chain is purely conjecture and probably bears no resemblance to reality. The unambiguous P_n velocity south of the trench is also higher than normal mantle P velocity; however, crustal thickening may be a factor here as well. The P_g velocities are in fair agreement with Shor's Aleutian refraction data.

In an attempt to ascertain whether or not there are propagation differences north and south of the arc as pertains to attenuation, Fourier transforms were taken over the P refraction arrivals from shots north and south of the arc at the longer offsets. Plots of total energy vs range indicate an approximate amplitude decay law of $\frac{1}{r^2}$; however, the scatter in the results was

greater than any likely difference between the north and south shots. A critical assumption here is that all the shots put out the same energy.
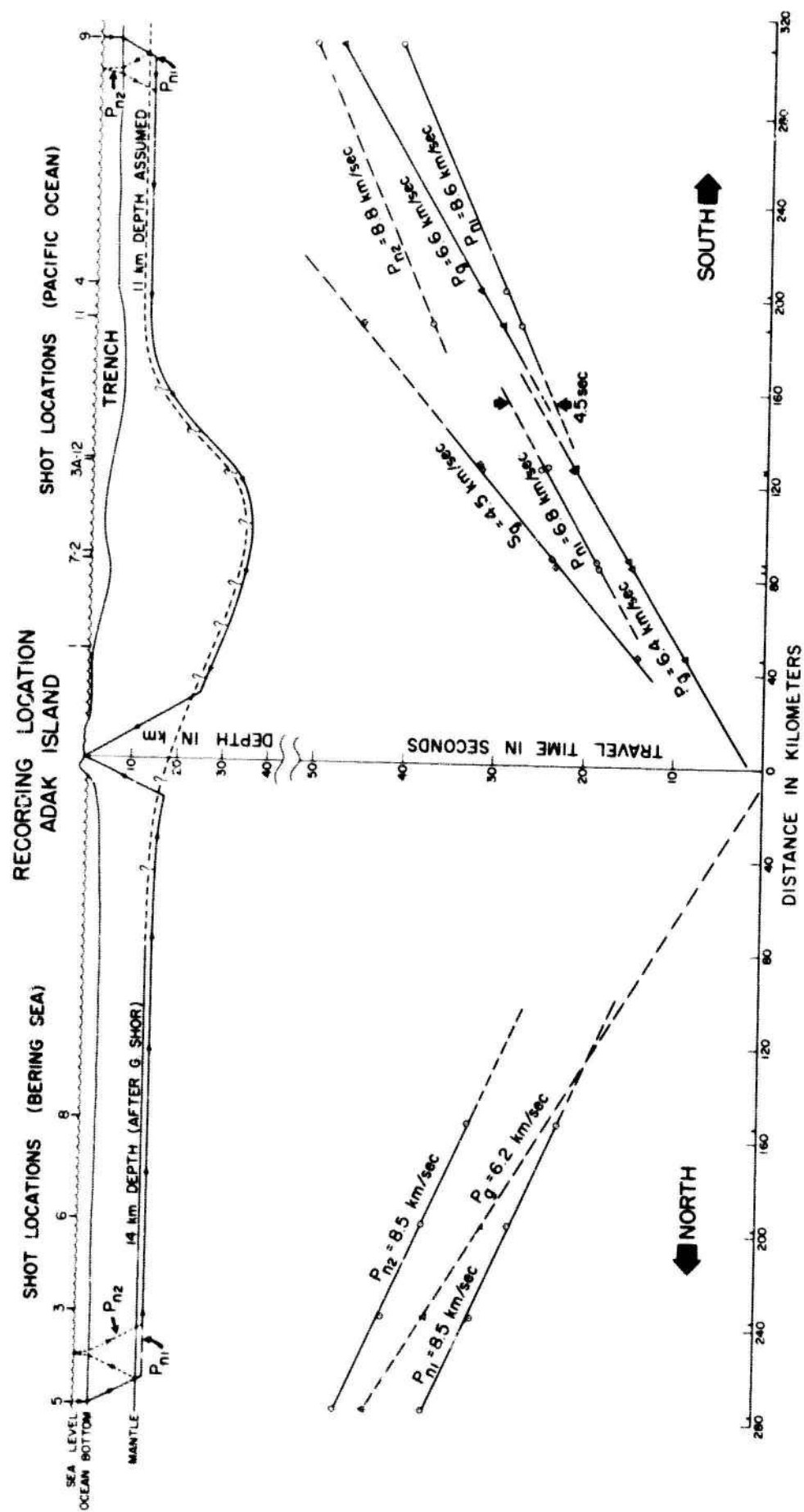
80

Figure 55. Aleutian Islands Seismic Refraction Study

SECTION III

STATISTICAL COMPILATION OF ANALYSIS RESULTS IN THE THREE PACIFIC COLLECTION AREAS

In order to distill and collect some of the more useful results of the noise analysis into a few curves, certain averages on the data have been performed. These relate to average noise spectra for the California, Aleutian and Hawaii areas.

These averages were obtained from all of the individual noise samples computed. The results were corrected for instrument response below 1 cps. Averages were computed in the one decade frequency band (0.2 to 2 cps). The low frequency limit is set by the resolution of the spectral estimate, and the high frequency limit was determined as the approximate useful upper limit on the ocean-bottom ambient. Noise at higher frequencies on the ocean bottom is more often than not in the instrument noise range due to low modulation levels.

Figure 56 shows the average noise spectra for the ocean-bottom vertical, pressure, and land vertical for the three drop areas. The numbers beside the curves indicate the number of days the average represents. Each day's spectrum is itself an average of five noise samples taken over a time span of approximately 5 hours. Therefore, an average of 10 days' noise is actually an average over 50 noise samples spanning approximately 50 hours of ocean-bottom recording. Perhaps the most significant result is the small variation in the average spectra between different Pacific Ocean provinces, particularly for the ocean-bottom components. The spread in noise between areas on the ocean bottom is about 5 db on the vertical component, and varies from 0 db at 2 cps on the pressure to 10 db at the lowest frequency(0.2 cps). The spread of land noise ranges between 5 and 15 db vs frequency. The increase in the Hawaii land noise above 1 cps is, of course, evident in the various spectral plots. It is most likely the result of recording close to the coast and picking up surf noise. The level difference between the land and ocean-bottom vertical components is evident from the figure, but can perhaps be viewed more quantitatively in Figure 57 showing the ocean-bottom-to-land noise power ratio vs frequency for the three areas. Notice the closeness of the Aleutian and California ratios, even to the hump at about 1.2 cps. The lower Hawaii ratio is principally the result of higher Hawaii land noise than lower ocean-bottom noise as Figure 56 indicates. All three curves decrease by about 10 db in going from lowest to highest frequency. This trend, if it continues would favor the ocean bottom as the quieter site at the higher frequencies, say $f > 3, 4$ cps. Unfortunately, our present data does not allow us to answer this unequivocally. The results of Bradner's 1964 Hawaii ocean-bottom-to-land noise comparisons are in substantial disagreement with these, in that
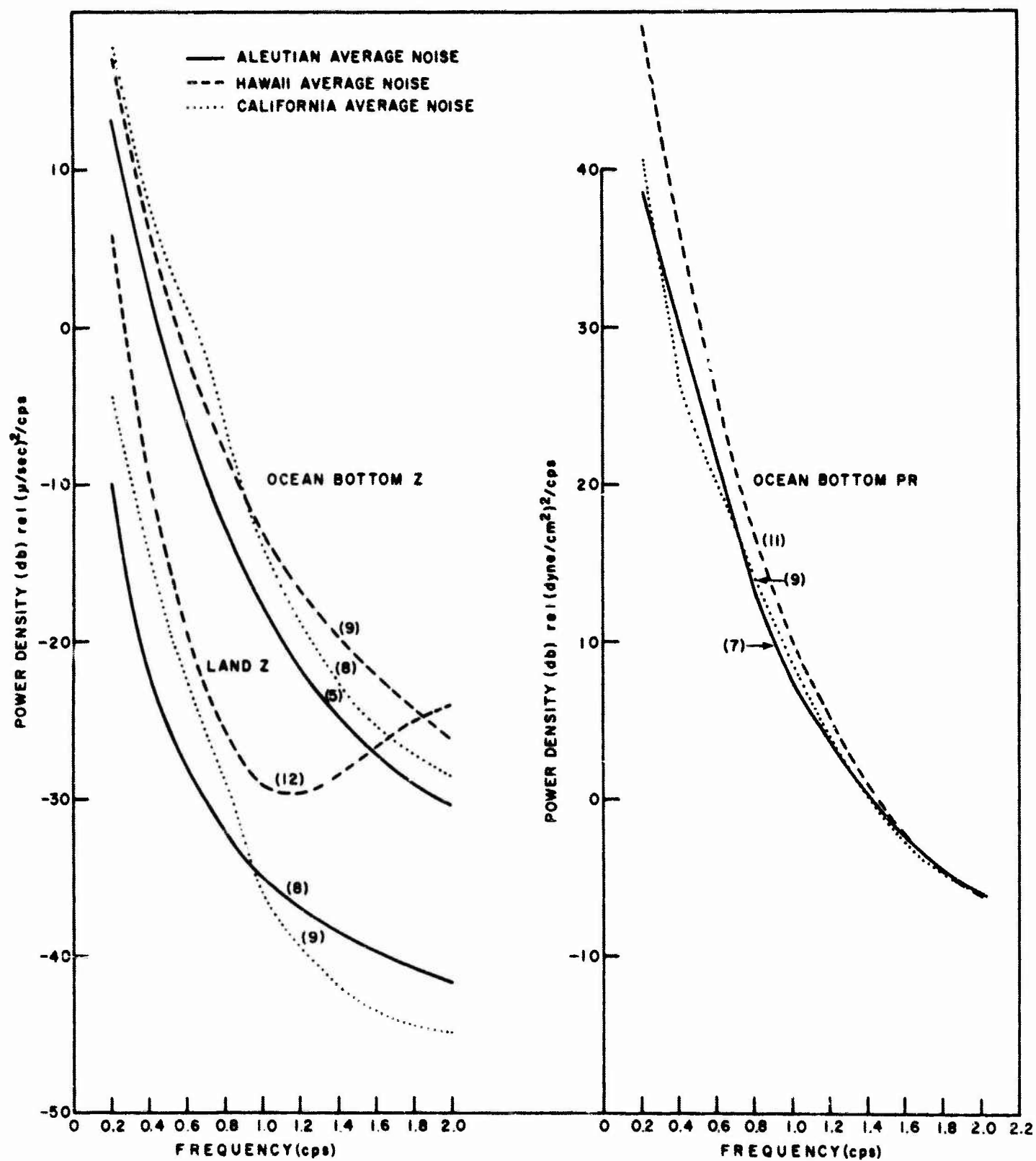
Figure 56.   Average Ocean Bottom and Land Spectra in the Aleutian, Hawaii and California Drop Areas
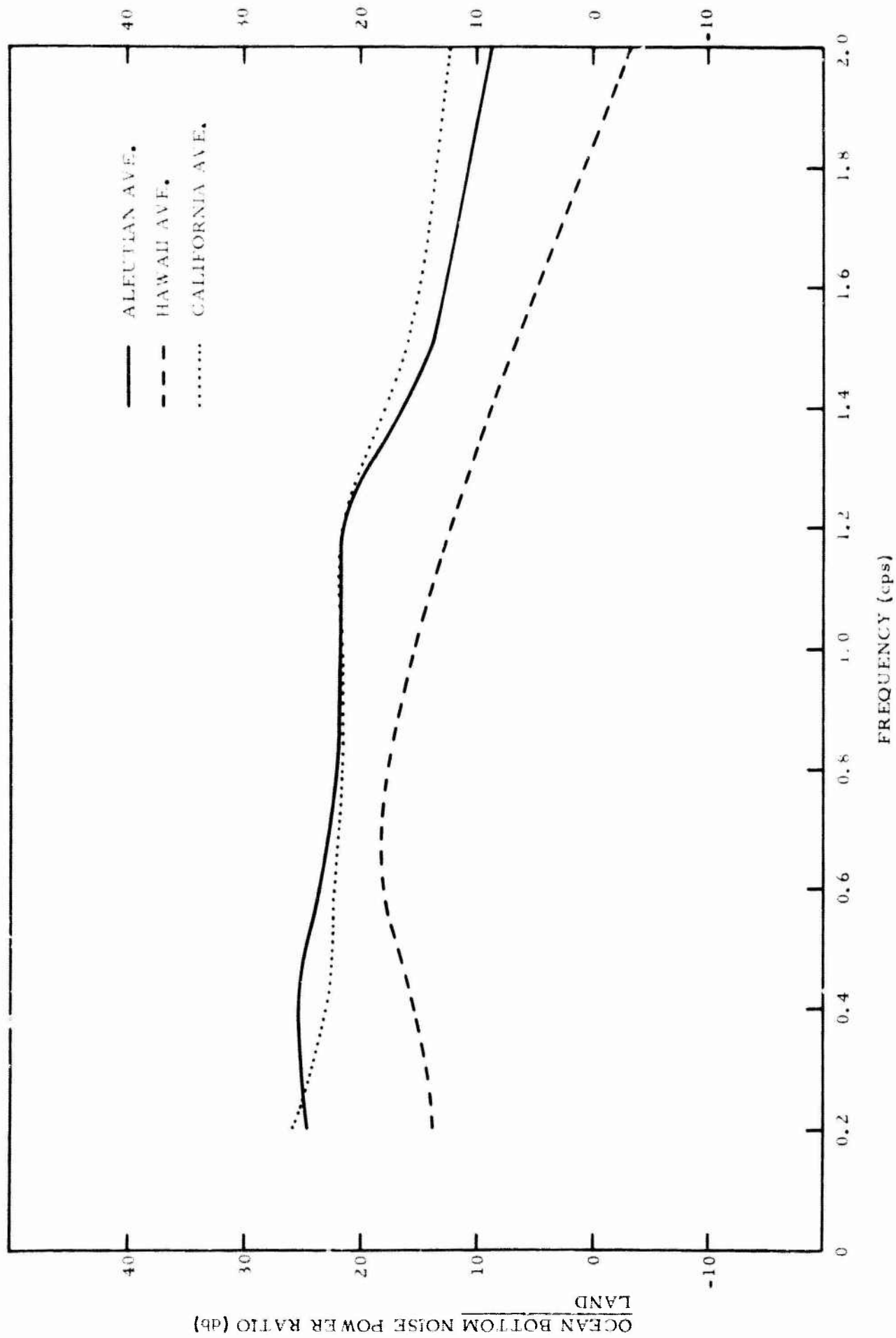
Figure 57. Ratio of Ocean Bottom to Land Noise Power vs Frequency

they show diverging noise levels with increasing frequency. In Figure 58 one of Bradner's noise sets for the Hawaii area is compared to the average obtained here.

Bradner's land instrument was located on Oahu in Waihole Tunnel, and the ocean-bottom instrument, at coordinates $19°$, $58'N$ and $151°$, $11'W$ in 17,300 ft of water. The comparison in Figure 58 is rather interesting in that the land results agree most closely up to about 0.6 cps, at which the surf noise presumably becomes important. The ocean-bottom comparison on the other hand is poor at all frequencies except the very lowest. We offer no explanation for the discrepancies in the ocean-bottom spectra, for they may well exist. We have not, however, observed the multitude of spectral peaks in our Hawaii noise analysis that Bradner reports; nor, for that matter, has such structure appeared in any of our ocean-bottom noise analysis (excluding resonance artifacts), save for one case off Point Reyes, California where the horizontal components show a well developed odd harmonic structure in the spectra unrelated to package resonance.
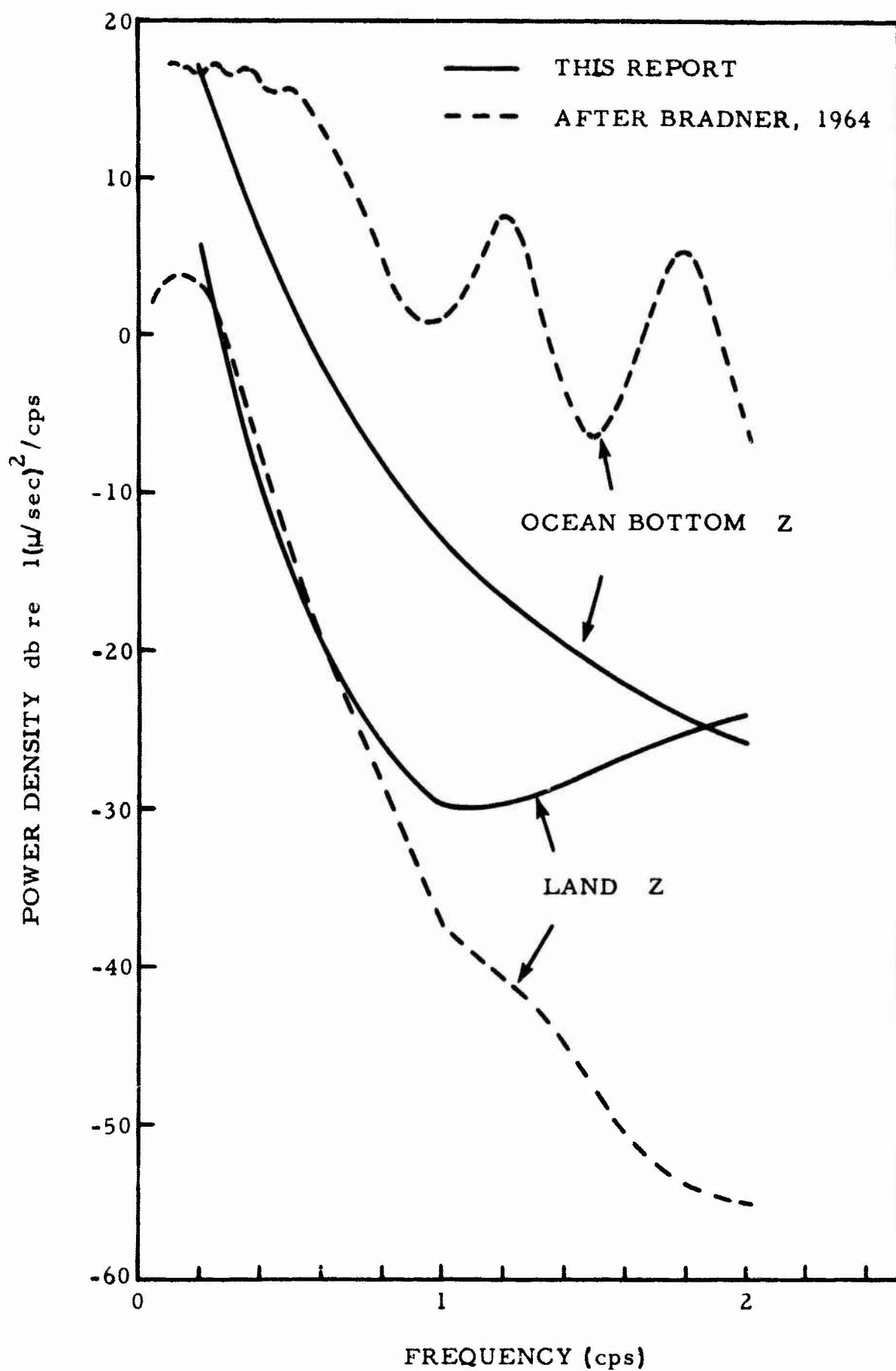
Figure 58. Comparison between Hawaii Ambient Noise Spectra Results Obtained in this Study and the Results Obtained by Bradner
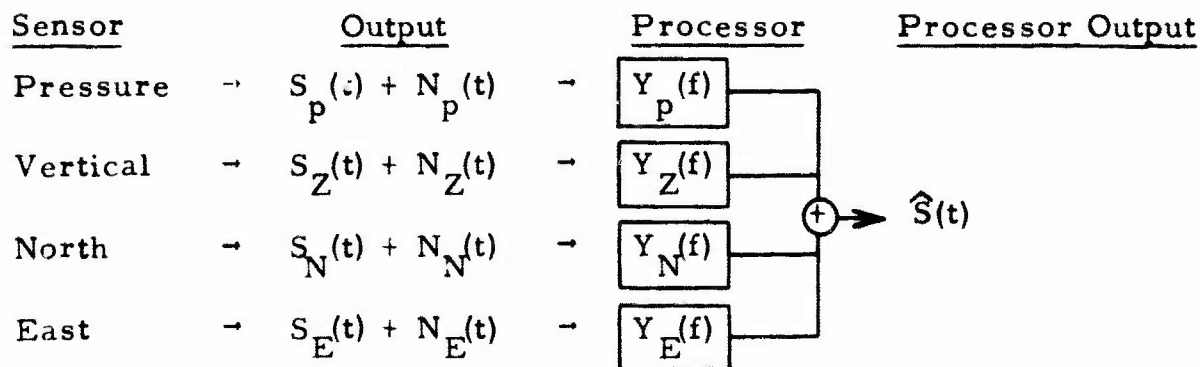
SECTION IV

PRESSURE - VELOCITY RELATIONSHIP

In previous analyses certain aspects of the pressure-vertical velocity relationship at the ocean bottom have been explored as they relate to signal detection and noise definition. In particular, studies of first motion, pressure-velocity power ratio, sum and difference traces have verified simple theoretical predictions for emergent signal events. (Semiannual Technical Report No. 3, Collection and Analysis of Pacific Ocean Bottom Seismic Data, Ocean Bottom Seismic Measurements off the Coast, 1964.) Our understanding of the noise field has also been assisted by examinations of the pressure and velocity relationships of the noise field. The two most consistent conclusions that can be drawn are: 1) the noise field appears to be non-directional the majority of the time, and 2) the low frequency end of the spectrum $0.1 < f < 1.0$ shows pressure-vertical velocity phase relationships consistent with normal mode propagation (see Section V, Ambient Noise).

In addition to studying the pressure-velocity relationships for the noise field to ascertain information about the latter concerning modes of propagation, directionality, time stationarity, etc., we are also vitally interested, from a signal extraction standpoint, to know what is the mutual dependence of one component upon the others for ambient noise on the ocean bottom.

If the noise field is strongly dependent between components, then a processing system can be devised which appropriately combines the components to simultaneously suppress or eliminate the noise and pass desired signal events. To illustrate the system, consider the schematic below:

Sensor		Output		Processor	Processor Output
Pressure	→	$S_p(t) + N_p(t)$	→	$Y_p(f)$	
Vertical	→	$S_Z(t) + N_Z(t)$	→	$Y_Z(f)$	
North	→	$S_N(t) + N_N(t)$	→	$Y_N(f)$	$\widehat{S}(t)$
East	→	$S_E(t) + N_E(t)$	→	$Y_E(f)$	

where $S_p(t)$ is the signal component on the pressure sensor and $N_p(t)$ is the ambient noise on the pressure component (etc., for vertical, north and east), and $\widehat{S}(t)$ is the system output. We would like this to represent as faithfully as possible some desired output S(t), which may represent for instance, the P_n

arrival from a certain azimuth, or a teleseismic P arrival at some Δ. At any rate we can specify the nature of S(t) and its constituent components on the four sensors. The appropriate filters $Y_p(f)$, $Y_Z(f)$, $Y_N(f)$ and $Y_E(f)$ to apply may be computed by minimizing the mean-square-error between the desired output S(t) and the actual system output $\hat{S}(t)$. That is, we wish to minimize the quantity

$$\min \overline{e(t)^2} = \overline{\left[S(t) - \hat{S}(t)\right]^2} \tag{1}$$

with respect to the filters Y_p Y_Z Y_N and Y_S. The minimization is performed by taking the partial derivatives of (1) with respect to the filters and equating to zero. This leads to a system of linear equations with the filters as unknowns. Details of the mathematics may be found in Levinson, 1947; Spieker, Burg, Backus and Strickland, 1961; and Burg, 1964. The coefficients in the equation involve knowledge of only the correlations (auto and cross) between signal and noise on the various sensors. The degree of correlation (or coherence) between signals and noise on the several channels ultimately determines how effective the processor will be in separating signal and noise. Of course, it goes without saying, that high coherence is necessary but not sufficient for separation of signal and noise. These must also be correlated differently between components.

For a preliminary evaluation of the four-channel processing system, it is sufficient to evaluate the mutual dependence (or coherence) of the noise field.

This was accomplished by computing filters to transform the pressure and horizontal components into the vertical noise components as follows:
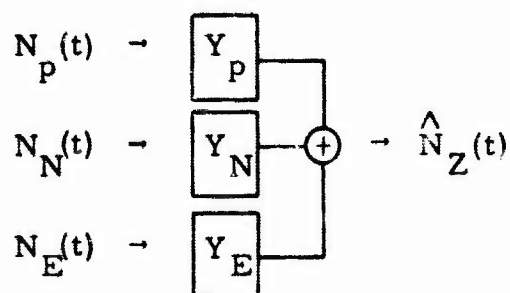
The filters were designed as before on the mean-square-error criteria to minimize the error between the vertical component noise $N_Z(t)$ and its estimate $\hat{N}_Z(t)$ as given above.

Examination of the power spectrum of $N_Z(t)$ and $\hat{N}_Z(t)$ enables one to draw quantitative conclusions about the percentage of the power which is coherent between components, as well as to estimate potential S/N improvement through implementation of such a system.

The analysis was performed on noise recorded on October 12, 1963 at 16,400 ft depth in the Hawaii area. The average power spectra for this day's noise are shown in Figure 24. The sample was selected primarily on the basis of having all components working properly and no strong package resonance. A small resonance at about 5.3 cps is evident on the velocity components in the figure; however, the low frequency portion of the spectra, f < 3 cps, looks "reasonable" on all components. The sample is also typical of all the Hawaii noise in spectrum level; however, no other claims are made for its being representative of all ocean-bottom noise.

The prediction analysis was carried out on an individual noise sample approximately 3-1/2 minutes long, and a noise ensemble average obtained from five 3-1/2 minute noise samples taken about one hour apart. The ensemble average of the noise correlation between components is shown in Figure 59. The pressure autocorrelation differs substantially from the velocity components having significantly more low frequency power. This is due primarily to the difference between pressure and velocity system response for frequencies below the cutoff of 1 cps. The pressure channel has 6 db per octave less attenuation than the velocity components. The cross-correlations are generally small between all components except the pressure and vertical velocity which has a correlation coefficient of approximately

$$\frac{\varphi_{pz}(0)}{\sqrt{\varphi_{pp}(0)\,\varphi_{zz}(0)}} \cong 0.4.$$

Thus, we can conclude without any further analysis that the components (except perhaps the pressure and vertical velocity) are not strongly dependent or coherent for noise averaged over a four or five hour period. It is of interest, however, to determine which spectral regions, if any, are predictable between components, even though we can say in advance the total power will be poorly predicted.

The prediction filters were computed from the ensemble average correlation set to predict the vertical component from the two horizontals, and from the horizontals and pressure. In addition, another set of prediction filters was designed for similar predictions using an individual noise correlation set to determine the amount of prediction improvement for short time interval noise correlation statics.

The filters (from both the ensemble and individual noise sets) were applied to the respective traces of the noise sample from which the individual correlation set was obtained, and the outputs were summed to give the various estimates of the vertical noise component $\hat{N}_z(t)$. The power spectra of the latter were computed and compared with the power spectrum of the vertical noise component $N_z(t)$ to be predicted. The results are shown in Figure 60.
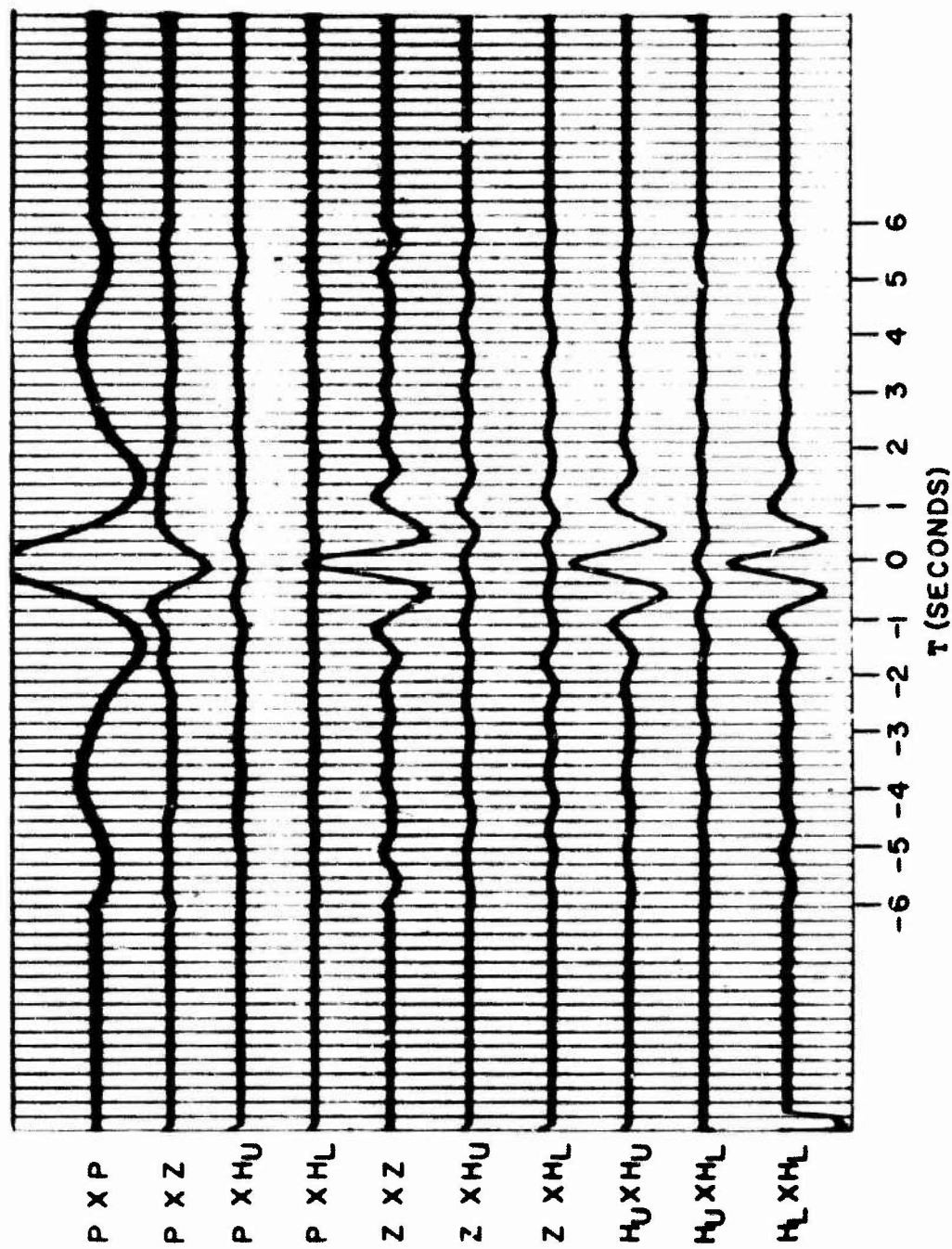
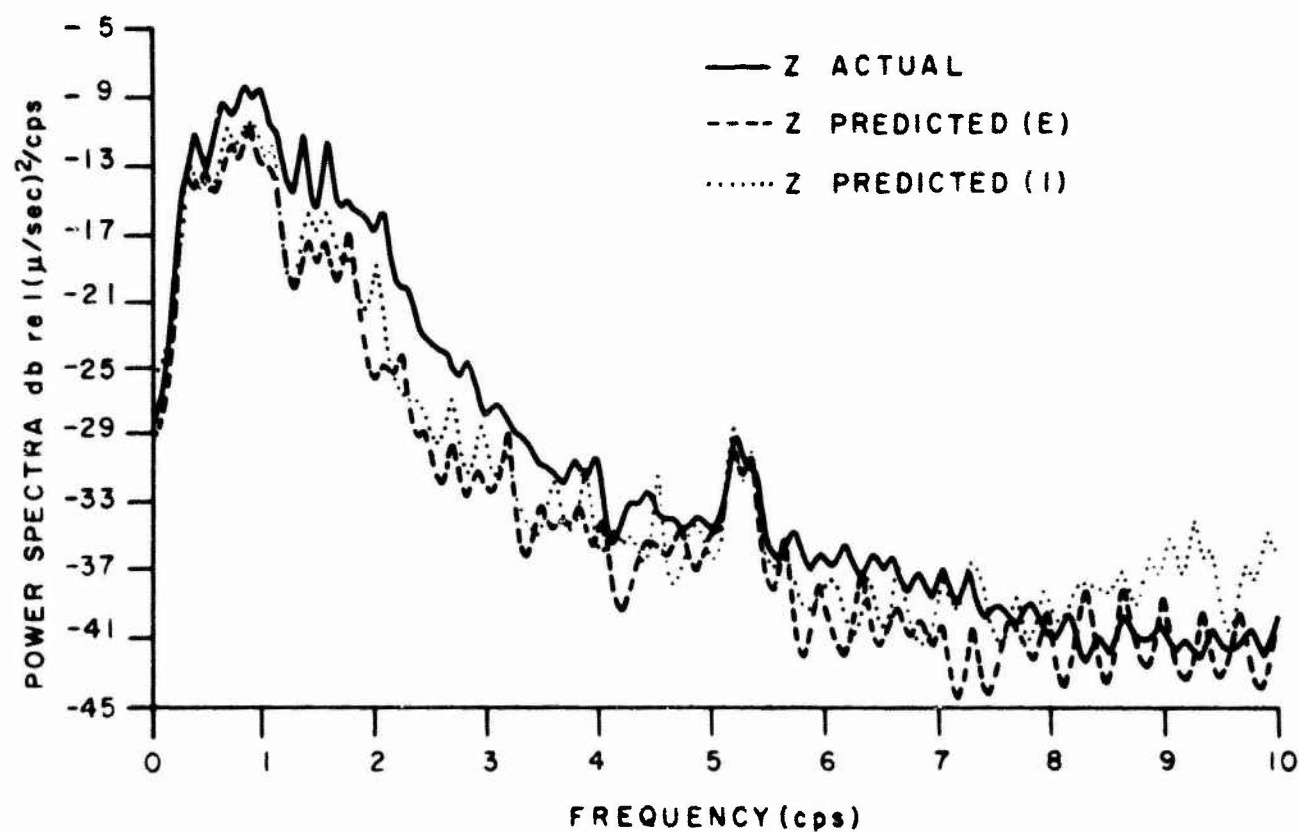Figure 59. Ensemble Average Correlations between OB Seis Components

Figure 60. Spectra of Vertical Component Predicted from Horizontal and Pressure

The top half of the figure displays the predictions using only the horizontals for both the individual (I) and the ensemble (E) correlations. The bottom half shows the predictions of the vertical noise using all three components. The horizontals are not able to predict the vertical component to any significant degree. In the peak region (0.2 to 2 cps) only about 10 - 15 per cent of the power is coherent between the vertical and horizontal components for the ensemble estimate. The individual estimate is an average of 3 to 6 db better than the ensemble over the total band, but still falls short of predicting a major part of the vertical spectrum. The small resonance band at 5.2 cps is nearly perfectly predicted by the horizontal components on both the individual and ensemble estimates. This says that this particular package resonance is linearly related between the three velocity components, and is stable over at least a five hour period.

The three channel predictions in the bottom half of the figure do substantially better in the low frequencies. This is solely due to the addition of the pressure trace, which boosts the coherent power to about 45 per cent over the total band. That is, approximately one half the total power on the vertical component is predictable from the pressure and horizontal components, with the pressure alone contributing about 35 per cent. The ensemble and individual predictions differ by only one - two per cent in total power for this case. In the low band of about 0.2 to 0.8 cps, the pressure prediction comes within about 2 db of the vertical spectrum. This is the region where high pressure-vertical velocity noise coherence is normally observed. The nearly perfect prediction of the 5.2 cps resonance is again due to the horizontals.

In summary, the noise prediction analysis allows the following tentative conclusions concerning use of the ocean-bottom seismometer as a point, four-channel processor for signal-to-noise improvement:

(1)   The horizontal components for noise appear to be very weakly coupled to the vertical and pressure on either a long or short term basis. This is consistent with the majority of our coherence computation between components. The horizontals consistently show low coherence except at obvious package resonances. Therefore, it is unlikely that the horizontals would be used in a signal enhancement processor.

(2)   The pressure and vertical velocity components are moderately coupled for noise at the low frequencies. If all the coherent noise between pressure and vertical is separable from signal, a signal-to-noise improvement of 3 db is indicated from the results. While this is not very astounding, it is believed sufficiently encouraging to pursue in conjunction with array studies from the multiple ocean-bottom units now in operation.

(3)   The per cent prediction of the noise does not improve
        significantly in going from an ensemble average over
        several hours to an individual correlation set from 3
        minutes of data.   This implies that the noise field is
        reasonably stationary in frequency distribution as well
        as spatial distribution for t'is day.   The generally poor
        prediction of the vertical noise from the horizontals even
        at the low frequencies implies that the noise field is rather
        omnidirectional in the horizontal plane.

(4)   The lack of noise prediction between the pressure and vertical
        in the 1 to 6 cps band is possibly due to:

        (a) presence of several higher noise modes, and/or

        (b) poor ambient to instrument noise ratio.

The dynamic range of the tape recorder is about 40 db from full modulation.
Forty decibles down from the vertical spectral peak occurs at about 4 cps, and
the data was not recorded at full modulation.   Therefore, it is reasonable to
expect that the data beyond 4 cps and possibly 2 cps is instrument or tape noise
corrupted.   Data from the new units will prewhiten the ambient noise and
make better use of the dynamic range, thus extending the upper limit of our
noise analysis.

SECTION V

AMBIENT NOISE

In addition to spectral averages computed for the ocean-bottom noise presented in Section III, certain other features of the noise field have been inferred from study of the relationships between components. The major analysis tools used in studying the inter-component relationships for ambient noise are t'.e cross-correlation, cross power amplitude and phase spectra, and coherences, which may be interpreted in terms of propagation modes and directionality. The propagation velocities are of course inaccessible with a single instrument, but will be studied with multiple ocean-bottom units.

Utility of the above-mentioned analyses in ferreting out information about the ambient noise field stems from the fact that the various possible modes of propagation in the oceanic waveguide have different pressure, particle velocity relationships. The degree to which these relationships manifest themselves in the quantities computed above determines what inferences may be made about the noise field.

Consider first the normal mode contribution to the ambient spectrum.

A. NORMAL MODES

The steady state displacement potential for the normal modes in a liquid over a layered half space (Ewing, Jardetzky, and Press, 1957) is given by

$$= \frac{2}{H}\sqrt{\frac{2}{r}} \sum_{n=1} \frac{1}{\sqrt{K_n}} e^{i(wt - K_n r - \frac{\pi}{4})} \tag{2}$$

$$x \cdot (K_n) \sin\left(K_n h \sqrt{\frac{C_n^2}{C^2} - 1}\right) \sin\left(K_n Z \sqrt{\frac{C_n^2}{C^2} - 1}\right)$$

where C = velocity of sound in water

$C_n = \frac{2\pi f}{K_n}$ = phase velocity of nth mode

and (K_n) = function of K_n and elastic constants of bottom layering.

The steady state pressure and vertical velocity at the bottom are obtained from (2) by differentiating with respect to time and the Z coordinate:

$$P(f) = \rho \left. \frac{\partial^2 \varphi}{\partial t^2} \right|_{Z = H}$$

$$V(f) = - \left. \frac{\partial^2 \varphi}{\partial t \partial Z} \right|_{Z = H} \tag{3}$$

and evaluating at $Z = H$.

Forming the ratio of pressure to vertical velocity we obtain for a single mode:

$$\left. \frac{P(f)}{\rho_c V(f)} \right|_{n = i} \frac{e^{i\frac{\pi}{2}}}{\sqrt{1 - \frac{C^2}{C_i^2}}} \tan \left[\frac{2\pi f H}{C} \sqrt{1 - \frac{C^2}{C_i^2}} \right] \tag{4}$$

where C_i = the phase velocity of the ith mode and H = the water depth.

Equation (4) shows that the pressure-velocity amplitude ratio is a fairly complicated function of frequency through the phase velocity $C_i = f_i(f)$. On the other hand, the phases of pressure and vertical velocity for normal modes differ by 90° independent of frequency. This holds as well for the sum of several modes; however, the amplitude ratio would be more complicated than (4) depending upon the relative excitation of the contributing modes.

Attempts to verify normal mode propagation by comparing the amplitude portion of (4) with measured amplitude ratios has not been conclusive. This is not unexpected, however, because: 1) the elastic parameters of the bottom layering are not known in general, and 2) if several modes are present we do not know their relative excitations vs frequency. Thus, the amplitude portion of (4) does not appear to be a useful diagnostic tool in understanding ocean-bottom ambient. The phase information, however, appears to be of considerable interpretational value.

All of the cross power phase spectra between pressure and vertical velocity reveal a phase difference of 90° at the low frequency end. That is, in the frequency band 0.1 to 0.5 cps, and occasionally to 2.0 cps, the phase difference between pressure and vertical velocity are consistent with normal mode propagation. Considering the frequencies and water depths, probably only the fundamental Rayleigh and first shear mode are contributing to the ambient spectrum for $f < 1.0$ cps. Figure 61 shows an example of the pressure-vertical cross power phase to 3 cps for average noise on October 12, 1963, recorded at the Hawaii map position 10 in 16,070 ft of water. The phase difference is within ± 10° of 90° out to approximately 2.5 cps, beyond which the fluctuations become random and uninterpretable due to low pressure-velocity correlation.
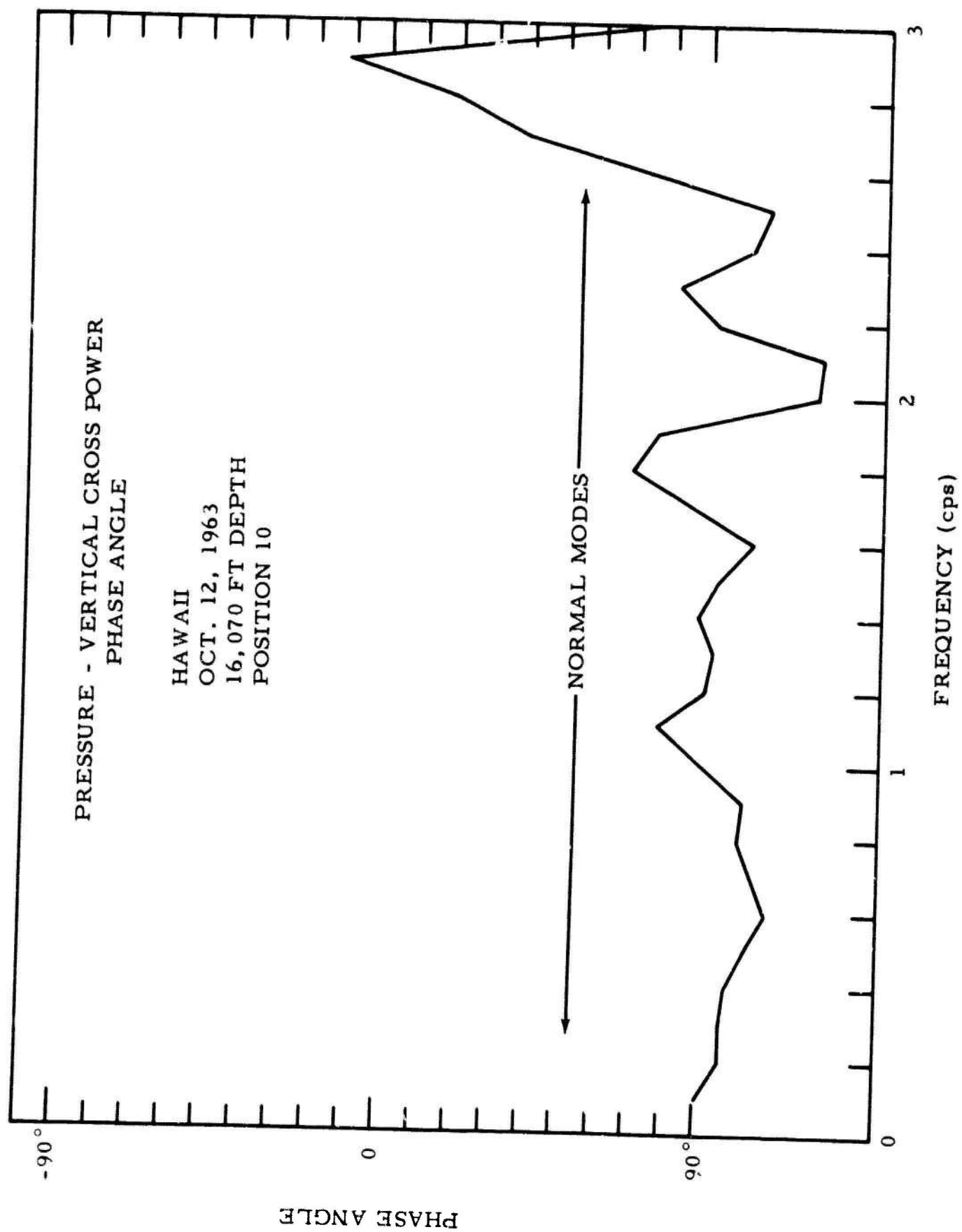
Figure 61. Pressure-Vertical Cross Power Phase Angle, Position 10

The coherence between pressure and vertical velocity is high (coh > 0.9) in this same low frequency band, but drops off rapidly above 1 cps as do the pressure and velocity auto spectra. The latter decrease in coherence between may be due to a combination of: 1) decrease in ambient to instrument noise ratio with increasing f and 2) presence of several modes independently generated.

The horizontal, vertical relationships provide additional information on the nature of the noise field in the low frequency part of the spectrum. For normal modes propagating from a single direction, equation (2) shows that the vertical and horizontal components are also ± 90° out of phase. The sign depends on direction of propagation relative to the orientation of the horizontal component. The ensemble average cross power phase spectra between the vertical and horizontal components do not show consistent ± 90° phase differences, and in fact, are quite random in the low frequency part of the spectra where the ambient energy is concentrated. In addition, the coherence between vertical and horizontal components at these same frequencies is consistently low.

The apparent contradiction between the phase difference and coherence of pressure-vertical which supports normal modes, and that of horizontal-vertical which seems not to, may be resolved by invoking a noise field consisting of the superposition of normal modes from many directions of about equal strength. The cross power spectrum between either pressure-vertical or horizontal-vertical is a pure imaginary quantity for normal modes. Let the noise field consist of a single mode uniformly distributed in azimuth. The contribution to the pressure-vertical cross power from the angular segment $d\theta$ is $i \dfrac{A(f)d\theta}{2\pi}$, and the total cross power becomes:

$$\Phi_{PV}(f) = \int_0^{2\pi} i \frac{A(f)}{2\pi} \, d\theta = i A(f) = A(f) \, e^{i\frac{\pi}{2}} \tag{5}$$

The contribution to the vertical-horizontal cross power from the angular segment $d\theta$ is $i \cos \theta \dfrac{B(f)}{2\pi} \, d\theta$, and the total cross power becomes

$$\Phi_{VH}(f) = \int_0^{2\pi} i \frac{B(f)}{2\pi} \cos \theta \, d\theta = i \frac{B(f)}{2\pi} \int_0^{2\pi} \cos \theta \, d\theta = 0. \tag{6}$$

The condition of perfect isotropy is seldom if ever reached in the oceans, consequently $\Phi_{VH}(f)$ would not vanish, but may be expected to be small if the noise sources are distributed in azimuth. Therefore, low vertical-horizontal coherence and "random-like" cross phase are not inconsistent with normal mode propagation, but rather imply a non-directional noise field in the spectral region

of 0.1 to 1 cps, which encompasses most of the ocean bottom ambient power. These results apply to spectral estimates averaged over several hours duration, and thus do not preclude the possibility that the noise field is directional with time varying directionality. Two findings which tend to indicate this is not the case are: 1) spectra computed from selected individual 3 minute noise samples have not shown high vertical-horizontal coherence, and 2) visual examination of most all the individual correlation sets used in obtaining the ensemble averages reveal that the vertical-horizontal cross-correlations are small (relative to the auto-correlations) before averaging.

In addition to the normal mode contribution to the ocean-bottom ambient spectrum, it has been suggested by Phinney, 1960, and observed by Bradner, 1964, that energy in organ pipe modes is also important.

B. ORGAN PIPE MODES

These modes represent energy multiply reflected within the water layer at angles of incidence less than the critical angle for P refraction in the bottom. These modes are not trapped, but leak energy into the solid bottom at each bottom reflection, and are classed as leaky modes. They suffer attenuated propagation, and are usually inconsequential relative to the normal modes when considering arrivals from a distant source such as an earthquake or explosion. Their possible importance in the ambient spectrum of the oceans results from two factors: 1) the organ pipe modes can persist in the water trap for relatively long times because of the high acoustic impedance at the bottom, and 2) the organ pipe modes may be excited locally within each area of the ocean and, continually replenished by surface wave action of the Longuet-Higgins, 1950, variety, barometric fluctuations, or emergent earthquake body waves.

In order to obtain the predicted pressure and velocity relationships for the organ pipe modes, consider the layer over half space problem depicted in Figure 62.
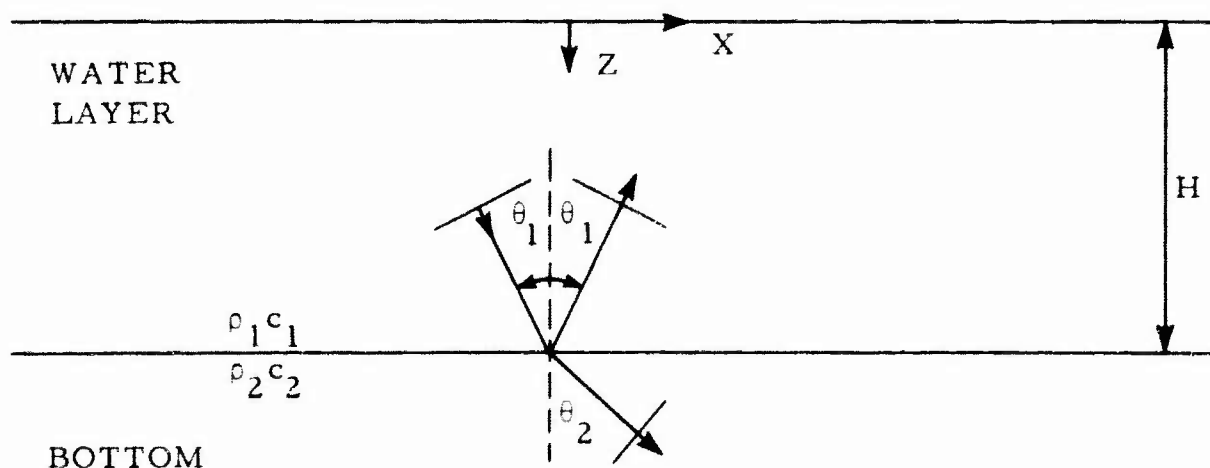
Figure 62. Layer Over Half Space Problem

The bottom is taken as liquid for simplicity; however, this should not alter the significant feature of the organ pipe modes. The velocity potential in the layer and bottom are given by:

$$\varphi_1 = e^{i\bar{w}\left(t - \frac{z\cos\theta_1}{C_1} - \frac{x\sin\theta_1}{C_1}\right)} - e^{i\bar{w}\left(t + \frac{z\cos\theta_1}{C_1} - \frac{x\sin\theta_1}{C_1}\right)}$$

$$\varphi_2 = A\, e^{i\bar{w}\left(t - \frac{z\cos\theta_2}{C_2} - \frac{x\sin\theta_2}{C_2}\right)} \tag{7}$$

The boundary condition at $z = 0$ is automatically satisfied by φ_1,

$$\varphi_1 = 0 \text{ at } z = 0.$$

The boundary conditions at $z = H$ are:

$$\rho_1 \frac{\partial\varphi_1}{\partial t} = \rho_2 \frac{\partial\varphi_2}{\partial t} \tag{8}$$

$$\frac{\partial\varphi_1}{\partial z} = \frac{\partial\varphi_2}{\partial z}$$

which lead to a set of equations:

$$e^{-i\bar{w}\frac{H\cos\theta_1}{C_1}} - e^{i\bar{w}\frac{H\cos\theta_1}{C_1}} = \frac{\rho_2}{\rho_1} A\, e^{-i\bar{w}\frac{H\cos\theta_2}{C_2}}$$

$$e^{-i\bar{w}\frac{H\cos\theta_1}{C_1}} + e^{i\bar{w}\frac{H\cos\theta_1}{C_1}} = \frac{C_1}{C_2} A\, e^{-i\bar{w}\frac{H\cos\theta_2}{C_2}} \tag{9}$$

where $\dfrac{\sin\theta_1}{C_1} = \dfrac{\sin\theta_2}{C_2}$ has been employed to eliminate the x dependence.

Solving the above for A,

$$A = \frac{2\rho_1 C_2 \cos\theta_1}{\rho_1 C_1 \cos\theta_2 + \rho_2 C_2 \cos\theta_1}\, e^{-i\bar{w}\, H\left(\frac{\cos\theta_1}{C_1} - \frac{\cos\theta_2}{C_2}\right)} \tag{10}$$

and substituting in (9) results in the expression,

$$e^{i\bar{w}\frac{2H \cos \theta_1}{C_1}} = -R \qquad (11)$$

where R is the plane wave reflection coefficient

$$R = \frac{\rho_2 C_2 \cos \theta_1 - \rho_1 C_1 \cos \theta_2}{\rho_1 C_1 \cos \theta_2 + \rho_2 C_2 \cos \theta_1} \; .$$

Equation (11) does not have a solution for arbitrary $\bar{w}$; in fact, it requires a complex angular frequency. This is more easily seen by taking the natural logarithm of both sides which gives

$$i\bar{w}\frac{2H \cos \theta_1}{C_1} = \ln -R = \ln R + i\pi(2n - 1) \qquad n = 1, 2, \ldots \qquad (12)$$

or

$$\bar{w} = -i\frac{C_1}{2H \cos \theta_1} \ln R + (n - 1/2)\frac{\pi C_1}{H \cos \theta_1} \; .$$

The real part of the complex frequency yields the organ pipe frequencies directly

$$\frac{1}{2\pi} \mathrm{Re}(\bar{w}) = \frac{(n - 1/2) C_1}{2H \cos \theta_1} \qquad (13)$$

and the imaginary part gives the amplitude decay of the waves due to bottom leakage

$$e^{-\mathrm{Im}(\bar{w}) t} = R^{\frac{C_1 t}{2H \cos \theta_1}} \; . \qquad (14)$$

Substituting the expressions for A and $\bar{w}$ into (7), performing the differentiations $\rho_1 \frac{\partial \varphi_1}{\partial t}$ and $-\frac{\partial \varphi_1}{\partial z}$ to obtain the pressure and vertical velocity, respectively, and evaluating at $z = H$ we obtain:

$$P_{z=H} = \rho_1 \frac{1 + R}{R^{1/2}} R^{\frac{C_1 t}{2H \cos \theta_1}} \sum_{n=1}^{\infty} (-1)^n |\bar{w}| \cos\left[\frac{(n - 1/2)\pi C_1 t}{H \cos \theta_1} + \psi\right] \quad (15)$$

103

$$V_{z=H} = \frac{\cos \theta_1}{C_1} \frac{1 - R}{R^{1/2}} R^{\frac{C_1 t}{2H \cos \theta_1}} \sum_{n=1}^{\infty} (-1)^n \left| \bar{w} \right| \cos \left[\frac{(n - 1/2) \pi C_1 t}{H \cos \theta_1} + \psi \right]$$

where

$$\psi = \tan^{-1} \frac{\ln R^{1/2}}{(n - 1/2)\pi}$$

The ratio of pressure-to-vertical velocity normalized by $\frac{\cos \theta_1}{\rho_1 C_1}$ results

in the remarkably simple expression

$$\frac{\cos \theta_1}{\rho_1 C_1} \left. \frac{P}{V} \right|_{z=H} = \frac{1 + R}{1 - R} \tag{16}$$

which shows that for the organ pipe modes, the pressure and vertical are in phase and differ by only a constant. If these modes are present in the measured ambient, the cross power amplitude spectrum should show the resonant frequencies

$$f_n = \frac{(n - 1/2) C_1}{2H \cos \theta_1} \text{ , with zero phase difference between pressure and vertical.}$$

As previously noted, the ambient energy below 1 cps appears to consist of normal mode propagation, based on the 90° phase shift between pressure and vertical. A number of the average noise cross spectra (about 20 per cent) do show near zero phase between pressure and vertical above 1 cps and extending to 2 or 3 cps depending upon where the instrument noise takes over. An example of the latter is shown in Figure 63 for average noise recorded on October 18, 1964, in 5.4 km (17,932 ft) of water at site 15. Note that the phase starts near -90° at the low end and changes to near zero rather smoothly, indicating the presence of both normal and organ pipe energy in the transition region of 0.5 to 1.5 cps.

This behavior is not nearly as consistent as the presence of a 90° phase shift in the low frequencies; however, it does occur often enough to suggest that the organ pipe modes do contribute to the ocean ambient spectrum. Their role at higher frequencies (2 to 10 cps) may be even more important, unfortunately our data is generally instrument-noise limited in that range.

The cross power amplitude spectrum associated with the phase in Figure 63 does not show the organ pipe frequencies; however, their separation in frequency $\Delta f = \frac{C_1}{2H \cos \theta_1} \sim 0.14$ cps is less than the resolution of the

spectral estimate, approximately 0.2 cps.
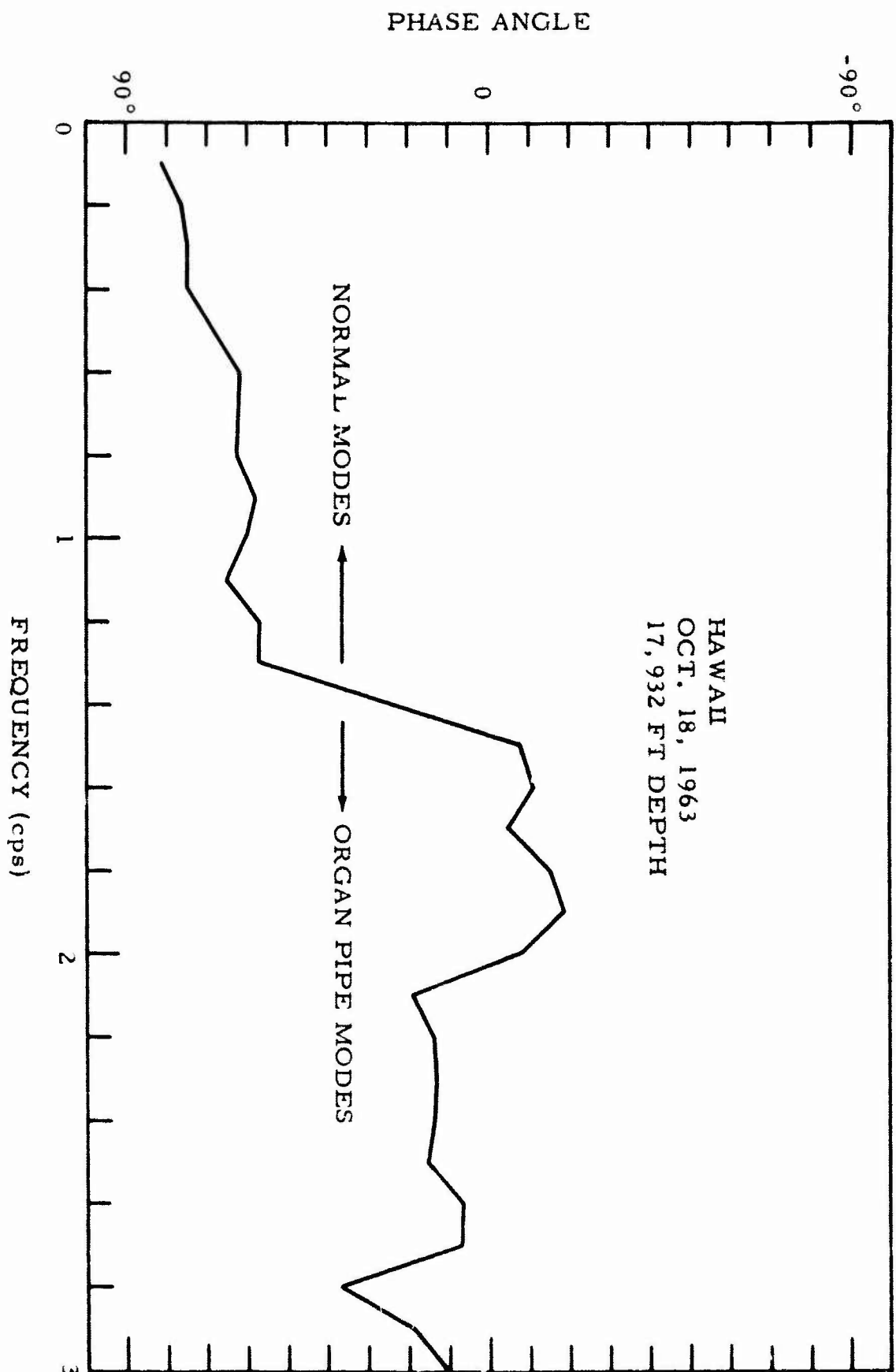
Figure 63. Pressure-Vertical Cross Power Phase Angle, Position 15

C. CONCLUSIONS REGARDING AMBIENT NOISE

In summary, the major conclusions about the nature of the ocean-bottom ambient noise field which can be drawn from the inter-component analysis are as follows:

(1)   For frequencies less than 1 cps the dominant energy is carried in normal modes, based on high pressure-vertical coherence and 90° phase shift. The lack of vertical-horizontal coherence in this band implies noise sources distributed in azimuth.

(2)   Approximately 20 per cent of the noise data indicates the presence of significant organ pipe energy in the band about 1 to 2 cps, based on the zero phase difference between pressure and velocity.

SECTION VI

SUMMARY AND CONCLUSIONS

The signal and noise studies compiled in this report and those of previous reports on ocean-bottom data collected in the Pacific Ocean under this contract, yield the following results and conclusions:

(1) Signal-to-noise ratios on the ocean bottom are generally inferior to those at a land control station by 0 to -10 db in two of the three Pacific areas investigated. The superior ocean-bottom (S/N) ratios in the Hawaii area are due principally to a "noisy" land site.

(2) No consistent differences in phase development on the ocean bottom and land have emerged from the study, other than effects associated with the free surface and the late arriving T phase.

(3) For near-regional and local events, the ocean-bottom seismogram quite often shows greater high frequency energy content than on land.

(4) Ocean-bottom magnification of signal energy by as much as 20 db is consistenly observed for teleseisms and occasionally for near regional and local events.

(5) Ambient noise levels on the ocean bottom are greater than at a land control station by about 20 db at the low frequencies in all three areas. The difference decreases with increasing frequency.

(6) The ocean-bottom ambient spectra do not vary significantly over the days and areas sampled. The ambient in the vicinity of the Hawaiian Islands showed no depth dependence from 4000 to 18,000 ft in the 0.2 to 2 cps band.

(7) Examination of inter-component relations such as cross spectra and coherence reveals that the predominant ambient noise in the low frequencies $(0.1 < f < 1.0$ cps$)$ consists of normal modes propagating in many directions. Some evidence also exists for the presence of organ pipe modes at higher frequencies.

The foregoing are based not on a few observations, but what we believe the largest sample of ocean-bottom seismic data yet amassed in the frequency range 0.1 to 10 cps. In spite of the number of hours of data

collected, the geographical sampling of the oceans is exceedingly small, and it is entirely possible that vast statistical variations from these results may exist in other locations. Our picture of the noise based on three widely separated areas is, however, one of remarkable uniformity. As data becomes available from ocean-bottom units which can record on the bottom for periods up to one month, and from fixed ocean-bottom installations, the long term variations of the ambient can be studied and correlated with storm activity. Recall that all the ambient analyzed in this report was collected under favorable local sea state conditions, and may be biased in that regard.

Results of the prediction analysis, which are neither exhaustive nor complete, suggest that signal detection gains of at least 3 db are possible by suitably combining pressure and vertical to suppress the coherent part of the noise energy. The inability of the horizontals to contribute is consistent with the picture of noise being fairly isotropic. Finally, it is significant to note that the pressure-vertical velocity phase difference for signal (first motion of upgoing plane wave) is 180°, while the major postulated noise modes, e.g., normal and organ pipe have 90° and 0° phase difference respectively. This, in principle, affords considerable potential for signal and noise separation employing a two-channel pressure and vertical velocity processor. The latter will be explored in future work.

REFERENCES

Bradner, H., and Dodds, J. G., (to be published), "Comparative Seismic Noise on the Ocean Bottom and on Land," Journal of Geophysical Research.

Burg, J. P., 1964, "Three-Dimensional Filtering with an Array of Seismometers," Geophysics, V. 29, No. 5, (to be published).

Ewing, M. W., Jardetzky, W. S., and Press, F., 1957, "Elastic Waves in Layered Media," New York, McGraw-Hill Book Company, Inc.

Levinson, N., 1947, "A Heuristic Exposition of Wiener's Mathematical Theory of Prediction and Filtering," Journal of Math and Physics, V. 26, p. 110-119.

Longuet-Higgins, M. S., 1950, "A Theory of the Origin of Microseisms," Philosophical Transactions of the Royal Society of London (A), V. 243.

Phinney, R. A., 1961, "Leaking Modes in the Crustal Waveguide," Part 1, "The Oceanic PL Wave," Journal of Geophysical Research, V. 66, No. 5, p. 1445-1469.

Schneider, W. A., Farrell, P. J., and Brannian, R. E., 1964, "Collection and Analysis of Pacific Ocean Bottom Seismic Data," Geophysics, V. 29, No. 5 (to be published).

Semiannual Technical Report Number 3, 1962, "Ocean-Bottom Seismometer Data Collection and Analysis," Texas Instruments Incorporated, Contract No. AF 19(604)-8368.

Semiannual Technical Report, Number 5, 1963, "Ocean-Bottom Seismometer Data Collection and Analysis," Texas Instruments Incorporated, Contract No. AF 19(604)-8368.

Shor, George G., Jr., 1962, "Seismic Refraction Studies Off the Coast of Alaska, 1956-19 7," Seismic Society of America Bulletin, V. 52, No. 1, p. 37-57.

Spieker, L. J., Burg, J. P., Backus, M. M., and Strickland, L., 1961, "Seismometer Array and Data Processing System," Final Report Phase I, AFTAC Contract AF 33(600)-41840, Project VT/077.

Air Force Cambridge Research Laboratories, Laurence
G. Hanacom Field, Bedford, Mass.
Rpt. No. AFCRL-64-666, OCEAN-BOTTOM SEISMOGRAPH DATA
COLLECTION ANALYSIS. Final Report, 12 October 1964. 108 p.
incl. illus., tables, 11 refs.

Unclassified Report

Ocean-bottom data from three independent geographical locations
in the Pacific Ocean has been studied for consideration of means
of detecting and identification of underground or underwater
nuclear explosions.

Signal-to-noise ratios on the ocean bottom are generally inferior to
those at a land control station by 0 to -10 db in two of the three
areas. The superior ocean-bottom (S/N) ratios in the Hawaii area
are due principally to a "noisy" land site. The study reveals no con-
sistant differences in phase development between the ocean bottom
and land other than effects associated with the free surface and the
late arriving T phase. For near regional and local events, the
ocean-bottom seismogram often shows greater high frequency energy
content than on land. Ocean-bottom magnification of signal energy
by as much as 20 db is consistently observed for teleseisms and
occasionally for near regional and local events. Ambient noise
levels on the ocean bottom are greater than at a land control station
by about 20 db at the low frequencies in all three areas. The differ-
ence decreases with increasing frequency.

The study of these data suggests that signal detection gains of at
least 3 db are possible by suitably combining pressure and vertical
to suppress the coherent part of the noise energy.

1. Ocean-bottom data analysis for
   the Aleutian drop area
2. Ocean-bottom data analysis for
   the Hawaii drop area
3. Ocean-bottom data analysis for
   the California drop area
4. Statistical compilation of analysis
   results in the three Pacific areas

I.   Project No. 8652
     Task No. 865205
II. Contract AF 19(604)-8368
III. Schneider, W. A.
IV. In ASTIA collection